ABSTRACT

WHITE, LEONARD WILSON. Compensation of Electric Arc Furnaces Based on LaGrange Minimization. (Under the direction of Subhashish Bhattacharya.)

Electric Arc Furnaces (EAFs), among the largest loads on the electrical system, are generally moderated by ancillary compensation, Static Compensators (STATCOMs) being the most common equipment used. The most usual compensation strategy, the goal of which is to remove the highly variable reactive component from the utility load, is fundamentally based upon an application of the Clarke transformation.

A detailed look at the Clarke transformation shows that, while it is mathematically correct, the particular the conditions under which it is applied do not match the constraints that were used in its derivation. The application mismatch results in only minor discrepancies in the output of the transformation itself; however, the compensation strategies that embody the transformation do not use the zero component, a more serious issue. EAF current waveforms are highly unbalanced, resulting in a significant zero component that remains uncompensated.

The present work uses LaGrange minimization to determine inactive currents that are then used to direct a STATCOM to provide these currents. In cases where there is significant unbalance, the technique results in reduced line currents and improvements to the magnitude and stability of power delivered to the arc. The real power delivered by the STATCOM under the LaGrange compensation technique is zero; in cases where there is no line imbalance the results are identical to those produced by use of the Clarke transformation.

The Clarke transformation-based compensation scheme is compared directly to the LaGrange scheme by the use of a *PSCad* model. The STATCOM and compensation model are fully developed; also included is a *PSCad* arc model that can be arranged in any desired configuration to simulate unbalanced EAF load currents.

Compensation of Electric Arc Furnaces Based on LaGrange Minimization

by
Leonard Wilson White

A dissertation submitted to the Graduate Faculty of
North Carolina State University
in partial fulfillment of the
requirements for the degree of
Doctor of Philosophy

Electrical Engineering

Raleigh, North Carolina

2012

APPROVED BY:

_____	_____
Subhashish Bhattacharya Committee Chair	Alex Q. Huang
_____	_____
Mesut E. Baran	Mo-Yuen Chow

BIOGRAPHY

Leonard W. White was born in Henderson, NC, USA in 1945. He received a BS from NC State University in 1969, in Engineering Operations, a MS in Electrical and Computer Engineering from NC State University in 1986, and is presently pursuing a PhD in Electrical Engineering at NC State University. His area of specialization is power quality with a special emphasis on mitigation of flicker phenomena and harmonics as caused by Electric Arc Furnaces and similar industrial equipment.

Mr. White is one of the founding partners and former Senior Principal of Stanford White, Inc., a mid-sized engineering firm specializing in engineering services for the construction industry. He is a Senior Member of IEEE, a registered Professional Engineer (PE) in eight states, a Registered Communications Distribution Designer (RCDD), and serves on the NFPA-99 hospital electrical systems committee.

TABLE OF CONTENTS

LIST OF TABLES

LIST OF FIGURES

1 – Introduction

"In physical investigations success depends often on a happy choice of co-ordinates."
C. L. Fortescue

The quotation above is from the seminal work of Charles Fortescue [1], published in 1918. Professor Fortescue recognized that by simply changing the way a particular system, any system, is viewed may provide insight into ways to simplify computations or to extract information from the system that was not immediately obvious from the original viewpoint. While his original work was subsequently modified by others into its presently used form, the method of Symmetrical Components is fundamental to the analysis of polyphase electrical systems. The Symmetrical Component method is a result; it is the *concept* of looking at a system from a different viewpoint that is the critical element to the advance.

The present work picks a different viewpoint from which to look at the flow of electrical energy into an Electric Arc Furnace (EAF), a load that is generally unbalanced and largely stochastic. The motivation behind such an approach is that EAFs are arguably the largest producer of industrial heat in the world and, as such, the energy that they consume is considerable. Further, EAF loads are extremely disruptive to the electrical grid; an operating EAF can disturb power quality for many miles around the facility that employs them.

1.1 – Compensation of EAFs

The load presented to the grid by an EAF is that of a large, rapidly varying, generally unbalanced, non-linear load with a lagging, relatively low, power factor. The combination of load characteristics, along with the magnitude of the loads – easily up to 100 MVA – mandates some type of compensation to avoid severe disturbances to other users of the electrical utility. The type of disturbance to the grid is generally fluctuating, distorted, and possibly unbalanced system voltages. (As an aside, EAFs are sized up to 300 MVA with equipment as manufactured by *Alstom, S. A.*) Compensation of EAFs is necessary with the multiple goals of the compensation – and EAF operation in general – to maximize production output, minimize electrode consumption, furnace wear as well as to reduce flicker and harmonic generation.

The major effects of EAFs is large and erratic current swings which in turn cause corresponding voltage drops across the reactive impedances of the AC system; the net result is

fluctuating terminal voltages at the utility Point of Delivery. The intent of compensation is to reduce this effect by providing reactive elements that can be controlled to counter effects of the EAF. Fixed passive and active filters have had success in providing power factor correction but have been less effective when applied to EAFs. [2] Likewise, Static VAR Compensators are not completely effective as, once triggered, the thyristor valves must remain in conduction until natural commutation occurs. Static Compensators (STATCOMs) offer a controllable, versatile, synchronous voltage source, one where the magnitude can be controlled at will. The goal of compensation will be to "supply those components of the arc furnace load comprising non-sinusoidal, unbalanced, randomly fluctuating currents, in addition to the fundamental reactive power." [3] It is noted that STATCOMs will not normally have a source of real power connected to its DC terminals, thus no sustained real power can be provided by the compensator. Work has been done to use ultra-capacitors as an Energy Storage System to enable a STATCOM to deliver real power [4] but, to the knowledge of the author, this technique has not yet been applied to a working EAF. In summary, STATCOM is generally acknowledged to be more effective than Static VAR Compensators in the mitigation of flicker as generated by EAFs. [5] The efficacy of STATCOM in the mitigation of the various problems caused by EAFs is such that this equipment is becoming a prerequisite for EAF installations. [6] The physical implications of the requirement to minimize flicker were observed first-hand during the site visits for the present work: The company that operates the 33 MVA EAF that is described hereinafter is prohibited by the electric utility from operating the EAF unless the plant STATCOM is on-line.

As will be seen, the efficacy of EAF compensation is closely related to the degree of balance of the load at the instant of time at which the compensation is applied. It is the method of determining the compensation at each instant of time that is the main subject of the present work. As indicated by [7] the purpose of any power theory is to, (1) describe the interchange of energy between a source and a load and, (2) provide information about how to (possibly) improve the energy exchange by means of compensation. As a part of the present work, various power theories will be examined with the specific goal of determining which of the assumptions are appropriate for application to the compensation of the load of EAFs.

Any theory, power or otherwise, must have assumptions upon which the theory is based. It is axiomatic that the final usefulness of the theory will be determined by the degree of accuracy with which the theory predicts the behavior of a physical, real-world system. Therefore, the present work will commence with a general description of an EAF, the nature of the current waveforms drawn by this type equipment, and the impact of such waveforms on an electrical distribution system. This will

be followed by a detailed description of the present methods of EAF compensation and the shortcomings of same. Finally, an alternate mathematical analysis will be presented, followed by a compensation scheme based upon the analysis and an active simulation demonstrating the overall efficacy of the proposed scheme.

1.2 – Basis of comparison

It is axiomatic that in any engineering endeavor, the evaluation of options involves a comparison of some variable that has significance to the operators of the system under review. For the comparison to be valid the basis of comparison must remain invariant under the various modalities under review. As EAFs are used only for commercial purposes, the production of steel and other metals, it is logical that the basis of comparison be economic in nature. This is a fundamental, but not necessarily obvious, conclusion about economic systems. [8]

Having made the general observation that an economic analysis is an effective method of comparison, it must be noted that there are many things that affect the economics of a situation, some of which are not readily quantifiable. For example, one compensation technique may result in a higher level of energy being delivered under similar conditions but result in such a poor input waveform as to effectively increase the cost of the method.

For the work at hand, the decision is taken to allow the basis of comparison to be the total real power delivered to the arcs of the EAF under equivalent conditions. It is obvious that if more energy is delivered to the arc, the total time required for the charge to remain in the EAF will be reduced and the production throughput will increase. In making "real power to the arc" the figure of merit as a basis of comparison of the compensation methods under consideration some effort will be expended to demonstrate that other operational features of the EAF that could have a negative economic impact are not exacerbated or are actually improved by the method under question.

2 – EAFs and EAF waveforms

EAFs melt steel, or other conductive materials, by directing an arching electrical current through the material contained within the furnace, the "charge." The charge is thus exposed to both the heating effect of the current through the net resistance of the metal (i^2r) and the high temperature of the arc. The electrode temperatures can be quite high, with 1,500°C being fairly typical. [9]

The basic purpose of an EAF is simple, to melt the charge so that metallurgical modifications may be made to the material in its liquid state; however, the actual operation is quite complex. Additionally, the amount of energy required to melt steel is large, on the order of 360-400 kWH per ton. With furnace capacities up to 400 ton, the power requirements are quite impressive; sizes of 120 MVA are common. [10] Considering the size of the equipment, the various operations, and the nature of an electric arc, it is to be expected that EAFs are not kind to an electrical distribution system. A schematic diagram of a typical EAF is shown in Fig. 2.1; a photograph of an actual EAF that matches the schematic is presented as Fig. 2.2.

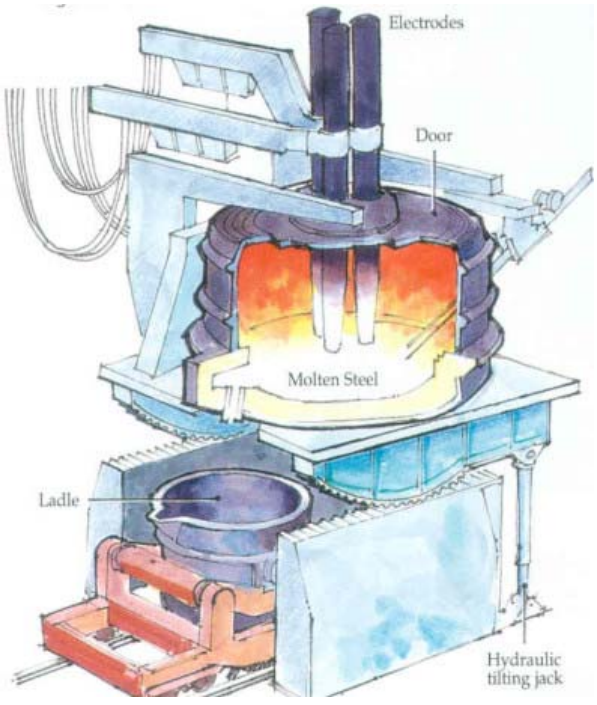

Fig. 2.1 Schematic Diagram of an Electric Arc Furnace

While, strictly speaking, it is not necessary to understand the physical details of EAF operation, such an understanding makes it easier to visualize the causes for the different waveforms that are produced during the cycle. The basic periods of a typical steel-making process are described in Table 2-1. [11] It is noted that a major EAF operating objective is to prevent damage to the EAF itself. The reason for this is fairly obvious when one considers that the electric arc is a plasma, with an effective temperature of 5,000°C – 20,000°C (9,032°F – 36,032°F). [12] No physical material can withstand temperatures of this magnitude, so it is necessary to limit the exposure of the internal parts of the furnace to the arc. This is accomplished by control of the arc current and by careful positioning of the electrodes during the steel-making cycle.

Fig. 2.2 Operating Electric Arc Furnace

It is the electrical considerations that are of concern. For a delta connected furnace, there is no current flow then the first electrode makes contact with the furnace charge; when the second electrode makes contact, there is a single-phase, line-to-line current flow. The load becomes a three-phase load when the third electrode makes contact with the furnace charge. Wide variations of load are

experienced during the ignition of the furnace. Because of movement of the charge within the furnace, the loads between the phases can go from the no-load condition, when the arc extinguishes, to the bolted-fault condition, when a part of the charge is displaced in a way such that it shorts two of the electrodes together. Physical movement of the electrodes is required to remedy either of these conditions. Disturbances of this type, and the resulting system unbalance, are short but random. In general, it is observed that electrical disturbances are most severe during the initial ignition of an EAF and early meltdown periods of the cycle. [13]

Table 2.1: The steel-making cycle

Period Name	Operating Objectives
Arc Ignition	1. To protect the furnace roof from the arc. 2. To stabilize the arc. 3. To rapidly submerge the electrode tip into the scrap.
Boring	1. To promote rapid melting by supplying high power and increasing the boring speed. 2. To increase the boring diameter.
Molten metal formation	1. To protect the furnace bottom from the arc spot.
Main melting	1. Arc is surrounded by molten metal: To provide maximum power permitted by the equipment.
Meltdown	1. To reduce any local damage near hot spots on furnace lining. 2. To rapidly melt remaining scrap.
Meltdown – heating	3. To reduce the heat radiation onto the lining. 4. To minimize hot-spot damage. 5. To rapidly increase the temperature of molten steel to the appropriate value for refining.

So, we see that, in general, an EAF of any type strikes and attempts to maintain an electric arc between a source, ultimately supplied by an electric utility, and a charge of conductive material. The operation of the arc under any conditions, but especially in the early stages of the steel-making

process, is unstable. It is extremely difficult to predict the characteristics of EAF load currents due to the stochastic nature of the system; the issue of prediction is further complicated by the non-linear and unbalanced nature of the load, the magnitude of the load, the mode of operation of the furnace, the characteristics of the particular charge, and the degree of wear of the electrode elements. Even so, serious work has been accomplished in an attempt to model EAF through various statistical and neural network schemes. The majority of these works appear to be directed toward control of the electrodes and control of the overall energy being put into the charge; representative examples are given by [14-16].

The goal of the present work is to develop a technique that improves the effectiveness of response to changes that have occurred in the load current of an EAF. Toward that end, it would be fitting to review some of the many EAF models that have been proposed in the literature and to finally present a series of waveforms captured from a working EAF.

The first thing to realize about EAF models is that the intent of such models is to produce an estimate of large-scale behavior of the EAF based on information that can be obtained from the furnace itself, the electrical system from which the furnace is supplied, and the type of operations that will be performed in the furnace. The intent is manifestly *not* to predict the small-scale, moment-to-moment, behavior of the furnace as this not possible because of the stochastic nature of the load. As we normally see the universe around us as a series of events occurring in linear time, it is logical to begin the review of EAF models with a time-domain approach.

A time-domain model is described by [17] that operates by applying a random number multiplier to an arc resistance range, really a difference between a maximum and a minimum arc resistance, that is dependent on the characteristics of a particular EAF. The random multiplier is then applied to a cosine function that is used to represent the modulation of the effective arc resistance; the scheme is applied independently to all three phases. The random number, distributed uniformly, is updated every half-cycle, at the zero crossing point of the current waveform. Validation of the model was accomplished by means of direct comparison of model results with actual operating EAFs with the measurements being made with an IEC compliant flickermeter [18]. While this model gives results that have overall errors of around 5%, it is not acceptable for accessing the impact of flicker mitigation equipment composed of a Static VAR Compensator (SVC) or a Static Synchronous Compensator (STATCOM) because of the fixed frequency of the modulation source.

Another time domain approach is presented by [19] in which an arc conductance representation for a low current arc is combined with a corresponding representation for a high

current arc by means of a transition factor; the transition factor is based on arc current. In this model again a random element is introduced; the voltage and current imbalance is obtained by using different values for the random variable for each of the three phases; no validation is provided.

The absence of validation is a concern with [19], however, the avowed purpose of this model is to provide a signal source that represents an EAF from within an operating *MatLab* [20] program. This use of the model is quite different from that of [17], where the goal is to predict the response of an electrical distribution system to a particular EAF. While no effort has been expended to duplicate the described MATLAB model, it is noted that the time-domain waveforms presented in the work as sample outputs from the model appear, at least visually, to be strikingly similar to real-time EAF data that was captured as a part of the present work.

In order to represent a time-domain function as a sum of sine and cosine waveforms, *i.e.*, as a Fourier series, the waveform under consideration must meet the Dirichlet conditions over the time period of interest. In general, this is not a problem with practical periodic waveforms, implying that a frequency-domain approach can be successfully used in the description and modeling of most real-world problems. [21] The problem of a frequency-domain representation of EAF phenomena arises due to the stochastic nature of the waveforms: The harmonic content of the various waveforms changes from period-to-period and in fact, as demonstrated by data captured as a part of the present work, the period itself can change significantly depending on how a 'period' is defined. For example, it will be seen that sample intervals based on a fixed time interval, based on zero-crossing point, and peak values will all result in different harmonic content. The inherent 'periodic' problems have not prevented frequency-domain based models of EAF behavior.

The particular methods used by [22-24] involve the selection of a generalized reference period composed of a integer number of elemental periods, *i.e.*, time intervals equal to the period of the fundamental frequency of the system; a system electrical model is described, from which component values are available. A dynamic arc is assumed, with the individual harmonics summing to the arc voltage. Two additional equations are available from the Kirchhoff's Law equations of the system electrical model. The set of equations is solved by Newton's Method; the current harmonics can be determined from the solution of the voltage equations.

The utility of the frequency domain models is in the ease of understanding of the individual harmonics and the simple application of the EAF model to the network model. The disadvantage of such models is that the frequency content of the current waveform changes from instant-to-instant; these changes are lost unless multiple analyses are conducted. As stated in [22], "...the harmonic

analysis...avoids the unexpected transients and deviation caused by time domain calculation." While this statement is undoubtedly true, it is these same "unexpected transients and deviations" that are the proximate cause of the flicker phenomenon and that are in fact the purpose for creating a model of the EAF.

Another approach to EAF modeling is taken by [25], where the EAF current waveform is represented as a state variable described by a Markov-like chain. This approach appears to have some merit as it is clear that the represented waveform is stochastic in nature. In effect, a Markov chain is nothing more than a sequence of random variable such that the value of the next state is dependent only upon the value of the present state. While it is obvious that the next state cannot be determined *a priori*, the statistical probability of any particular value of the state can be predicted.

Initially, it was believed that an EAF model would serve no real purpose in the present work, except perhaps as a means to perform early-on testing of the efficacy of the proposed harmonic reduction scheme. Even there, the utility would be somewhat limited as data is available from real-time measurements taken at an actual operating EAF. These data have been used to compare the various extant EAF compensation schemes with the present method. It is believed that the inclusion of modeling information is academically helpful, if only to highlight the significant amount of work that has been devoted to EAFs.

EAFs are used primarily to melt and process steel; the closest steel-making EAFs to the Raleigh, NC area are the following:

Nucor Steel
300 Steel Mill Rd.
Darlington, SC 29540
http://www.nucor.com

CMC Steel South Carolina
310 New State Road
Cayce, SC 29033
www.cmcsteel-sc.com

In spite of a serious effort, it was not possible to secure permission from either of the above facilities to capture real-time load information from their operations. The reason offered was "legal concerns" about the use of the data, frustrating but understandable, given the highly disruptive nature of a typical EAF facility. An alternate facility was selected.

A 4 MVA EAF is located at a manufacturing facility just north of Greensboro, NC, USA. The furnace is used to reduce copper scrap to the molten state for further processing into finned cooling tubes for use in heat-transfer equipment. The subject EAF is operated continuously, on a 24/7 basis. Arrangements were made with the manufacturing facility and the local utility, *Duke Energy*, to obtain metering from the utility substation, located adjacent to the manufacturing facility's property. The furnace and related items are shown in Figs 2.3 – 2.5.

Fig. 2.3 Subject Electric Arc Furnace in operation

The subject EAF is a dedicated load, supplied by a dedicated *Duke Energy* transmission, operating at the 88 kV level. There are three, single-phase substation transformers, each rated 2 MVA, 88:12.47 kV; the substation transformers are connected Δ:Y, with the voltage to the EAF transformer being 12,470gndY/7,200 Volt. The transformer impedance is 6.42%Z; the X/R ratio is unknown.

Input voltage and current were captured from the subject EAF on March 9, 2009, at a time when the furnace was operating in its normal reduction mode. The instrument used to capture the data, was a *Fluke 434* Power Quality Analyzer. The memory capacity of the *434* is somewhat limited, allowing the capture of eight (8) sets of data, each composed of 300 data points; four (4) values are captured for both voltage and current. The timing of the capture -cycle is such that two full cycles of data are captured. Although the memory is limited, the spacing of the data points at 2.4° (electrical) between points provides a perfectly acceptable resolution for the present purpose.

Captured data for a typical data-capture cycle is presented in Figs. 2.6 and 2.7. These data are used in further analysis in this work; refer to Appendix A for a listing of the software used to generate the plots. The generally complex relationship between the voltage and current waveforms is shown in Fig. 2.8, where typical plots of single-cycle voltage *vs.* current are presented.

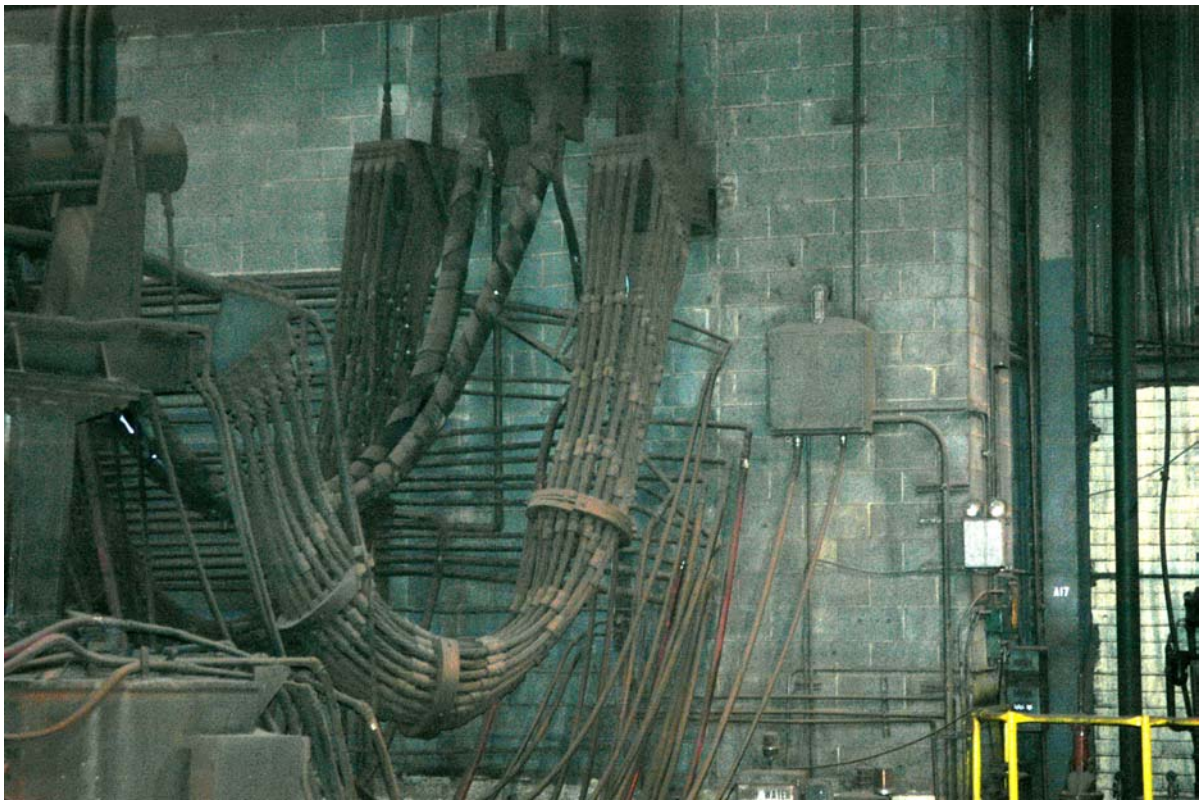

Fig. 2.4 Subject EAF electrode feeders

The captured waveforms for only one data set are presented but, in general, all captured data waveforms are similar. In reviewing the captured data, several points become obvious:

- The waveforms are non-sinusoidal.
- The waveforms are non-periodic, *i.e.*, they are not identical cycle-to-cycle.
- The waveforms have no obvious symmetry.
- The peak values of the waveforms are different from phase-to-phase.
- The peak values of the waveforms are different from cycle-to-cycle.
- There are multiple zero-crossing points within one cycle.

- The waveforms do not originate from a system in the 'steady-state,' as this is usually defined.

Each of the bulleted points listed above has direct implications for the analysis that will follow.

Fig. 2.5 *Duke Energy* substation

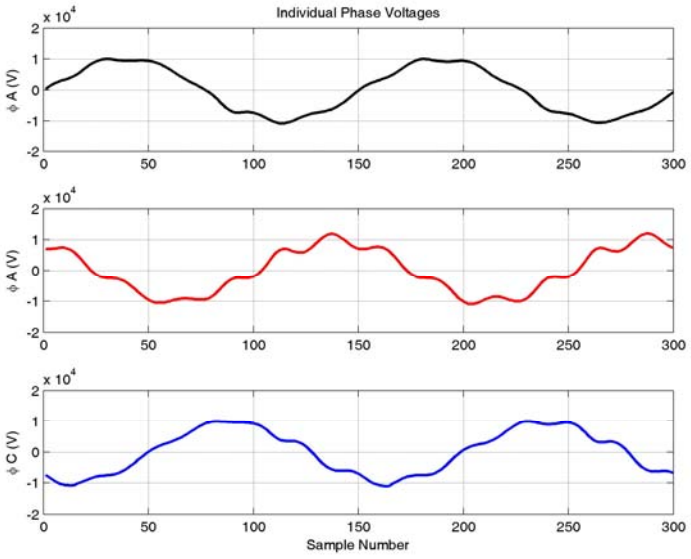

Fig. 2.6 Subject EAF input voltages

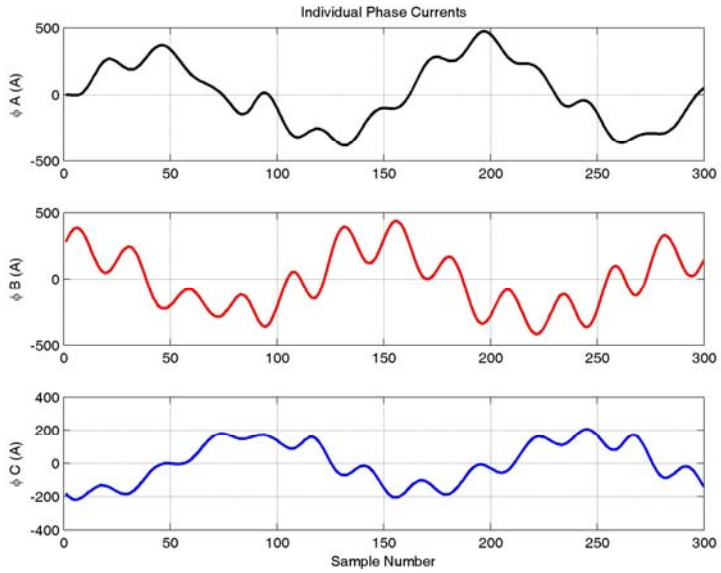

Fig. 2.7 Subject EAF input currents

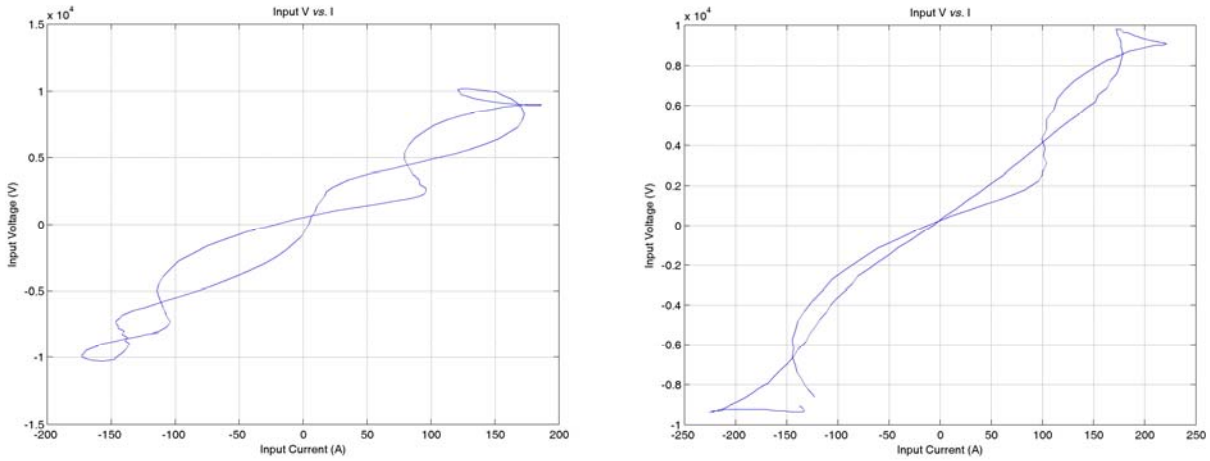

Fig. 2.8 Typical voltage *vs.* current plots for captured data

3 – Literature Review

The definitions of real power and reactive power under steady-state, sinusoidal conditions are well known and can be found in any basic AC theory textbook [26-28]. When we move away from the well-known conditions into the realm of instantaneous values we discover a wide variation in terms and expressions to describe the various mathematical and physical attributes of the instantaneous values. In the power quality literature, both active power and passive power are defined imprecisely. Unfortunately, the available definitions exhibit both synonymy, *i.e.*, use of two different words with equivalent meaning, and polysemy, *i.e.*, use of the same word to mean different things. Further, the latter includes differences in level of abstraction, as well as in concept coverage. Standard terms and definitions, also called *controlled vocabulary*, are required to unambiguously and precisely specify the concepts active and passive power. The disambiguation obtained through solid terminological methods [29-30] is necessary for the specificity required of mathematical models.

It is noted that [29-30] are oriented specifically toward a medical environment where a controlled vocabulary is necessary to convey information quickly and accurately in a life-critical situations. Although is it obvious that what is needed is a unifying set of definitions, as suggested by the references, the development of such a set will take the cooperation of multiple standards agencies and is clearly beyond the scope of the present work. The present approach will be to identify differences in terms where the difference would influence an understanding of the work.

The initial work in instantaneous power theory was by Akagi, Kanazawa, and Nabae in the early 1980s. This work, generally known as the *pq*-theory, was expanded and presented in [31] as the definitive text on the subject. This text deals with all aspects of instantaneous power, but the main emphasis is on systems that are periodic. A great deal attention is paid to sinusoidal systems, which are a subset of the more generalized deterministic periodic systems. The generalized approach taken by [31] is one of transformation of the instantaneous system values of voltage and current as measured in the *abc* reference frame to the $\alpha\beta$ or $\alpha\beta 0$ reference frame as described by the work of Edith Clarke. [32]

The representation of a three-phase electrical system and its loads as described in [32] is very well suited to the control of motors, applications involving active filters, and in other situations where the phase-to-phase variations of the system, in particular the angles, are so small as to become insignificant. Under such conditions the mathematical mapping of an *abc* reference frame to a

$\alpha\beta 0$ reference frame is both one-to-one and onto, *i.e.*, no information is lost in the transformations back and forth between the two reference system.

In a more general sense, a three-phase set of current or voltage waveforms has six degrees of freedom as was recognized in 1918 by Fortescue. [1] This seminal work described a completely non-symmetric system and demonstrated how such a system could be represented as any other system where the number of degrees of freedom was preserved by both the transformation and the reversing transformation between representation formats. This work is the basis of the commonly-used symmetrical components analysis techniques. More importantly, it sets the stage for representation of a system in an infinitely large number of formats whose commonality is only that they all preserve the number of degrees of freedom.

Our first concern is to eliminate various works that reduce the number of degrees of freedom, that is, works based on [32-34] that use the methods based on a generalized assumption that the angles between the vectors are all equal, effectively reducing the number of degrees of freedom from six to four. The number of references based on reduction of degree of freedom is extensive, many hundreds, and comprises the vast majority of the literature. As an aside, it is noted that since any one of the six degrees of freedom may be arbitrarily selected as a reference without loss of generality, the net effect of any of these works is to reduce the number of degrees of freedom from six to three; mathematically speaking, all of these transforms are "one-to-one", but not "onto".

Another series of works is based on the efforts of Fryze [35-36], Buchholz [37], and Depenbrock [38-42] is generally known as the FBD method. The works of Fryze, Buchholz, and Depenbrock, in the German and Polish languages, have been summarized and analyzed in detail in a review paper by Staudt. [7] As an aside, this work, in a limited fashion, deals with the problem of definitions of terms that was previously discussed; at several points divergent definitions are identified; a brief list of definitions is provided so that meanings with regard to the work are absolutely clear.

The major developmental concepts of the FBD method are the definitions of active current, i_{a1}, and non-active current, i_{x1}, the assertion that these two current quantities are orthogonal, and the definition of active power, p_a, in terms of the square of active current. The operation of the definitions is demonstrated by the use of a single-phase circuit with sinusoidal excitation and loads. For the sinusoidal case, with active current based on an equivalent active conductance the following the modeled system matches the results of the classical phasor method. As with that method, reactive power, which is signed, and apparent power are not physical quantities. It is again noted that active

current and non-active current are orthogonal quantities, so that while these two terms sum to the total current, the addition is a *vector* addition, not an arithmetic addition. When working in the realm of sinusoidal functions this is a natural conclusion, a result of Euler's definition. [43] It should be kept in mind that this definition has no real meaning when non-deterministic, time-varying functions are under discussion.

The work is extended to the non-sinusoidal case by means of a circuit containing a pure resistance and an ideal switch. The major conclusion of this work is that switching can cause non-active power even though energy flows in only one direction and no power is associated with the operation of the switch itself. It is acknowledged that the generally accepted definition of reactive power does not apply under these conditions; it is further acknowledged that the current can always be decomposed into active and non-active components *if one period of current and voltage is known*. It is precisely this condition that leads to difficulties in the case of EAFs, where the current waveform is unbalanced, nonlinear, time-varying, [24] and where the exact moment control is desired is during a deviation from a normal periodic waveform.

Considerable effort is expended in [7] to consider the FBD method in frequency domain. The conclusions drawn appear to be valid, but from the prospective of the present work, these results are not important: We are not dealing with a known, consistent period for the current waveform under consideration.

A pair of publications [44-45] summarizes the FBD method, *pq*-theory, and a third decomposition method known as Conservative Power Theory (CPT). CPT, originally proposed in [46], is based on the assumption of a known periodic waveform from which average values can be defined as an integrals. The work defines operators, identified as homo-variables, that satisfy Kirchhoff's Laws, are mathematically complete within the set of defined values, and are conservative with respect to defined complex powers. The major difficulty with this theory, which offers some advantages over the FDB method and *pq*-theory, is the assumption of a fixed period, a condition that cannot be reliably assumed with the operation of an EAF.

Furuhashi [47] comes to the point quite quickly, but immediately runs into difficulties with definitions, particularity that of "reactive power", which is formally defined only in terms of sinusoidal systems. The technique used is one of establishing a performance function for the system and then minimizing this function subject to a separate constraining function; the assumption is made that the power source is balanced. The method is applied to a generalized three-phase, three-wire

system. A control algorithm is developed for the described system and is applied to a generalized load; a simulation is provided to demonstrate validity.

The major difficulty of this work is the assumption of a balanced supply source, an assumption that essentially reduces the degrees of freedom of the voltage from five (assuming an arbitrary reference) to three. Under this set of restrictions, the methods of [31] can be applied with good results. Even so, the work of [47] is otherwise valid and sets the stage for the present work, in which the instantaneous system values will be considered where there are absolutely no restrictions to waveform types, or periods, that is only information that is available instantaneously will be considered, *viz*., the magnitude of the three phase voltages and the magnitudes of the three phase currents.

As Staudt [7] points out so eloquently, a general theory becomes invalid if but one counter-example exists. That is precisely the point of the present work as the particular loads of interest occur at points where other 'theories' are not valid for one reason or another.

4 – Comparison of various instantaneous representations

4.1 – Introduction

There are several methods of representing electrical phenomena as instantaneous events or points in time. The validity of these various methods depends almost entirely on the assumptions that are made about the underlying electrical system, *i.e.*, the types of waveforms that are being observed. Before embarking on an EAF compensation scheme, it is appropriate to review the various methods that are presently in use. These methods can be generally broken down into the four (4) types, listed below:

- Fryze-Buchholz-Depenbrock (FBD) power theory
- *dq* theory
- *dq0* theory
- Constant Power (CP) Method

A great deal of emphasis is given in the literature to the physical meaning of the derived values of an instantaneous power theory. It can be taken as axiomatic that a physical representation of a mathematical construct aids in visualization; however, such a representation is in no way necessary to allow an understanding of the construct or even to allow to the construct to be utilized in a compensation strategy. The following is a general summary of the various methods of representing instantaneous power in electrical systems, each followed by a statement of the general utility of the method for the compensation of EAFs.

4.2 – Fryze-Buchholz-Depenbrock (FBD) power theory

The FBD power theory as, summarized by [7], is based on splitting a single phase load into two parts, an active part represented by a pure resistance (or conductance) and a current source. The pure resistance is selected such that the same energy per period is transferred to the active load as was transferred with the original circuit being modeled. The remainder of the total current into the original circuit is represented by a controlled current source. A major feature of the division of the currents is that the active current and non-active current are constructed to be orthogonal functions. The implication of orthogonality is that the active current can make no contribution to the non-active current and *vice-versa*.

In looking at the active portion of the divided load, it is immediately observed that the power is the product of the voltage across the resistance times the current through the resistance; the same result is obtained by dividing the voltage squared by the resistance. Both these results are the normal expectations for power delivered to a pure resistance. When the applied voltage waveform is sinusoidal, the results of the splitting of the input current into orthogonal active and non-active parts results in same circuit division as if the load is considered as a complex load, *i.e.*, a load composed of a real part and a reactive part. This same situation will result if the load contains controlled electronic elements so that it *appears* to be reactive. For sinusoidal voltage input to the original system, the various currents and voltages can be presented as phasors; phasor representation offers no real mathematical advantage, but provides easy visualization of the various quantities.

With the FBD representation scheme, active power is given by the dot-product of voltage and active current; this value corresponds to measured physical power. Reactive power, Q, determined in a similar way, has no physical significance. The apparent power under the FBD power theory, S, is determined by using the orthogonality of the individual components; the valued determined has no physical significance.

Under conditions of a non-sinusoidal voltage source with a pure resistance a load current similar to those with a non-linear load can be encountered. The circuit voltages and currents are determined as before, but the reference to 'reactive' components is lost as this designation applies only to sinusoidal conditions. In a similar way, the FBD analysis can be extended into the frequency domain, however there are problems when computing the total power by the usual method of summing all the individual frequency powers.

The FBD method may be extended to polyphase systems of dimension n in cases where currents and voltages sum to zero around some common point. The extension is straightforward and is based on the treatment of all instantaneous values of voltage and current being treated collectively.

Compensation schemes may be devised that exploit the non-active power of the FBD theory, as may all instantaneous power theories. The goal of such a scheme is to provide compensation such that the non-active currents delivered by the voltage source are reduced to zero. Since these currents cause no net energy to be transferred between voltage source and the load, in the ideal situation, the energy cost of such compensation is nil.

The following general observations may be made about the FBD power theory:

- In general the time function of optimal real power is not a constant but varies with the square of the voltage time function.

- The difference between actual current and active current is non-active current; this is a vector difference rather than an arithmetic difference.
- The reactive current can be modeled by equivalent reactive circuit elements. The apparent of reactive elements is equal to the absolute value of their reactive power. It is noted that reactive power is a signed quantity.
- Reactive power and apparent power are not physical quantities.
- A non-linear voltage source may cause non-active power even though energy flows only in one direction and there is no power associated with the non-linear elements in the voltage source.
- Reactive power, as it is classically defined, does not exist except under sinusoidal conditions.
- For a non-linear voltage source, non-active power is always positive; in general it can not be associated with reactive circuit elements.
- For a non-linear voltage source, there is no physical interpretation of non-active power.
- The decomposition into active and non-active components is always possible *if one period of current and voltage is known* and if these values do not change from cycle to cycle.
- Active current has a clearly defined time function, the instantaneous active current.
- Non-active current has a clearly defined time function, the instantaneous non-active current.
- Non-active current can be computed without using non-active power or 'fictitious' voltages.

In order to use FBD as a compensation method for non-linear loads it is first necessary to compute the value of the non-active current based on real-time measurements. If the non-linear load is stable from cycle-to-cycle the information is available to a control scheme and the value of the compensation can be computed. In the specific case of an EAF, there are cycle-to-cycle variations in not only the non-active portion of the load current but also in the active portion. For this reason, FBD is not an appropriate instantaneous power theory to develop further for EAF power quality control.

4.3 – *dq* Method: *abc* ↔ *dq* transformation

The *dq* method, first developed by Edith Clarke in [32], has arguably become the *de facto* method for determining compensation for a wide variety of compensation and control schemes. The transformation creates a two-phase system from a three-phase system, the mathematic equivalent of the Scott-T transformer (also known as the Scott connection). [48] The transformation can be successfully applied in cases where the waveforms are deterministic, periodic, sinusoidal, and balanced; the transformation can be used equally well for either voltage or current. For applicable systems, the waveforms can be expressed in frequency domain as phasors. A typical system to which a*bc* ↔ *dq* transformation can be successfully applied is shown below in Fig. 4.1.

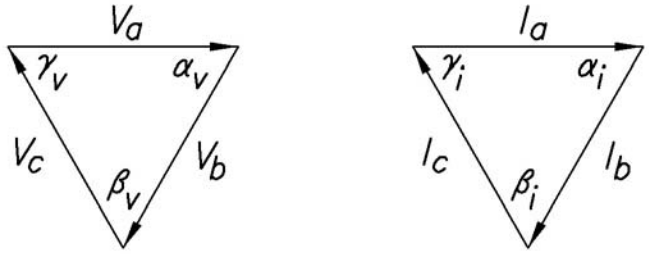

Fig. 4.1 Appropriate systems for use of the *abc* ↔ *dq* transformation

The following are the restrictions on the *abc* system to/from which the transformation is applied:

$$\begin{aligned} \vec{V}_a + \vec{V}_b + \vec{V}_c &\equiv 0 \\ \vec{I}_a + \vec{I}_b + \vec{I}_c &\equiv 0 \end{aligned} \tag{4-1}$$

The implications on the restrictions of (4-1) are that the angles between the vectors composing the system are also equal, as shown in (4-2) . This restriction is not generally stated, but is implied by the method of derivation, as will be shown later.

$$\begin{aligned} \alpha_v = \beta_v = \gamma_v &= 60° \\ \alpha_i = \beta_i = \gamma_i &= 60° \end{aligned} \tag{4-2}$$

The system as described above has three entering degrees of freedom for either a voltage or a current vector set. Specifically, the degrees of freedom are two (2) voltage (or current) magnitudes, and 1 angle, usually selected arbitrarily. Note that the 3rd voltage (or current) magnitude is fixed by restrictions of (4-1).

The *abc* → *dq* transformation is shown graphically in Fig. 4.2; the transformation is bi-directional.

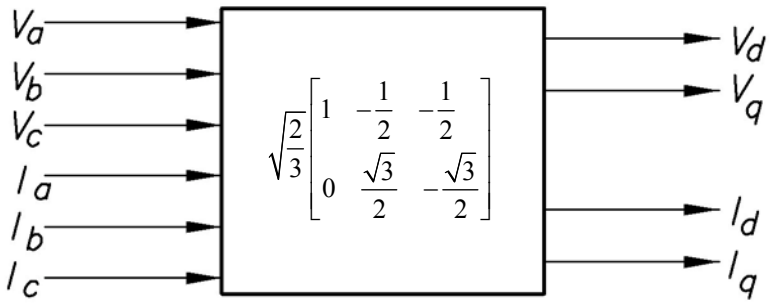

Fig. 4.2 Graphic representation of the *abc* → *dq* transformation

There are output restrictions on the *abc* ↔ *dq* transformation. For voltage representations, $\vec{V}_d$ is 90° out of phase with $\vec{V}_q$. For a current representation, $\vec{I}_d$ is 90° out of phase with $\vec{I}_q$. There are three (3) exit degrees of freedom, *viz.*, $\left|\vec{V}_d\right|$, $\left|\vec{V}_q\right|$, angle for voltage and, for current systems, $\left|\vec{I}_d\right|$, $\left|\vec{I}_q\right|$, angle for current. Since the number of degrees of freedom on both sides of the transformation is the same the transformation is both 'one-to-one' and 'onto.'

The power relationships that result from the *abc* ↔ *dq* transformation are presented for reference in (4-3) below:

$$\begin{aligned} S &= VI^{\dagger} = (V_d + jV_q)(I_d - jI_q) \\ S &= P + jQ \\ P &= V_d I_d + V_q I_q \\ Q &= (V_q I_d - V_d I_q) \end{aligned} \tag{4-3}$$

As will be seen in the sequel, the issues with the *abc* ↔ *dq* transformation come not from the transformation itself but rather from applying the transformation to a situation that does meet the specific requirement of the derivation.

4.4 – *dq0* Method: *abc* ↔ *dq0* transformation

The *dq0* method is an expansion of the *dq* method previously described into a method that has fewer constraints on its use. The balanced constraint has been relaxed with the *dq0* method, so

the transformation can be successfully applied in cases where the waveforms are deterministic, periodic, sinusoidal, and unbalanced; as with the *dq* transformation, *dq0* can be used equally well for either voltage or current and, as before, the waveforms can be expressed in frequency domain as phasors. A typical system to which a*bc* ↔ *dq0* transformation can be successfully applied is shown below in Fig. 4.3.

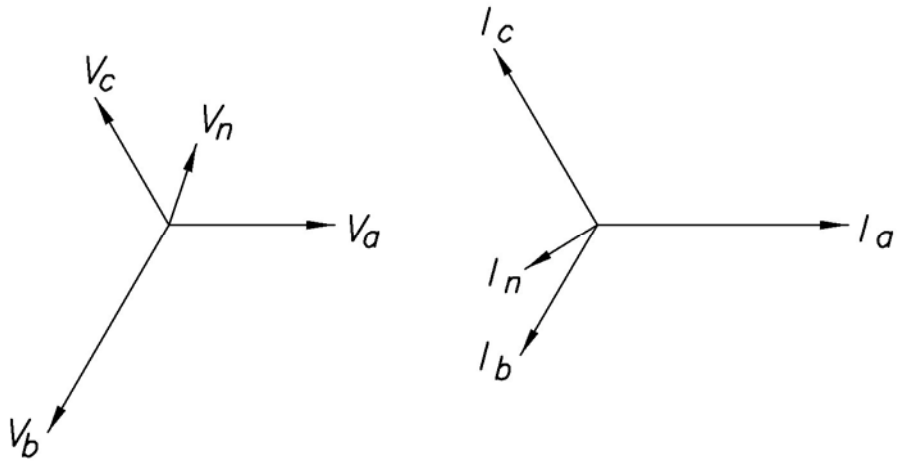

Fig. 4.3 Appropriate systems for use of the *abc* ↔ *dq0* transformation

The following are the restrictions on the *abc* system to/from which the transformation is applied:

$$\begin{aligned} \vec{V}_a + \vec{V}_b + \vec{V}_c + \vec{V}_n &\equiv 0 \\ \vec{I}_a + \vec{I}_b + \vec{I}_c + \vec{I}_n &\equiv 0 \end{aligned} \tag{4-4}$$

The angles between the vectors is also constrained in the *dq0* method, although they are not directly constrained as a result of (4-4). In this case the angles are assumed to be 120° by the derivation of the method. The method will be developed in detail in a later chapter.

There are four (4) degrees of freedom of the source ABC system, three (3) voltages (or current) magnitudes, and one (1) angle – usually an arbitrary selection; on the exit side, the degrees of freedom are the same, three (3) voltages (or current) magnitudes and one (1) angle, again usually an arbitrary selection. The transformation is bi-directional, *i.e.*, it works for either the *abc* → *dq0* transformation or the reverse, *dq0* → *abc*; mathematically, the transformation is one-to-one and onto. A graphic presentation of the transformation is presented in Fig. 4.4.

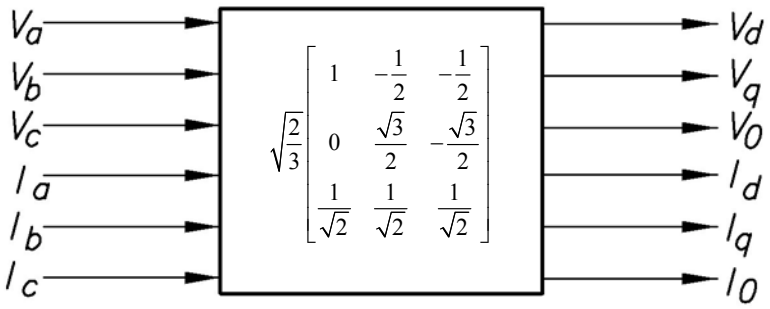

Fig. 4.4 Graphic representation of the $abc \rightarrow dq0$ transformation

The output of the transformation is, for voltage, $\vec{V}_d$ is 90° out of phase with $\vec{V}_q$, and, for current, $\vec{I}_d$ is 90° out of phase with $\vec{I}_q$. The neutral values, $\vec{V}_n$ and $\vec{I}_n$, are not a part of the *d* and *q* relationships. The power relationships are the following:

$$\begin{aligned} P &= V_d I_d + V_q I_q \\ Q &= j(V_q I_d - V_d I_q) \\ S &= P + jQ + S_n \end{aligned} \tag{4-5}$$

Where S_n is a single phase complex power such that $|S_n| = V_n I_n$.

There are difficulties with the application of both the *dq* and *dq0* transformations to the problem of EAF compensation. The problems arise due to the violation of initial conditions assumed during the derivation of the transformation and the inability to properly deal with the residual complex power that is a part of the zero term.

4.5 – Conservative power theory

The framework for Conservative Power Theory (CPT) has been well described by [49]. The CPT concept is based upon the definition of instantaneous complex power under non-sinusoidal conditions; the original work was based on a single phase system, but the concept is easily expanded to three-phase systems.

The fundamental concept of CPT is the definition of "homo-variables", variables that are the results of integral and derivates that are defined under periodic conditions. The fundamental definitions are the following, expressed using the notation that is presented in [44-45] :

$$\hat{v}_\mu = \omega\left(v_{\mu\int}(t) - \bar{v}_{\mu\int}\right)$$
$$\hat{i}_\mu = \omega\left(i_{\mu\int}(t) - \bar{i}_{\mu\int}\right) \tag{4-6}$$

Where the homo-integrals of the voltages, v_μ, and the current, i_μ, are given by:

$$v_{\mu\int}(t) = \int_0^T v_\mu(\tau)d\tau$$
$$i_{\mu\int}(t) = \int_0^T i_\mu(\tau)d\tau \tag{4-7}$$

With $\bar{v}_{\mu\int}$ and $\bar{i}_{\mu\int}$ being the average values of v_μ and i_μ, respectively, over the period *T*.

In a similar way, the homo-derivatives of the voltages and currents are given by the following:

$$\breve{v}_\mu(t) = \frac{1}{\omega}\frac{dv_\mu(t)}{dt}$$
$$\breve{i}_\mu(t) = \frac{1}{\omega}\frac{di_\mu(t)}{dt} \tag{4-8}$$

In all cases, $\omega = \frac{2\pi}{T}$.

The entire CPT framework is now based on the homo-voltages and currents being amenable to Kirchhoff's Laws. From this beginning, it is now possible to define active power, reactive power, active current, and reactive current. A new term is also defined, *void current*, a residual term that conveys neither active power (*P*) nor reactive power (*Q*).

The CPT framework is complete, and the computed powers, both real and reactive agree with the results of the time domain analysis, frequency domain analysis, FBD, *d0*, and *dq0* (collectively the *pq*-theory) representations when sinusoidal signals are considered. From [45], FBD and *pq*-theory can lead to invalid conclusions under certain conditions. These items are interesting academically, and are arguably necessary to a full presentation of the methods, but they are not cogent to the problem at hand, determining an effective framework for compensation of an EAF. In particular, the item that causes CPT to be unacceptable to the task at hand is the requirement that the waveforms under consideration be periodic. In general, EAF current waveforms have periods that vary from cycle-to-cycle in a stochastic manner.

4.6 – Instantaneous minimization methods

In brief, none of the extant power theories offer a reasonable way to accurately deal with a system of voltage and current waveforms as are generated by an operating EAF. Another approach to the problem involves looking at the instantaneous values of voltage and current and then separating the current into active and passive components. The goal of this approach will be to minimize the total passive current while maintaining the total power into the system. In taking this approach, it should be noted that the goal is not to create yet another unified instantaneous power theory, even though such may be possible. The goal is to develop an understanding of the system such that compensation can be introduced to a working EAF that will result in improved performance as compared with that which can be achieved using present techniques. The starting point for such work is a complete examination of the method of choice for EAF compensation, *pq*-theory, as based on the Clarke Transformations, and the limitations that such a scheme has when applied to the EAF.

5 – The Clarke transformations

5.1 Derivation of the Clarke transformations

The Clarke Transformations, [32] referenced in the previous chapter as the *abc* ↔ *dq* and *abc* ↔ *dq0* transformations, are important and should be examined in some detail, including a complete mathematical derivation of same. Toward that end, consider a three phase electrical system, the voltage equations of which are approximated by the equations below:

$$\begin{aligned} v_a(t) &= \sqrt{2}V_{RMS}\cos(\omega t) \\ v_b(t) &= \sqrt{2}V_{RMS}\cos(\omega t - \tfrac{2\pi}{3}) \\ v_c(t) &= \sqrt{2}V_{RMS}\cos(\omega t + \tfrac{2\pi}{3}) \end{aligned} \tag{5-1}$$

The set of equations presented as (5-1) shows a simple set of idealized voltages, without harmonic content. Data from actual EAFs, as previously presented, indicates that the expressions are considerably more complex, with harmonics higher than the 40th being common. [50] The present simplification is justified and, in the sequel, it will be demonstrated that the actual complexity of the waveform does not affect the analysis.

A simplified current waveform set that corresponds to the above voltage set is given by (5-2). In this expression the ϕ term is the phase shift of the current waveform, assumed in the simplistic case to be a constant. Again, in the sequel, this will become unimportant.

$$\begin{aligned} i_a(t) &= \sqrt{2}I_{RMS}\cos(\omega t - \phi) \\ i_b(t) &= \sqrt{2}I_{RMS}\cos(\omega t - \tfrac{2\pi}{3} - \phi) \\ i_c(t) &= \sqrt{2}I_{RMS}\cos(\omega t + \tfrac{2\pi}{3} - \phi) \end{aligned} \tag{5-2}$$

The traditional analysis of (5-1) and (5-2) assumes the system is in equilibrium, *i.e.*, steady state, and that the time domain equations can be accurately represented by an exponential format where the exponential representation is assumed to rotate at the angular speed of the system, ωt. This representation is based on the complex variable definition [43] of the cosine function, generally expressed as:

$$\cos(\omega t) = \frac{e^{j\omega t} + e^{-j\omega t}}{2} \tag{5-3}$$

In this representation, the positive value of the exponent of e is generally taken as both the positive value and the negative value carries the same information about the system. The classical representation of the system of (5-2) becomes:

$$\begin{aligned} i_a(t) &= \sqrt{2} I_{RMS} e^{(j\omega t - \phi)} \\ i_b(t) &= \sqrt{2} I_{RMS} e^{(j\omega t - \frac{2\pi}{3} - \phi)} \\ i_c(t) &= \sqrt{2} I_{RMS} e^{(j\omega t + \frac{2\pi}{3} - \phi)} \end{aligned} \tag{5-4}$$

This is shortened even further by reduction to *phasor* notation in which the electrical angular velocity, ωt , is assumed to be a known constant and the RMS value of the waveform is used. The resulting format, expressed in phasor notation, then becomes: [26]

$$\begin{aligned} i_a &= I \angle (0 - \phi) \\ i_b &= I \angle (-120^\circ - \phi) \\ i_c &= I \angle (120^\circ - \phi) \end{aligned} \tag{5-5}$$

It is noted in passing that the simplified phasor format can be used to represent a system with an unbounded number of harmonics by introducing a phasor term for each harmonic. The only general requirement for this representation is the same as for the original development, *viz.*, that it be a steady state representation.

Graphically and analytically the system of (5-5) and, through extension, the earlier versions, can be represented as a system of three related vectors. The vectors all have the same length and are rotated one from the other by equal angles of 120˚. Such a system can be completely defined by only two variables, the magnitude of *V* and the and the value of the rotation displacement, ϕ . Mathematically, this system has two degrees of freedom.

The system can be generalized by allowing the magnitude to vary from phase-to-phase and removing the equal-angle restriction on the angle between the vectors. The resulting generalized system becomes:

$$\begin{aligned} i_a &= I_a \angle (0 - \phi_a) \\ i_b &= I_b \angle (-120^\circ - \phi_b) \\ i_c &= I_c \angle (120^\circ - \phi_c) \end{aligned} \tag{5-6}$$

The system of (5-6) has six degrees of freedom as each vector is totally independent of the other vectors, *i.e.,* each of the vectors of this 3 vector coplanar set can be positioned in 2-space without regard to the other vectors. The observation is made that the vectors may be positioned in

any order (ABC or ACB rotation), with a common tie point (*wye* connection), or joined tail-to-head (*delta* connection) without affecting the conclusions of the present work.

If we apply the generalized notation of (5-6) to the current equation set of (5-2) we end up with a generalized set of equations, for which we have a exponential or phasor representation, with which we can begin a more detailed look as instantaneous values. The generalized set is presented below for reference:

$$\begin{aligned} i_a(t) &= \sqrt{2} I_{aRMS} \cos(\omega t - \phi_a) \\ i_b(t) &= \sqrt{2} I_{bRMS} \cos(\omega t - \tfrac{2\pi}{3} - \phi_b) \\ i_c(t) &= \sqrt{2} I_{cRMS} \cos(\omega t + \tfrac{2\pi}{3} - \phi_c) \end{aligned} \tag{5-7}$$

To represent harmonics in this notation, the vector representing each succeeding harmonic is simply added to the end of the vector of the harmonic below it but rotates at twice the electrical angular velocity.

The equation set of (5-7) is the starting point for the two-phase representation introduced by Edith Clarke in. [32] For technical completeness this work will be developed along the same lines as the original development. Then, the method will be examined to determine the tacit underlying assumptions and its suitability for use in EAF compensation.

Consider a three phase vector system that is based on equation set (5-7). The system is labeled as currents, but voltages can be used with no loss of generality. The three-phase set can be superimposed on a set of orthogonal axes labeled as d and q, with the 'a' phase of the three-phase set being aligned with the d phase of the two-phase set. (Aside: The two-axis set of vectors is the same as would be used to describe a 2-phase, 5-wire system as was occasionally used in the early days of electrical power distribution systems [51]. The axis system was described as being composed of a *direct* axis, d, and a quadrature axis, q.) The basic concept will be to project the three-phase, a, b, c, set of vectors onto the two-phase, $d, q,$ set of axes and then to sum the value into a total contribution for the particular two-phase axis.

For the 'd' axis, the contribution of the 'a' vector is $\sqrt{2} I_{aRMS} \cos 0°$, that of the '$b$' vector is $\sqrt{2} I_{bRMS} \cos(-120°)$, and that of the '$c$' vector is $\sqrt{2} I_{cRMS} \cos(120°)$. Evaluating the trigonometric expressions and summing gives:

$$I_d = \sqrt{2}\left(I_{aRMS} - \frac{1}{2} I_{bRMS} - \frac{1}{2} I_{cRMS} \right) \tag{5-8}$$

In a similar way, for the 'q' axis, the contribution of the 'a' vector is $\sqrt{2} I_{aRMS} \cos 90°$, that of the '$b$' vector is $\sqrt{2} I_{bRMS} \sin(-120°)$, and that of the '$c$' vector is $\sqrt{2} I_{cRMS} \sin(120°)$. Evaluating the trigonometric expressions and summing gives:

$$I_q = \sqrt{2}\left(0 + \frac{\sqrt{3}}{2} I_{bRMS} - \frac{\sqrt{3}}{2} I_{cRMS} \right) \tag{5-9}$$

The unbalance component, I_0, often misleadingly called the *zero sequence* component, is given by a simple summation of one third of the individual phase values:

$$I_0 = \left(\frac{1}{3} I_{aRMS} + \frac{1}{3} I_{bRMS} + \frac{1}{3} I_{cRMS} \right) \tag{5-10}$$

Arranging (5-8),(5-9), and (5-10) gives:

$$\begin{bmatrix} I_d \\ I_q \\ I_0 \end{bmatrix} = \begin{bmatrix} 1 & -\frac{1}{2} & -\frac{1}{2} \\ 0 & \frac{\sqrt{3}}{2} & -\frac{\sqrt{3}}{2} \\ \frac{1}{3} & \frac{1}{3} & \frac{1}{3} \end{bmatrix} \begin{bmatrix} I_a \\ I_b \\ I_c \end{bmatrix} \tag{5-11}$$

The expression of (5-11) is based on an input vector of RMS values; if peak values are used, each element of the 3x3 transition matrix is divided by $\sqrt{2}$. Another commonly applied modification is made by multiplying the matrix by $\sqrt{\frac{2}{3}}$ so that the magnitude of the vectors in *dq0* space are the same as the magnitude of the vectors in *abc* space [52]. The final result of this change is presented below:

$$\begin{bmatrix} I_d \\ I_q \\ I_0 \end{bmatrix} = \sqrt{\frac{2}{3}} \begin{bmatrix} 1 & -\frac{1}{2} & -\frac{1}{2} \\ 0 & \frac{\sqrt{3}}{2} & -\frac{\sqrt{3}}{2} \\ \frac{1}{3} & \frac{1}{3} & \frac{1}{3} \end{bmatrix} \begin{bmatrix} I_a \\ I_b \\ I_c \end{bmatrix} \tag{5-12}$$

Defining the Clarke transformation, T_C, as:

$$\mathrm{T}_C \triangleq \sqrt{\frac{2}{3}} \begin{bmatrix} 1 & -\frac{1}{2} & -\frac{1}{2} \\ 0 & \frac{\sqrt{3}}{2} & -\frac{\sqrt{3}}{2} \\ \frac{1}{3} & \frac{1}{3} & \frac{1}{3} \end{bmatrix} \tag{5-13}$$

Allows the following shorthand notation to be used:

$$I_{dq0} = \left[\mathrm{T}_C\right] I_{abc} \tag{5-14}$$

Now, the inverse of T_C, T_C^{-1}, is given by:

$$\mathrm{T}_C^{-1} = \sqrt{\frac{2}{3}} \begin{bmatrix} 1 & 0 & 1 \\ -\frac{1}{2} & \frac{\sqrt{3}}{2} & 1 \\ -\frac{1}{2} & -\frac{\sqrt{3}}{2} & 1 \end{bmatrix} \tag{5-15}$$

From which it follows that:

$$I_{abc} = \left[\mathrm{T}_c^{-1}\right] I_{dq0} \tag{5-16}$$

Some comments about the derivation of the $abc \rightarrow dq0$ transformation are appropriate at this point. First, is the general assumption of the existence of vectors in the derivation. The use of vectors implies that the quantities represented are in the steady state, something that is certainly possible but

not really the intent of using the transformation for work with instantaneous power. When used for instantaneous power the values of the abc system are not *a priori* known to be part of a system of sinusoidal functions; further, the normal inputs to the transformation is an instantaneous value, not a value as determined from a frequency-domain quantity.

Second, and more important, is the fact that the method of the derivation assumes that the angles between the vectors are fixed at 120°. In the general case, even with sinusoidal functions, this cannot be guaranteed to be true. In the general case the $abc \rightarrow dq0$ transformation losses information in that the overall number of degrees of freedom in the abc system is greater than that of the *dq0* system.

5.2 – Degrees of freedom

A vector is a line segment in *n*-space that is completely defined by the coordinates in that space of the end points, or by any two independent variables that can be translated by mathematical operations into the coordinates of the end points of the line segment. [53] As line segment is completely defined by two points, a vector is said to have two degrees of freedom. As defined, a vector is free-floating, that is, it does not have any fixed relationship to the base coordinate of the space within which it is located. Fixing the vector by relating one end to a defined point in the defining space does not alter the number of degrees of freedom. A common way of defining a vector in *xy*-space, a subset of *n*-space, is shown in Fig. 5.1. Any two of the variables shown in the figure can be used to define the vector. Since any of the variables can be referenced to particular points in *xy*-space there are an infinite number of ways to derive the two the pieces of information necessary to define the two degrees of freedom.

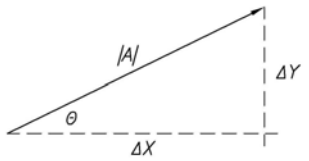

Fig. 5.1 Generalized vector in 2-space

Vector notation is commonly used to represent steady state electrical quantities. [26] In the case of a three phase electrical system, there are three vectors, one for each phase; it follows from the above discussion that such a system, composed of three unrelated vectors, has six degrees of freedom. Joining the vectors at a common point does not change the number of degrees of freedom as each

vector still has an independent magnitude and direction or some equivalent representation. Such a system of three vectors is shown in Fig. 5.2.

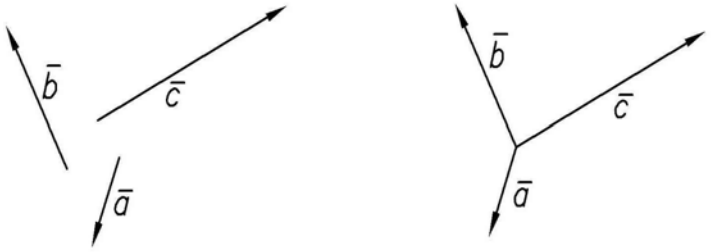

Fig. 5.2 Three vectors in 2-space

5.3 – Loss of degrees of freedom

The vectors presented in Fig. 5.2 are unrelated, one to the other. Obviously, if these vectors are used to represent some quantity, *e.g.*, a set of three-phase voltages, a relationship exists, or *may* exist, between the represented quantities but no relationship among the vectors themselves is implied; the number of degrees of freedom remains at six.

The system can be constrained in various ways to reduce the number of degrees of freedom. Consider the case where the set of three vectors is constrained such that the vector sum of all three vectors must be zero. Under this restriction, if two of the vectors are known, the third is pre-determined. The number of degrees of freedom has been reduced by two. Such a case is shown in Fig. 5.3 below, where vectors $\overrightarrow{ca}$ and $\overrightarrow{ab}$ are known; vector $\overrightarrow{bc}$ can be determined with no additional information.

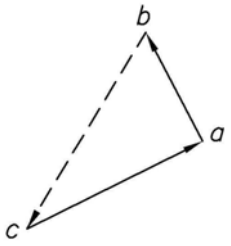

Fig. 5.3 Constrained set of vectors: $\overrightarrow{bc} = \overrightarrow{ca} + \overrightarrow{ab}$

A three-phase system constrained so that the vector sum is zero has four degrees of freedom. The number of degrees of freedom can be further reduced if the additional requirement is made that the angles between the vectors is equal. Such a system is shown in Fig. 5.4, presented in both a closed configuration and as a system with a common point, a so-called "wye" configuration.

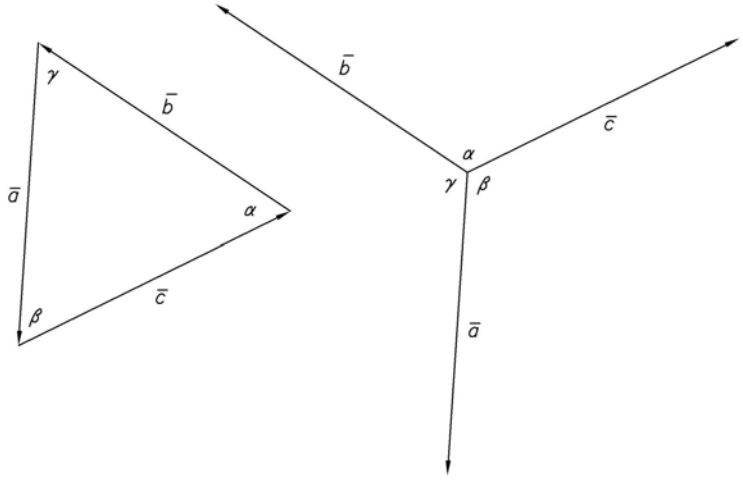

Fig. 5.4 Constrained set of vectors with two degrees of freedom

The additional constraint of equal angles has also forced a change in the length of the vectors as, in accordance with the *Law of Sines*, the system must obey (5-17).

$$\frac{|\bar{a}|}{\sin\alpha} = \frac{|\bar{b}|}{\sin\beta} = \frac{|\bar{c}|}{\sin\gamma} \tag{5-17}$$

A system thus constrained has two remaining degrees of freedom, which are typically expressed as a magnitude of the vector set and an angle that the vector set has been rotated around some arbitrary reference. When used to express three-phase electrical system quantities, such a set is known as a balanced 3-phase system.

Consider a set of three independent vectors of different magnitudes that are separated in space by equal angles; a set of vectors meeting these conditions is shown in Fig. 5.5. As shown, the set can be configured in a 'wye' arrangement as before, but when arranged head-to-tail the three vectors do not sum to zero; the difference in the closure is $\bar{\varepsilon}$. The initial set of three unconstrained

vectors had a total of six degrees of freedom. By constraining all angles to be equal the degree of freedom of the set is reduced by two, leaving a set with four degrees of freedom.

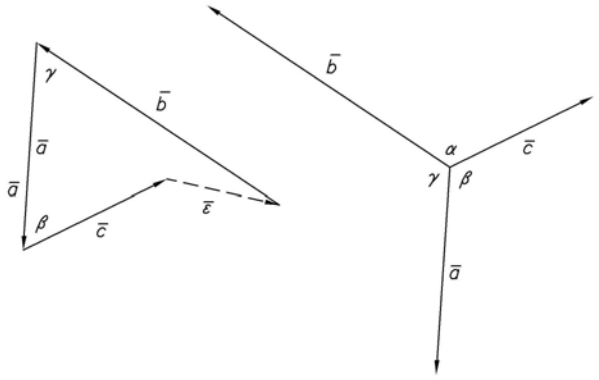

Fig. 5.5 Constrained set of vectors with four degrees of freedom

There are two major points relate to the above that directly apply to the work at hand, *viz.*, the $abc \rightarrow dq0$ transformation and the related inverse transformation, $dq0 \rightarrow abc$:

- When starting with an unconstrained, unbalanced, three-phase system, the $abc \rightarrow dq0$ transformation reduces the number of degrees of freedom from six (6) to three (3).
- When starting with an unconstrained, unbalanced, three-phase system, the $abc \rightarrow dq$ transformation reduces the number of degrees of freedom from six (6) to two (2).
- When starting with a constrained, balanced, three-phase system, the $abc \rightarrow dq$ transformation does not cause loss of degrees of freedom.
- Once a degree of freedom has been lost, it cannot be recovered by any mathematical operation or combination of operations. The information, such as it may be, contained in a lost degree of freedom cannot be used for any form of system manipulation or control.

The loss of degrees of freedom and the mapping of one variable space onto another is well understood mathematically, especially in the understanding of under and over-constrained mechanical systems. [54] It is the implications of the mapping that is important in the present work, especially as it relates to the use of a truncated space as a part of an EAF compensation scheme.

5.4 – The significance of a loss of degree of freedom

It is logical to extend Instantaneous Power Theory [31] into the problem of compensation of EAFs. The load presented to an electrical system from an EAF is essentially a non-linear load, and has many of the same characteristics demonstrated by loads driven by electronic control systems, *e.g.*, variable speed motor drives, with the added complexity of phase-to-phase independence, and stochastic current values, cycle-to-cycle. [5] A number of published works dating from the mid-1980s, beginning with [55], advocate the use of a compensation scheme that converts voltages and currents in *abc* format to *dq* format, perform power calculations, makes various adjustments to the power, determines the resulting voltages and currents, and then converts the voltages and currents back to *abc* format for injection into the system. Compensation schemes using this approach work well when the three phase waveforms are reasonably balanced, but fail when there are large phase-to-phase variations.

The reason for the problem with the above approach is that the $abc \rightarrow dq$ transformation is not symmetric, *i.e.*, the conversion is one-to-one when going from *abc* format to the *dq* format but there can be many points in the *dq* plane that map to the same points in the *abc* frame when the reversing transformation is made. This can be easily shown by creating an arbitrary unbalanced waveform set and then performing the transformation and a reversing transformation on these data. This has been done for demonstration purposes below.

Consider the following three phase current waveform set as could be obtained from a 4-wire system. All values are arbitrarily chosen for the purpose of demonstration.

$$\begin{aligned} I_a &= 5\sqrt{2}\sin(377t) \\ I_b &= 4\sqrt{2}\sin(377t - \frac{3\pi}{2}) \\ I_c &= 6\sqrt{2}\sin(377t + \frac{3\pi}{2}) \end{aligned} \tag{5-18}$$

The waveforms are transformed to the *dq* plane by the following transformation:

$$T_{2C} = \sqrt{\frac{2}{3}}\begin{bmatrix} 1 & -\frac{1}{2} & -\frac{1}{2} \\ 0 & \frac{\sqrt{3}}{2} & \frac{\sqrt{3}}{2} \end{bmatrix} \tag{5-19}$$

And then re-transformed to the *abc* reference frame by a reversing transformation:

$$T_{2CI} = \sqrt{\frac{2}{3}} \begin{bmatrix} 1 & 0 \\ -\frac{1}{2} & \frac{\sqrt{3}}{2} \\ -\frac{1}{2} & -\frac{\sqrt{3}}{2} \end{bmatrix} \tag{5-20}$$

One full cycle of each of the equations that results from this series of transformations is shown in Fig. 5.6. This plot graphically indicates the error introduced by using a $abc \leftrightarrow dq$ transformation in a situation where there is phase-to-phase unbalance in the system waveforms; refer to Appendix B for a listing of the software used to generate the plot. It is obvious that if the fidelity of the transformations cannot be guaranteed, any compensation scheme that uses these transformations cannot be expected to provide a high-level of performance. It has been previously shown that the waveforms produced by an operating EAF show large phase-to-phase variations, *inter alia*; the conclusion to be drawn is that compensation schemes using $abc \leftrightarrow dq$ transformations are not ideally suited for EAF compensation.

The apparent failure of the $abc \leftrightarrow dq$ transformations to maintain fidelity begs the question of how this method would fare if the neutral were to be considered in the transformation, *i.e.*, if the more complete $abc \leftrightarrow dq0$ transformation were to be used. The answer is that this transformation and the retransformation is complete and is fully reversible. Mathematically, the operations are both "one-to-one" and "onto". The problem as presented above does not exist and the results of the transformation and retransformation would yield waveforms that exactly matched each other. However, there is still a problem, albeit it more subtle.

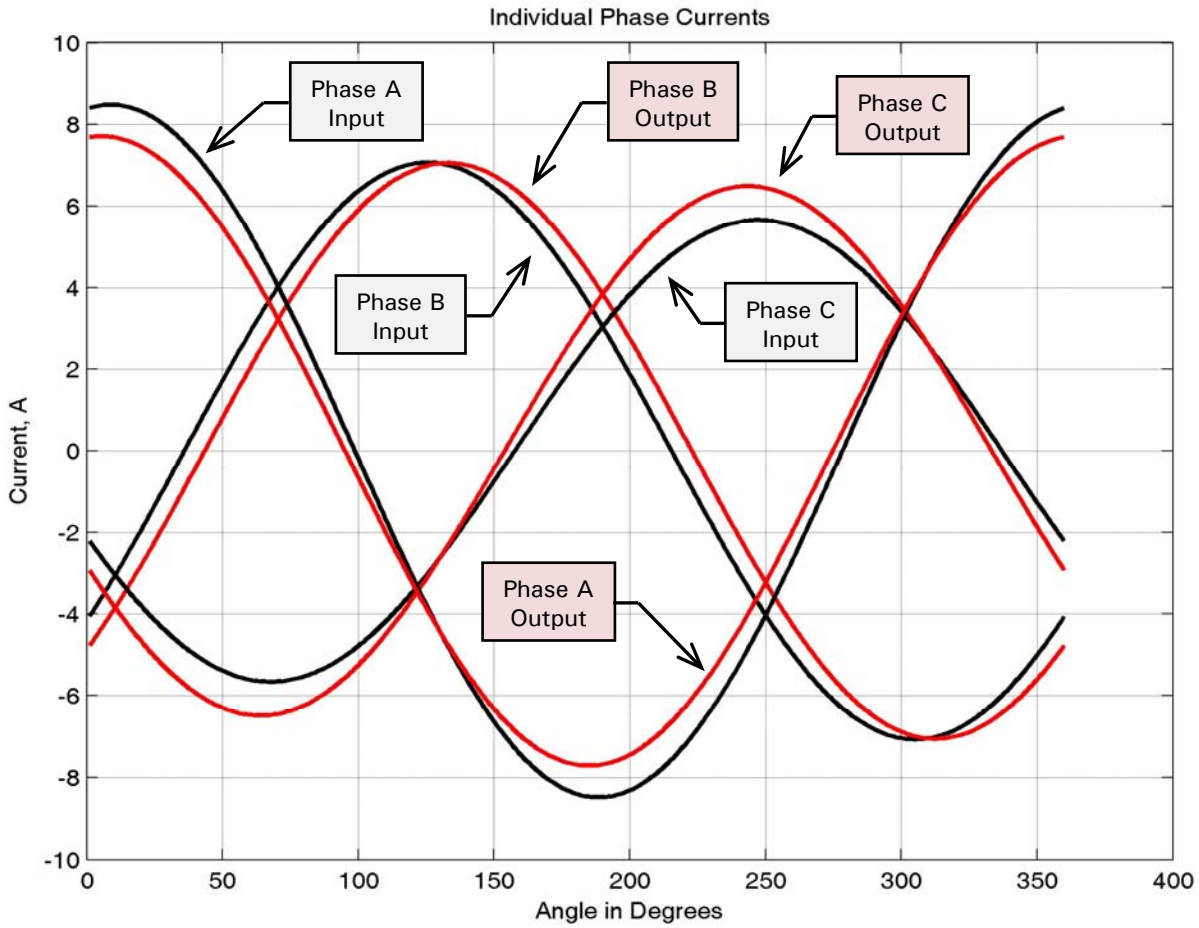

Fig. 5.6 $abc \leftrightarrow dq$ comparative waveforms

With the $abc \leftrightarrow dq$ transformation where the phases are balanced the angles between the source vectors are identical. When the transformation is expanded to allow for a 4-wire system, the same general assumption is made but the angles are no longer constrained by the topology of the system. This fact is not immediately obvious but leads to error in the transformation and retransformation.

Consider an illustrative example as presented in left-hand side of Fig. 5.7, where the phases are unbalanced but the angles are all equal, at 120° each. Using the complete $abc \rightarrow dq0$ transformation, (5-21), on the points that are represent these vectors at the point that $I1_a = 0$, gives the instantaneous vector shown as in (5-22).

$$T_C = \sqrt{\frac{2}{3}} \begin{bmatrix} 1 & -\frac{1}{2} & -\frac{1}{2} \\ 0 & \frac{\sqrt{3}}{2} & -\frac{\sqrt{3}}{2} \\ \frac{1}{\sqrt{2}} & \frac{1}{\sqrt{2}} & \frac{1}{\sqrt{2}} \end{bmatrix} \tag{5-21}$$

$$I1_{dq0} = \begin{bmatrix} -1.0000 \\ -8.6603 \\ 1.4142 \end{bmatrix} \tag{5-22}$$

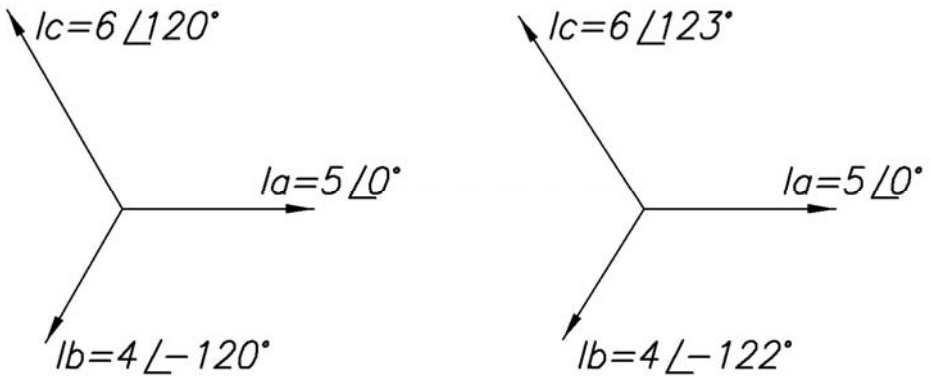

Fig. 5.7 Unbalanced 3-phase currents, equal angles (left) and unequal angles (right)

For the comparison, the phase B vector is shifted 2° in a clockwise direction and the Phase C vector is shifted 3° in a counterclockwise direction. The vector arrangement of this configuration is shown as the right-hand side of Fig. 5.7. For comparative purposes the complete waveforms of Phase C in time domain are shown in Fig. 5.8. The main purpose for presenting this particular representation is to make it clear that a shift of 3° is a relatively minor shift that could easily go unnoticed on a typical visual display instrument.

The results of performing the $abc \rightarrow dq0$ transformation to the shifted waveform, at the same point, *viz.*, the point where $I2_a = 0$, gives the following instantaneous vector:

$$I2_{dq0} = \begin{bmatrix} -0.9468 \\ -8.4242 \\ 1.3389 \end{bmatrix} \tag{5-23}$$

Under the assumption that the original, un-shifted values as shown in (5-22) are the "correct" values, the following percentages of error can be computed.

$$\begin{aligned} \varepsilon_D &= 5.32\% \\ \varepsilon_Q &= 2.73\% \\ \varepsilon_0 &= 5.32\% \\ \varepsilon_{NORM} &= 2.82\% \end{aligned} \tag{5-24}$$

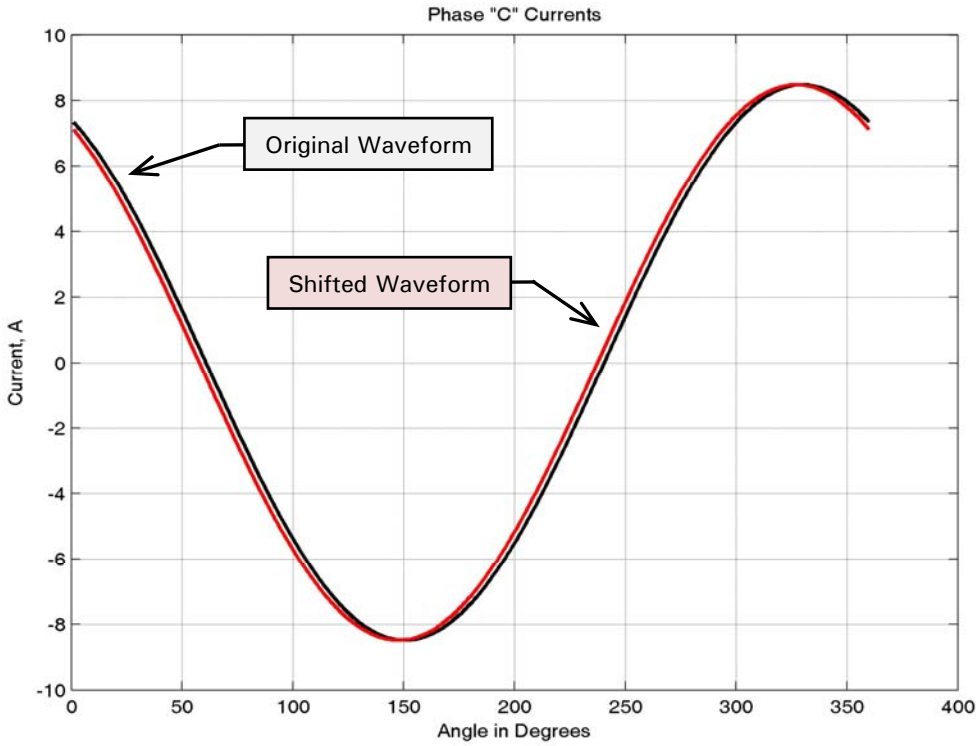

Fig. 5.8 Sinusoidal waveform shifted by 3°

While these appear to be relatively nominal values, it must be remembered that these errors are based on an sinusoidal waveforms where the only differences in the actual values and the values as determined by the methods of [31] are caused by the angle differences. When the actual waveforms are not sinusoidal the differences become more striking. Fig. 5.9 below shows the voltage waveform at the Point of Common Coupling (PCC) of an operating EAF, part of the data gathered during the site visits conducted to the EAF facility. The waveforms, presented for comparison purposes, are in black, the actual phase voltage data at the PCC and, in red, the waveform that results from transforming the original data to the *dq* domain and then re-transforming it back to the *abc* domain. For the voltage waveform the difference in not remarkable; the black, original data waveform is plotted with a wide pen width and the red transformed waveform is plotted with a narrower pen width. This visual presentation technique allows differences in the waveforms to be very obvious. Although it is noted that a close zoom-in will reveal minor differences in the two waveforms, the overall differences are small and are not worthy of further consideration. The current waveform is significantly different.

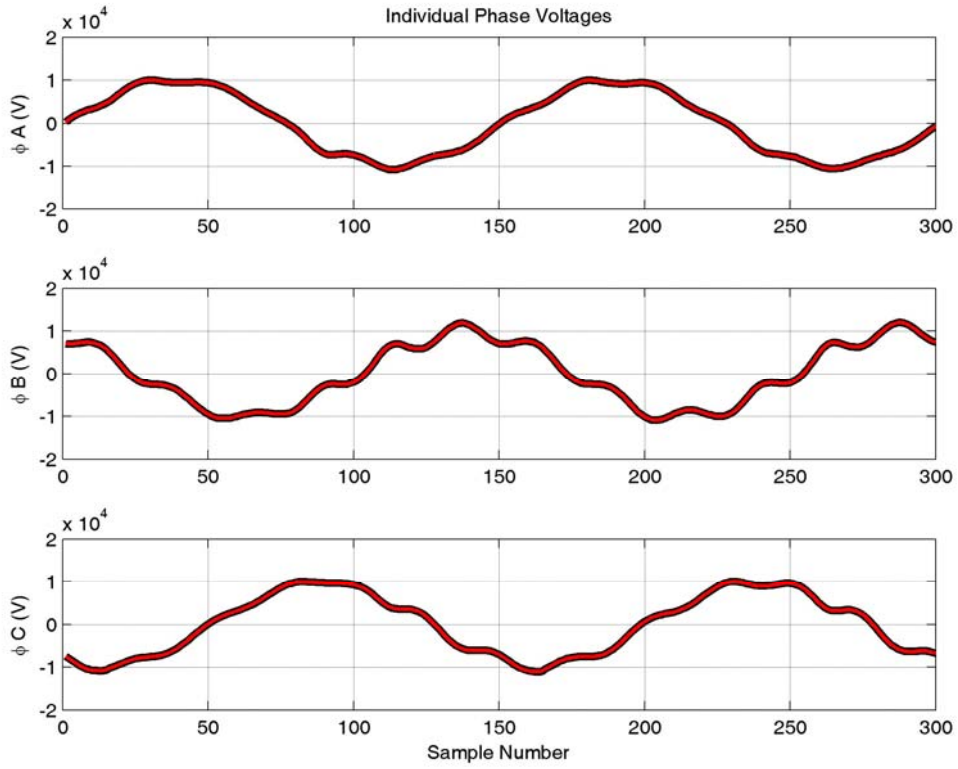

Fig. 5.9 EAF voltage comparison: original data *vs.* transformed data

Fig. 5.10 shows the current waveforms for the same load, again presented with the black waveform being the original data and the red being the transformed/retransformed data. The two waveforms are significantly different, in all three phases. The differences in the waveforms under these conditions are expected due to the amount of unbalance in the individual phase currents and the fact that the *dq* method does not deal with unbalance currents; further, EAF compensation schemes that use *dq* method also have no mechanism to adequately deal with unbalance currents and tacitly assume that the currents for all phases are balanced, an assumption that is rooted in the *dq* method itself.

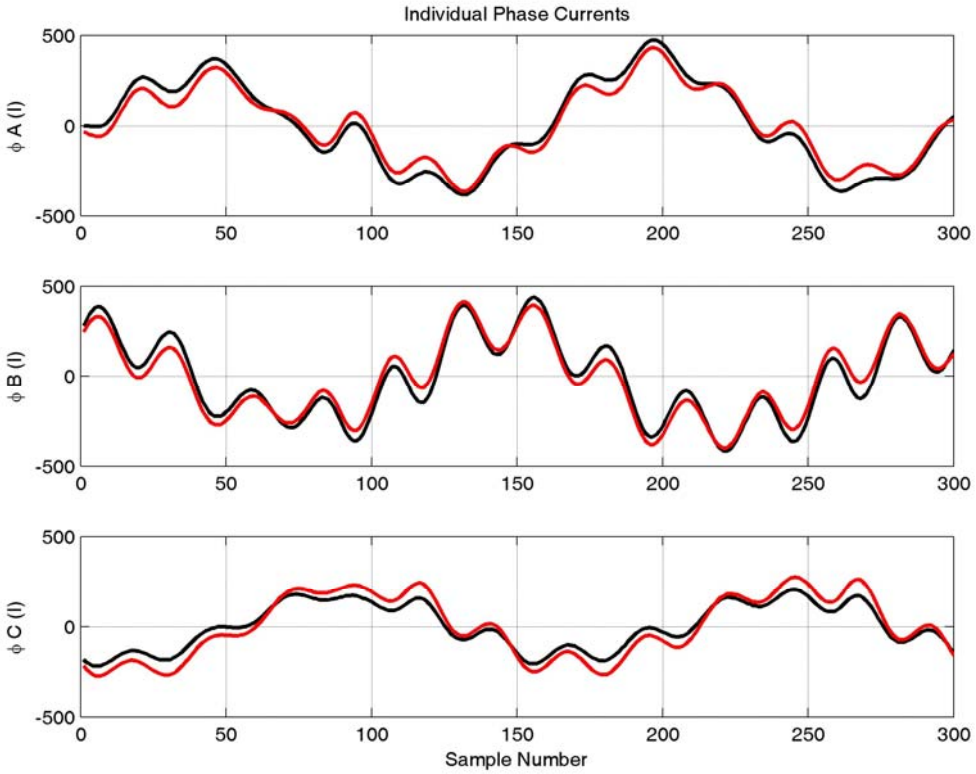

Fig. 5.10 EAF current comparison: original data *vs.* transformed data

It is obvious from the current plots that the differences are significant and that if the calculation method assumes sinusoidal waveforms, especially for voltage, and the waveforms vary significantly from the assumption, the calculations resulting from these assumptions will be in error. As an aside, it is noted that the point at which the waveforms deviate from the sinusoidal ideal are the

precise point where it is necessary to apply compensation to achieve a particular outcome. Refer to Appendix C for a listing of the software used to generate Figs. 5.9 and 5.10.

6 – Instantaneous power in the *abc* reference frame

6.1 – Introduction

The "normal" way that an electrical system is defined is based on the *abc* system, where each of the system phases is represented in time domain on a common horizontal axis that has units of time, or units that can be converted into time. The values that appear on the vertical axis are voltages, currents, powers, or some unit that is the result of the manipulation of these basic quantities. The single item of significance about the *abc* system is that the only information that is available about the system is the actual measured values at a particular instant of time. All other information about the system is based upon assumptions about the waveforms, *e.g.*, that they are sinusoidal, that they have a certain frequency content, that they are periodic, *etc*. It is when these assumptions do not match the actual conditions that the calculations made based upon the assumptions fail to match the reality of the situation.

The following development makes no *a priori* assumptions on the waveforms that comprise the *abc* system. The only constraints on the waveforms are those imposed by the physical connections of the components. A generalized connection of such a system, shown as a wye system to remove voltage constraints, is presented below in Fig. 6.1.

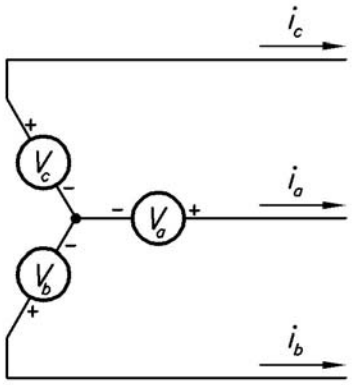

Fig. 6.1 Wye connected system without neutral connection

6.2 – Development of 3-phase, 3-wire equations

Consider a three phase electrical system similar to the system shown above in Fig. 6.1, except that we are no longer considering this system to be sinusoidal, balanced, or to have any fixed relationship between the voltages and currents that appear on the individual phases. The only constraints that we are presently placing on the system is that the voltage and currents be some differentiable function, $V(v_a, v_b, v_c): R^3 \to R$ and $I(i_a, i_b, i_c): R^3 \to R$.

We will be looking at the individual phase voltages and currents at some instant of time with the goal of determining the instantaneous magnitude of the portion of the current that contributes to the delivery of real power and that portion of the current that contributes to reactive power; the presentation that follows is conceptually described in [31]. Again, for technical completeness, it is noted that the usual way 'real' and 'reactive' power are defined is based entirely on a sinusoidal system. As those constraints do not apply to the present situation it should be expected that the meaning of the terms will turn out to be somewhat different. In order to avoid any confusion of terms the expressions 'active power' and 'passive power' will be used.

As a first step, partition the line currents into two parts, one that will represent the portion of the total current that contributes to active power with the remainder contributing to passive; the currents are taken to be magnitudes measured at a particular instant in time, so the addition is arithmetic. Over all three phases the current expression is the following:

$$\begin{bmatrix} i_a \\ i_b \\ i_c \end{bmatrix} = \begin{bmatrix} i_{Aa} + i_{Pa} \\ i_{Ab} + i_{Pb} \\ i_{Ac} + i_{Pc} \end{bmatrix}. \tag{6-1}$$

With regard to the partitioning of the currents into two parts, and the resultant definitions of power, it is noted that the terms 'active power' and 'passive power' are arbitrary to the extent that they do not (in general) correspond to the definitions of the FBD method previously presented. The major difference in the definitions between FBD and the present case is that the FBD begins with the assumption that the active current and non-active current – the two terms used in the FBD presentation – are orthogonal one to the other. This is a perfectly valid assumption when the functions involved are sinusoidal but the concept has no strict meaning when applied to the stochastic waveforms that result from EAF operation.

The goal of the present exercise is to determine the particular values of the components of the line currents as shown in (6-1) such that active currents, i_{Aa}, i_{Ab} and i_{Ac}, are minimized while at the same time guaranteeing that the passive currents, i_{Pa}, i_{Pb} and i_{Pc} do not contribute to the active power over the three phases. Symbolically, this minimization can be described as:

Minimize:

$$\mathcal{J}(i_{Pa}, i_{Pb}, i_{Pc}) = (i_a - i_{Pa})^2 + (i_b - i_{Pb})^2 + (i_c - i_{Pc})^2 \tag{6-2}$$

Subject to:

$$\mathcal{C}(i_{Pa}, i_{Pb}, i_{Pc}) = v_a i_{Pa} + v_b i_{Pb} + v_c i_{Pc} = 0. \tag{6-3}$$

To solve this set, a LaGrange multiplier, λ, will be introduced [56] and the current and constraint equations re-written as:

$$F(i_{Pa}, i_{Pb}, i_{Pc}, \lambda) = (i_a - i_{Pa})^2 + (i_b - i_{Pb})^2 + (i_c - i_{Pc})^2 + \lambda(v_a i_{Pa} + v_b i_{Pb} + v_c i_{Pc}). \tag{6-4}$$

Note that the introduction of the LaGrange multiplier does not change the overall relationship of (6-2) as the value of the constraining function is zero. The object now becomes to determine λ such that

$$\nabla F(i_{Pa}, i_{Pb}, i_{Pc}, \lambda) = 0. \tag{6-5}$$

Evaluating each of the four partial derivatives of *F* in turn gives the following equations:

$$\begin{aligned}
\frac{\partial F}{\partial i_{Pa}} &= -2(i_a - i_{Pa}) + \lambda v_a = 0 \\
\frac{\partial F}{\partial i_{Pb}} &= -2(i_b - i_{Pb}) + \lambda v_b = 0 \\
\frac{\partial F}{\partial i_{Pc}} &= -2(i_c - i_{Pc}) + \lambda v_c = 0 \\
\frac{\partial F}{\partial \lambda} &= v_a i_{Pa} + v_b i_{Pb} + v_c i_{Pc} = 0.
\end{aligned} \tag{6-6}$$

Using a matrix format gives:

$$\begin{bmatrix} 2 & 0 & 0 & v_a \\ 0 & 2 & 0 & v_b \\ 0 & 0 & 2 & v_c \\ v_a & v_b & v_c & 0 \end{bmatrix} \begin{bmatrix} i_{Pa} \\ i_{Pb} \\ i_{Pc} \\ \lambda \end{bmatrix} = \begin{bmatrix} 2i_a \\ 2i_b \\ 2i_c \\ 0 \end{bmatrix}. \tag{6-7}$$

Solving this set for λ gives:

$$\lambda = \frac{2(v_a i_a + v_b i_b + v_c i_c)}{v_a^2 + v_b^2 + v_c^2} \tag{6-8}$$

from which the passive currents can be directly determined as:

$$\begin{bmatrix} i_{Pa} \\ i_{Pb} \\ i_{Pc} \end{bmatrix} = \begin{bmatrix} i_a \\ i_b \\ i_c \end{bmatrix} - \frac{(v_a i_a + v_b i_b + v_c i_c)}{v_a^2 + v_b^2 + v_c^2} \begin{bmatrix} v_a \\ v_b \\ v_c \end{bmatrix} \tag{6-9}$$

with the active currents being:

$$\begin{bmatrix} i_{Aa} \\ i_{Ab} \\ i_{Ac} \end{bmatrix} = \frac{(v_a i_a + v_b i_b + v_c i_c)}{v_a^2 + v_b^2 + v_c^2} \begin{bmatrix} v_a \\ v_b \\ v_c \end{bmatrix}. \tag{6-10}$$

Although our initial assumptions assumed no mathematical constraints on the voltages and currents, there are the physical constraints imposed on the circuit arrangement by Kirchhoff's Laws: For a delta-connected circuit the phase voltages $v_a, v_b,$ and v_c must sum to zero as must the phase currents $i_a, i_b,$ and i_c.

6.3 – Evaluation of 3-phase, 3-wire equations

For the expressions developed above to be useful for non-sinusoidal and non-periodic conditions they also must be valid for the well-known sinusoidal case. For a demonstration of the sinusoidal case an arbitrary single-phase set of values is selected and the waveforms generated by the classic approach, as defined by elementary AC theory texts, *e.g.* [57], compared to the waveforms that would result from application of equations (6-9) and (6-10).

Consider the following time-domain expressions for voltage and current:

$$\begin{aligned} V_a(t) &= V_{aRMS}\sqrt{2}\cos(\omega t) \\ I_a(t) &= I_{aRMS}\sqrt{2}\cos(\omega t + \phi). \end{aligned} \tag{6-11}$$

Power, in time-domain, is the product of the voltage and current,

$$P_a(t) = V_a(t)\,I_a(t) = 2V_{aRMS}I_{aRMS}\cos(\omega t)\cos(\omega t + \phi). \tag{6-12}$$

It is noted that equation (6-12) can be partitioned by the use of a trigonometric identity for the product of two sine functions,

$$\sin(\alpha)\sin(\beta) \equiv \tfrac{1}{2}\cos(\alpha - \beta) - \tfrac{1}{2}\cos(\alpha + \beta)$$

into

$$P_a(t) = V_{aRMS} I_{aRMS} \cos(\phi) + V_{aRMS} I_{aRMS} \cos(2\omega t + \phi). \quad (6\text{-}13)$$

Equation (6-13) is technically accurate, but the interpretation of the two parts does not match the way we usually think about single-phase power. The equation implies that there is a constant power that is always positive when $-\frac{\pi}{2} \le \phi \le \frac{\pi}{2}$. We know that power is in fact *not* constant in this situation, as can be easily demonstrated with a low frequency generator, an inductor, and a test lamp.

Fig. 6.2 shows, *inter alia*, a demonstration plot of equations (6-12) and the two component parts of this total as described by equations (6-9) and (6-10). For this demonstration, arbitrary values have for voltage, current, and current phase shift have been selected as:

$$V_{aRMS} = 12 \text{ Volts}$$
$$I_{aRMS} = 5 \text{ Amperes}$$
$$\phi = 35°.$$

The voltage, current, and the components of the partitioned equation are identified.

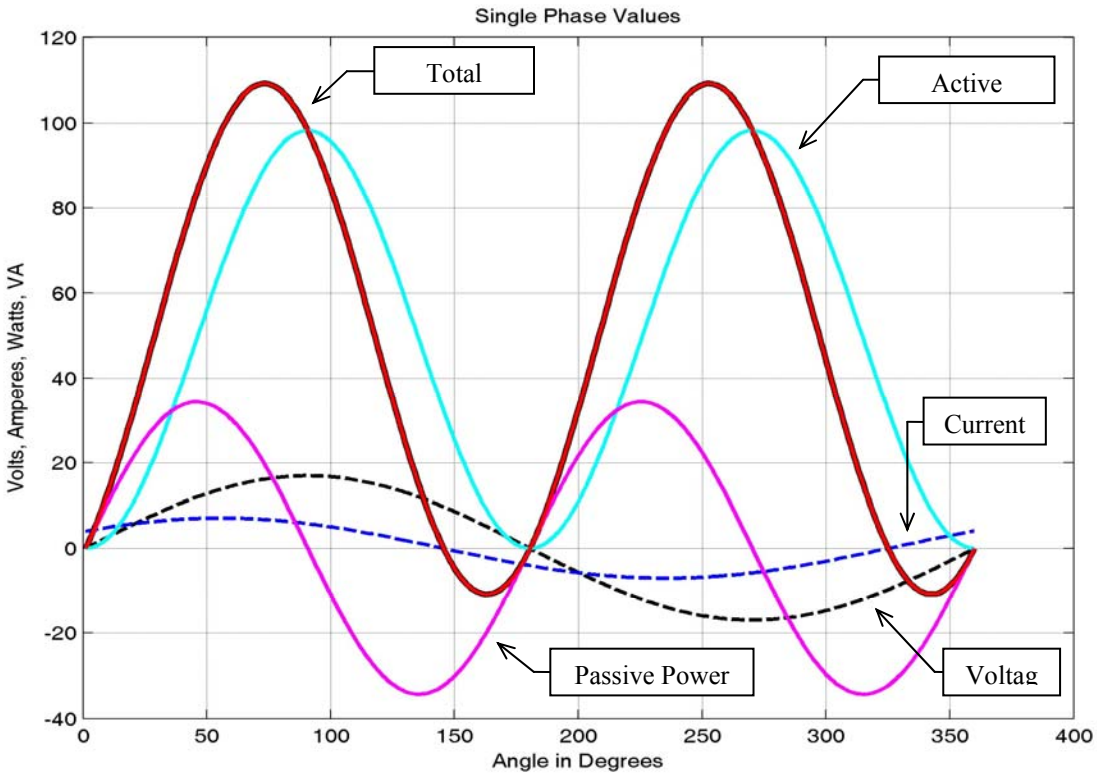

Fig. 6.2 Single phase power components

The demonstration associated with Fig. 6.2 involves two independent calculations for the Total Power. One calculation is based on direct plot of equation (6-12) for the particular values selected for the demonstration; this trace is drawn with a wide black pen. A separate calculation of active and passive power that is based on equations (6-9) and (6-10) is also provided, the values being calculated as follows:

$$\begin{aligned} P_{active} &= i_{Aa} v_a \\ P_{passive} &= i_{Pa} v_a . \end{aligned} \tag{6-14}$$

The Total Power, $P_{active} + P_{passive}$, is again presented, this time with the trace in red. It is observed that the values computed based on instantaneous values evaluated in (6-14) are identical to the corresponding values as previously described. In order to present this information clearly, one of the plots is plotted with a wide pen in black; the equivalent plot is shown in red with a narrower pen with so that any differences will be easily observable. It should be obvious that in a 3-phase evaluation where the individual powers are as determined above, the total power is the sum of the three phase powers.

The above demonstration was created with an arbitrary set of single phase values. In the sequel it will be demonstrated that the same relationships are valid for a completely random set of data as captured from an operating EAF.

6.4 – Development of 3-phase, 4-wire equations

The work presented in [31] is based on a 3-phase, 3-wire system and thus omits the neutral current and the neutral voltage with respect to ground; this work is expanded by the following presentation.

As we are considering the most general case possible, it would be well to modify the system to account for a system neutral; such a system is shown in Fig. 6.3. There are two possible approaches.

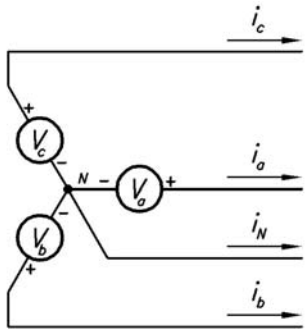

Fig. 6.3 Wye connected system with neutral connection

One approach would be to define the neutral voltage with respect to ground in terms of the phase voltages and then, similarly, define the neutral current in terms of the individual phase currents. That approach would have the effect of allowing the circuit to be unbalanced in terms of either voltages and/or currents but it would also conceal the neutral values within the computations.

A second approach simply defines the neutral components in a similar way to the phase components and relies on the circuit configuration to (perhaps) force the total of the voltages and the total of the currents to zero. The second approach has the advantage of providing a value of instantaneous neutral active and passive currents that would be lost with the first option. In the sequel it will be seen that the availability of neutral values is useful in the compensation scheme.

As before, the line currents will be partitioned into two parts, one that will represent the portion that contributes to real power and one that contributes to reactive power. Over the three phases and neutral the current expression is the following:

$$\begin{bmatrix} i_a \\ i_b \\ i_c \\ i_n \end{bmatrix} = \begin{bmatrix} i_{Aa} + i_{Pa} \\ i_{Ab} + i_{Pb} \\ i_{Ac} + i_{Pc} \\ i_{An} + i_{Pn} \end{bmatrix}. \tag{6-15}$$

The goal of the exercise now becomes the determination of the particular values of the components of the line and neutral currents as shown in (6-15) such that active currents, i_{Aa}, i_{Ab}, i_{Ac} and i_{An}, are minimized while at the same time guaranteeing that the passive currents, i_{Pa}, i_{Pb}, i_{Pc} and i_{Pn} do not contribute to the passive power over the three phases and neutral. Symbolically, this minimization can be described as:

Minimize:

$$\mathcal{J}(i_{Pa}, i_{Pb}, i_{Pc}, i_{Pn}) = (i_a - i_{Pa})^2 + (i_b - i_{Pb})^2 + (i_c - i_{Pc})^2 + (i_n - i_{Pn})^2 \tag{6-16}$$

subject to:

$$\mathcal{C}(i_{Pa}, i_{Pb}, i_{Pc}, i_{Pn}) = v_a i_{Pa} + v_b i_{Pb} + v_c i_{Pc} + v_n i_{Pn} = 0. \tag{6-17}$$

To solve this set, again a LaGrange multiplier, λ, will be introduced. Again, note that the value of the constraining function (6-17) is zero, so the addition of the product of this term and the LaGrange multiplier does not change the overall value of the function to be minimized.

The current and constraint equations are re-written as:

$$\begin{aligned} &F(i_{Pa}, i_{Pb}, i_{Pc}, i_{Pn}, \lambda) = \\ &(i_a - i_{Pa})^2 + (i_b - i_{Pb})^2 + (i_c - i_{Pc})^2 + (i_n - i_{Pn})^2 + \lambda(v_a i_{Pa} + v_b i_{Pb} + v_c i_{Pc} + v_n i_{Pn}). \end{aligned} \tag{6-18}$$

The object now becomes to determine λ such that

$$\nabla F(i_{Pa}, i_{Pb}, i_{Pc}, i_{Pn}, \lambda) = 0. \tag{6-19}$$

Evaluating each of the four partial derivatives of F in turn gives the following equations:

$$\begin{aligned} \frac{\partial F}{\partial i_{Pa}} &= -2(i_a - i_{Pa}) + \lambda v_a = 0 \\ \frac{\partial F}{\partial i_{Pb}} &= -2(i_b - i_{Pb}) + \lambda v_b = 0 \\ \frac{\partial F}{\partial i_{Pc}} &= -2(i_c - i_{Pc}) + \lambda v_c = 0 \\ \frac{\partial F}{\partial i_{Pn}} &= -2(i_n - i_{Pn}) + \lambda v_n = 0 \\ \frac{\partial F}{\partial \lambda} &= v_a i_{Pa} + v_b i_{Pb} + v_c i_{Pc} + v_n i_{Pn} = 0. \end{aligned} \tag{6-20}$$

Using a matrix format gives:

$$\begin{bmatrix} 2 & 0 & 0 & 0 & v_a \\ 0 & 2 & 0 & 0 & v_b \\ 0 & 0 & 2 & 0 & v_c \\ 0 & 0 & 0 & 2 & v_n \\ v_a & v_b & v_c & v_n & 0 \end{bmatrix} \begin{bmatrix} i_{Pa} \\ i_{Pb} \\ i_{Pc} \\ i_{Pn} \\ \lambda \end{bmatrix} = \begin{bmatrix} 2i_a \\ 2i_b \\ 2i_c \\ 2i_n \\ 0 \end{bmatrix}. \tag{6-21}$$

Solving this set for λ gives:

$$\lambda = \frac{2(v_a i_a + v_b i_b + v_c i_c + v_n i_n)}{v_a^2 + v_b^2 + v_c^2 + v_n^2} \tag{6-22}$$

from which the reactive currents can be directly determined as:

$$\begin{bmatrix} i_{Pa} \\ i_{Pb} \\ i_{Pc} \\ i_{Pn} \end{bmatrix} = \begin{bmatrix} i_a \\ i_b \\ i_c \\ i_n \end{bmatrix} - \frac{(v_a i_a + v_b i_b + v_c i_c + v_n i_n)}{v_a^2 + v_b^2 + v_c^2 + v_n^2} \begin{bmatrix} v_a \\ v_b \\ v_c \\ v_n \end{bmatrix} \tag{6-23}$$

with the real currents being:

$$\begin{bmatrix} i_{Aa} \\ i_{Ab} \\ i_{Ac} \\ i_{An} \end{bmatrix} = \frac{(v_a i_a + v_b i_b + v_c i_c + v_n i_n)}{v_a^2 + v_b^2 + v_c^2 + v_n^2} \begin{bmatrix} v_a \\ v_b \\ v_c \\ v_n \end{bmatrix}. \tag{6-24}$$

Again, our initial assumptions placed no mathematical constraints on the voltages and currents but physical constraints can be imposed on the circuit arrangement by Kirchhoff's Laws. In particular, note the total of the three phase currents and the neutral current must sum to zero.

6.5 – Evaluation of 3-phase, 4-wire equations

Similar to the approach taken for the single phase case, a demonstration of a 3-phase situation is now considered. In order to fully display the capabilities of the method a set of arbitrary sinusoidal waveforms is selected. Except for the phase shift of the "*a*" phase voltage waveform, which is selected to be zero as a reference, all other values are completely arbitrary.

Consider the following time-domain expressions for voltage and current:

$$
\begin{aligned}
V_a(t) &= V_{aRMS}\sqrt{2}\cos(\omega t + \alpha_a) \\
V_b(t) &= V_{bRMS}\sqrt{2}\cos(\omega t + \alpha_b) \\
V_c(t) &= V_{cRMS}\sqrt{2}\cos(\omega t + \alpha_c)
\end{aligned}
\tag{6-25}
$$

$$
\begin{aligned}
I_a(t) &= I_{aRMS}\sqrt{2}\cos(\omega t + \beta_a + \phi_a) \\
I_b(t) &= I_{bRMS}\sqrt{2}\cos(\omega t + \beta_b + \phi_b) \\
I_c(t) &= I_{cRMS}\sqrt{2}\cos(\omega t + \beta_c + \phi_c).
\end{aligned}
$$

where the values of the parameters are as follow:

$$
\begin{array}{lllll}
V_{aRMS} = 12 & \alpha_a = 0 & I_{aRMS} = 5 & \beta_a = 4° & \phi_a = -35° \\
V_{bRMS} = 15 & \alpha_b = -115° & I_{bRMS} = 4 & \beta_b = -122° & \phi_b = -35° \\
V_{cRMS} = 10 & \alpha_c = 121° & I_{cRMS} = 6 & \beta_c = 112° & \phi_c = -35°.
\end{array}
$$

Note that although the value of ϕ_x is allowed to be a constant -35° in this example, the net phase shift for current is the sum of $\beta_x + \phi_x$; the value of ϕ_x can be held constant without losing generality.

The base value to which the LaGrange method is compared is determined similar to the single phase case, that is,

$$
P_{total}(t) = \sum_{x=a,b,c} V_x(t)\, I_x(t) = \sum_{x=a,b,c} V_{xRMS} I_{xRMS} \cos(\omega t + \alpha_x)\cos(\omega t + \beta_x + \phi_x). \tag{6-26}
$$

Fig. 6.4 shows a plot of equation (6-26) and the two component parts of this total as described by equations (6-23) and (6-24). As before, the component parts of the partitioned equation are identified. The trace based on a direct calculation is drawn with a wide black pen. The calculation of active and passive power that is based on the LaGrange minimization is computed by the following relationships:

$$
\begin{aligned}
P_{active} &= \sum_{x=a,b,c} i_{Ax} v_x \\
P_{passive} &= \sum_{x=a,b,c} i_{Px} v_x.
\end{aligned}
\tag{6-27}
$$

Total Power, $P_{active} + P_{passive}$, is again presented, this time with the trace in red. It is observed that the values obtained by the two methods are again identical. Note that line voltages and currents are not presented in this plot to avoid cluttering.

One final verification is made for this system. It is expected that if both the system current and voltages are balanced, the active power will be a constant. Under these conditions, if the load is considered as a three phase load – not as three individual single phase loads – the passive power will be zero; in the sequel, a formal proof is presented to demonstrate that, for sinusoidal waveforms, the passive power across all three phases is identically zero. A third plot showing these conditions is presented as Fig. 6.5. For this plot a value of 12 Volts is used for all RMS voltages, with the RMS currents being 5 Amp; the current phase shift is -35°.

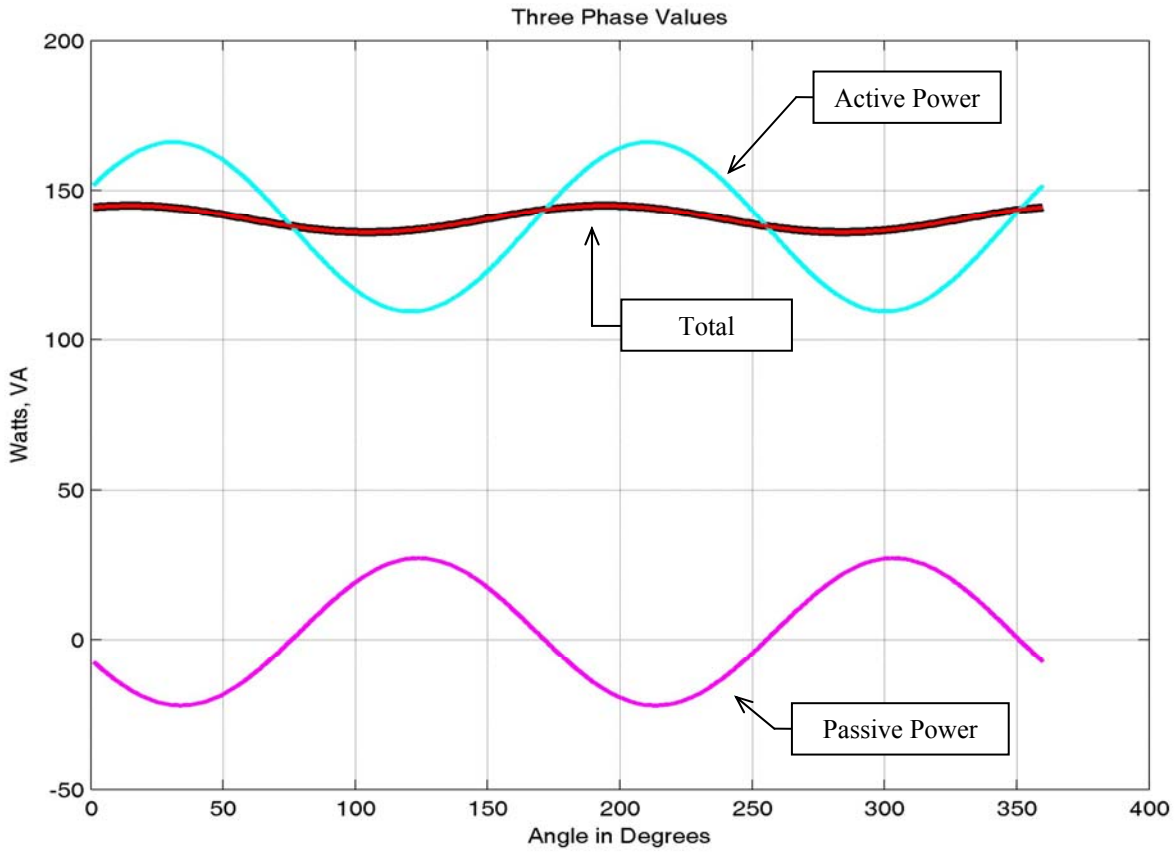

Fig. 6.4 Three phase power components

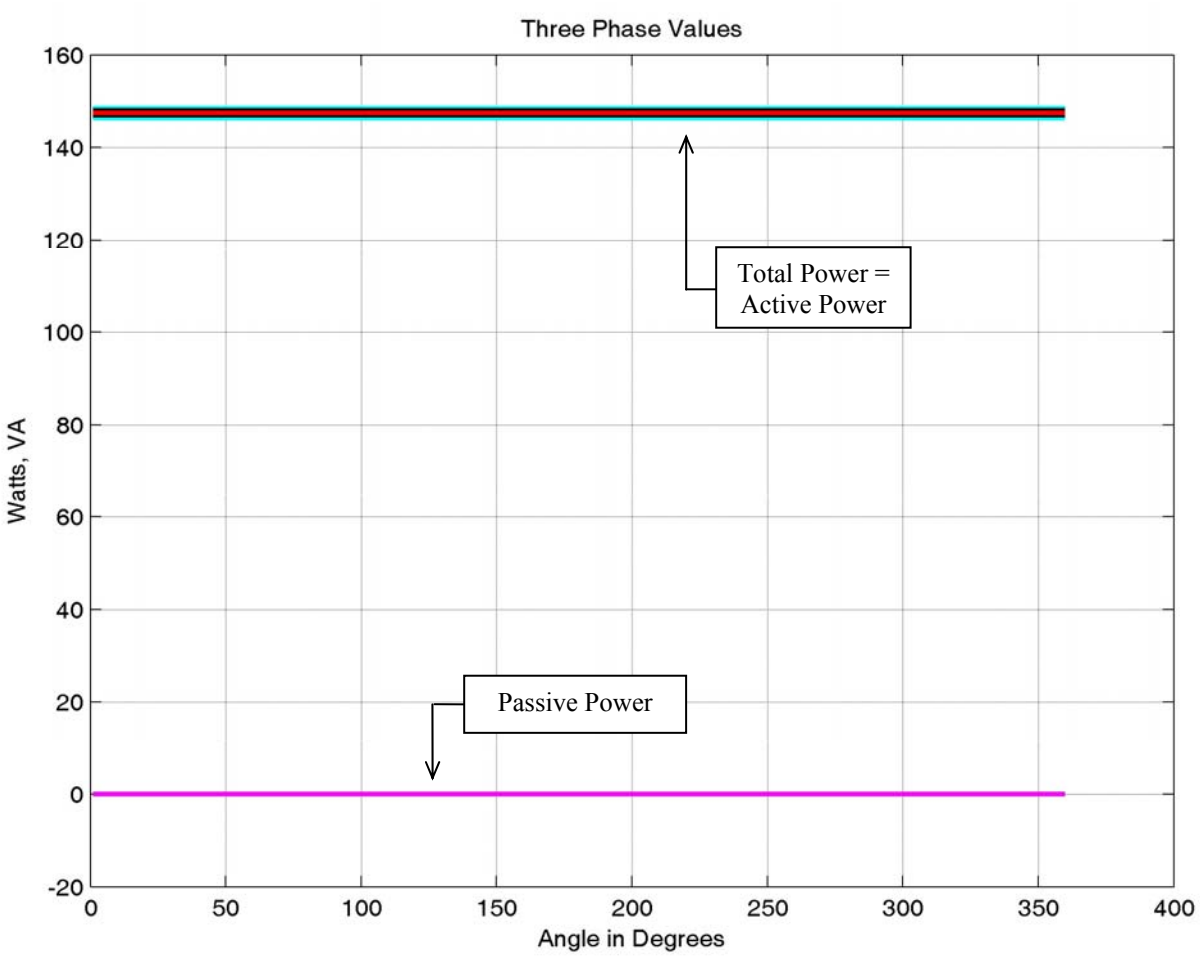

Fig. 6.5 Three phase power components with balanced system

7 – Application of the LaGrange minimization to the captured data

7.1 – Validations with captured data

The next logical step in the development of an effective use of the LaGrange minimization process is an evaluation of the method in comparison with other ways of describing power in a three-phase system. For comparison purposes, this will now be done, using the standardized method of expressing power, actually the FBD presentation, and the *dq*-theory method. The goal is to demonstrate that the results of using active currents from the LaGrange minimization method will produce identically the same results as would be obtained by using either of the other two systems.

The base definition of total power in the *abc* system is the following:

$$S_{abc} = V_a I_a + V_b I_b + V_c I_c \tag{7-1}$$

where V_a, V_b, and V_c are the individual phase voltages and I_a, I_b, and I_c are the individual phase currents. This is the classical definition of total power that matches the FBD power theory definitions.

The second item in the comparison is the total power as determined by the *pq*-theory. Under this system, total power is defined as:

$$S_{dq0} = v_d i_d + v_q i_q + v_0 i_0 \tag{7-2}$$

where v_d, and i_d are the direct axis voltage and currents, v_q, and i_q are the quadrature axis components, and v_0, and i_0 are unbalance components (the so-called 'zero sequence' components). These are the classical definitions under the *pq*-theory.

The item being compared it the total active power as determined by the LaGrange minimization method. This value is defined as:

$$S_L = V_a I_{Aa} + V_b I_{Ab} + V_c I_{Ac} \tag{7-3}$$

where V_a, V_b, and V_c are the individual phase voltages and I_{Aa}, I_{Ab}, and I_{Ac} are the individual phase *active* currents.

The result of the comparison is shown in graphic form in Fig. 7.1. In this graphic, the different items being evaluated are plotted in pens of varying width so that any deviations are immediately obvious; refer to Appendix D for a listing of the software used to generate the plot.

The values as determined by the use of (7-1) are plotted in the widest pen, in black. The values as determined by the use of (7-2) are plotted in the medium width pen in yellow; the values as

determined by the use of (7-3) are plotted in the narrowest pen in red. It is observed that there is no difference in the plots within the limits of the resolution of the *MatLab* program.

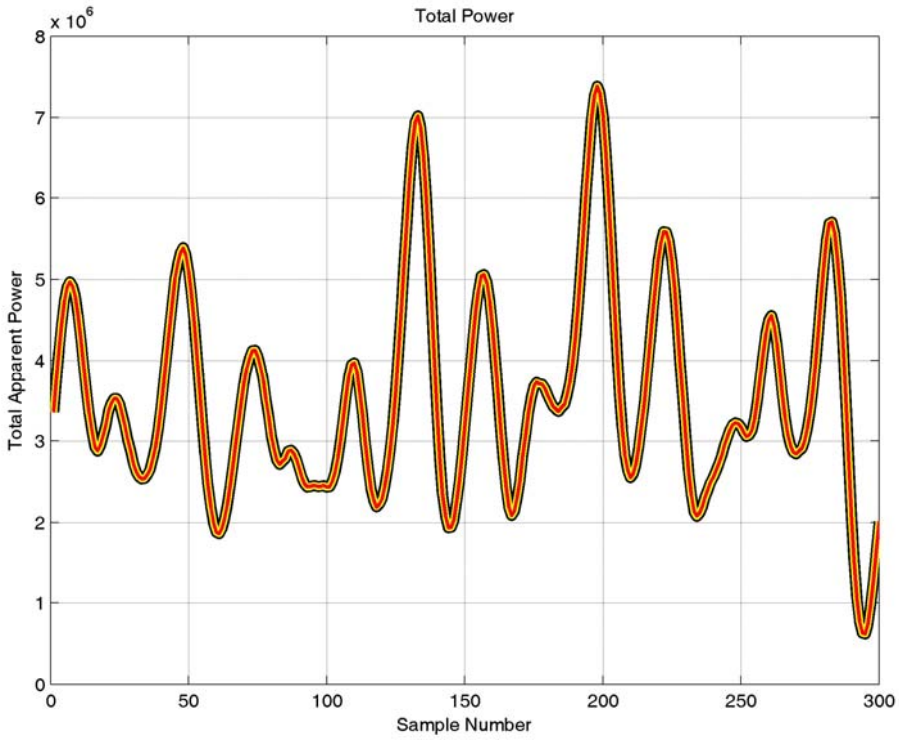

Fig. 7.1 Comparison of power resulting from various computational methods

The question that immediately comes to mind upon seeing these results is to inquire how the total values can be same when the same phase voltages are used for both the classic method and the LaGrange minimization method. The answer is that while the phase voltages are the same, the currents are in fact different from phase-to-phase; the total product of the voltages and currents, taken over all three phases, sums to the same value at any point in the data set. The differences in phase current are significant. In Fig. 7.2, the actual input current is show in black; the active portion of the current is shown in red; all three phases are presented for comparison purposes.

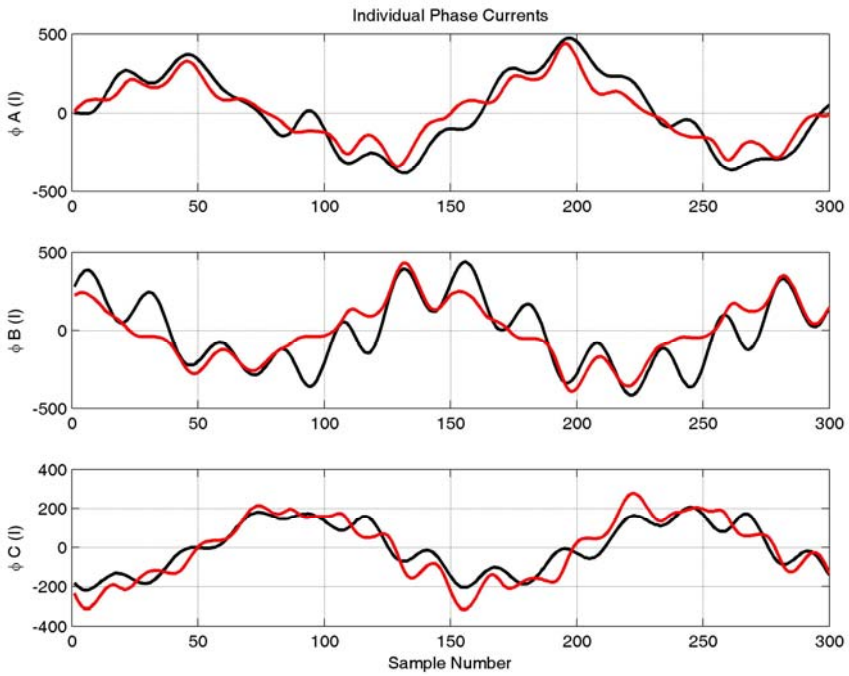

Fig. 7.2 Comparison of phase currents; measured current in black, active current in red

7.2 – Application to captured data

The goal of the work is to reduce the harmonic content of the input current waveform. Toward this end the LaGrange minimization will now be used to determine a current to be injected into the supply source of an EAF. The result of this compensation is the active current waveform, as shown in red in Fig. 7.2. The following spectrum analyses are presented to show the result of LaGrange compensation. The first set of harmonic bar charts, Figs 7.3 and 7.4, show each phase of the uncompensated EAF under normal operating conditions. There are two cycles of data, each of which is presented in a separate plot; refer to Appendices F, and G for listings of the software used to generate these plots.

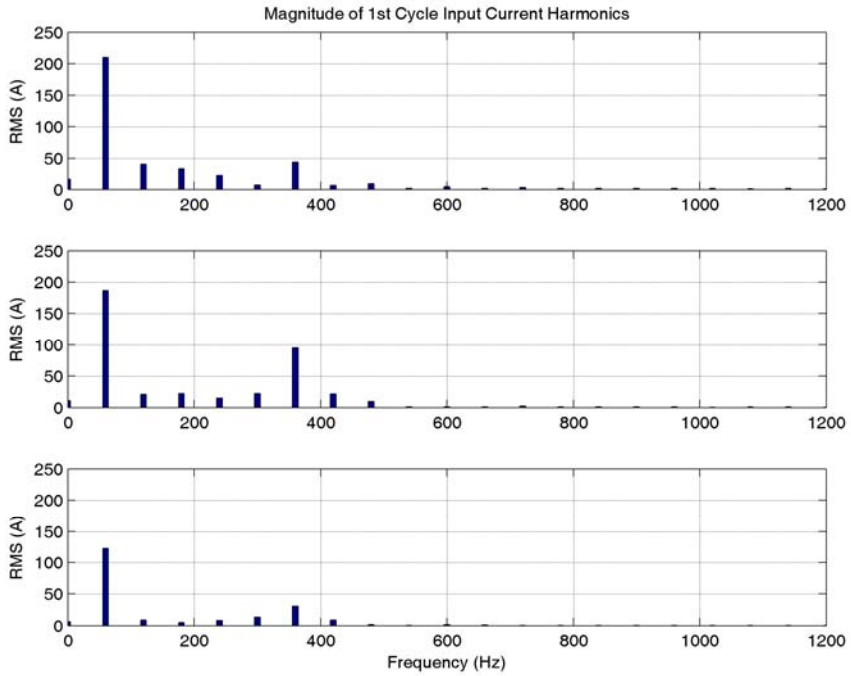

Fig. 7.3 Uncompensated EAF harmonic content, 1st cycle of data

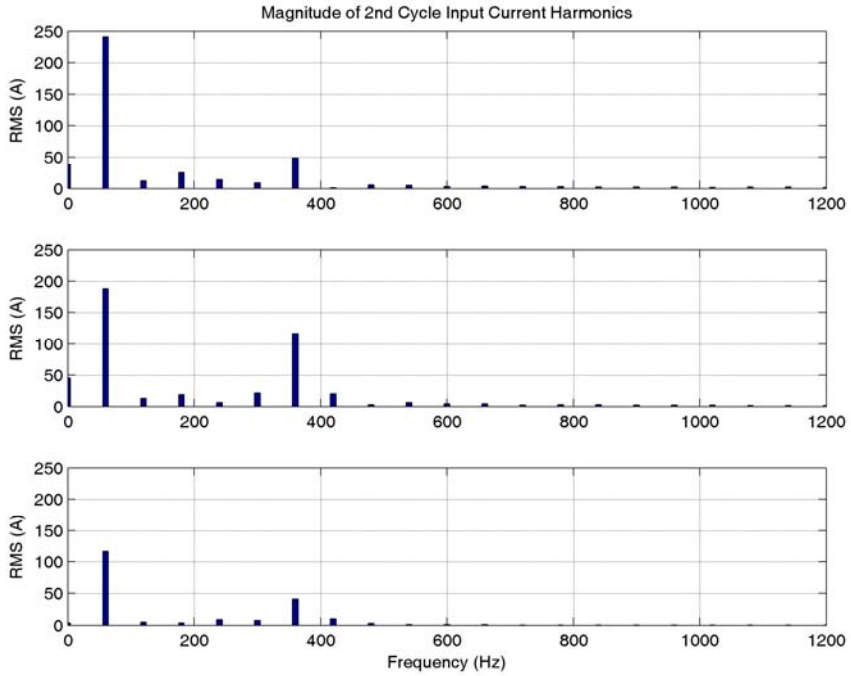

Fig. 7.4 Uncompensated EAF harmonic content, 2nd cycle of data

The next set of figures, Figs. 7.5 and 7.6, depict the same EAF input waveform as was used in the uncompensated case, but in this instance the traditional *dq*-theory compensation technique has been used for compensation. In brief, these waveforms have been modified such that the Q component of power has been removed. Again, both the first and second cycles of data have been plotted as separate bar charts. The important observation to be made about this set of waveforms is that while the total current of the fundamental has been reduced, there is actually much more harmonic content at upper frequencies than there was in the initial uncompensated waveforms.

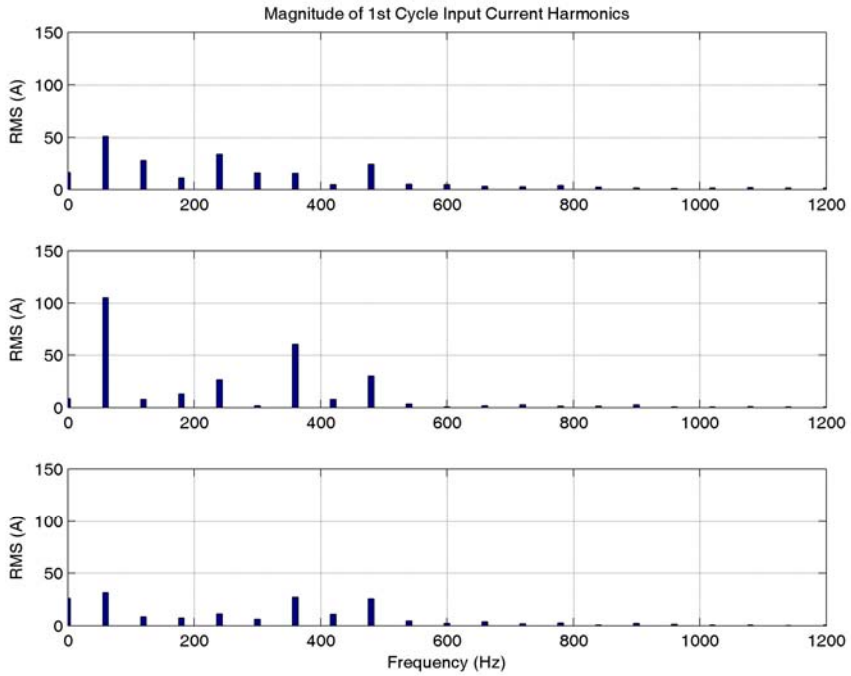

Fig. 7.5 *dq*-compensated EAF harmonic content, 1st cycle of data

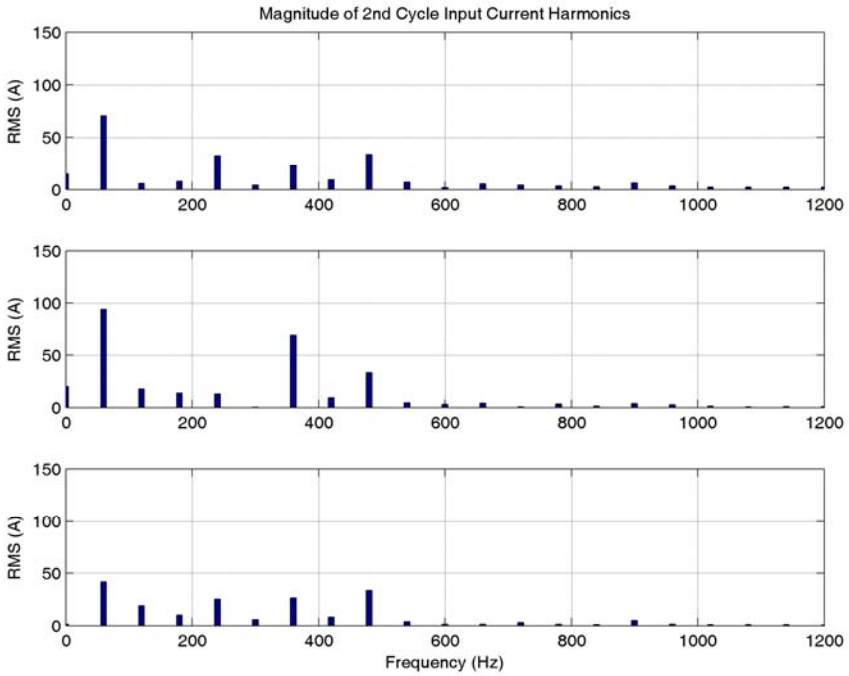

Fig. 7.6 *dq*-compensated EAF harmonic content, 2nd cycle of data

LaGrange compensation is now applied to the same data, with the results as shown in Figs. 7.7 and 7.8. The result of the compensation is that the magnitude of the fundamental component is significantly increased and the magnitude of the higher frequency components is depressed. The improvements in harmonic content of input current as compared with the *dq*-theory compensated case is typical for all data captured from the subject EAF; refer to Appendix H for a listing of the software used to generate these plots.

The total power of the EAF, over all three phases, in the two cycles of data presented is shown in Fig. 7.9, along with the average value of the power. It is noted that the average power over these two cycles of data is approximately 3.5 MVA. As the rating of the subject EAF is 4 MVA, and the data were captured at a time when the EAF was under nominal loading conditions, this is a welcomed confirmation that the overall calculations are, in general, correct.

An item of extreme interest is the amount of power that must be applied to the compensating waveform. The power, over all three phases, of the compensating waveform is essentially zero, as shown in Fig. 7.10; refer to Appendix I for a listing of the software used to generate Figs. 7.9 and 7.10.

The implication is that the LaGrange compensation method, similar to the *dq*-theory method, can be used without the application of real power. For reference, the power in the compensating waveform is determined by the following relationship:

$$S_{comp} = V_a I_{Pa} + V_b I_{Pb} + V_c I_{Pc} \tag{7-4}$$

where the compensating currents, I_{Pa}, I_{Pb}, and I_{Pc} are the inactive components of the LaGrange results and the voltages, V_a, V_b, and V_c are the voltages against which the compensating currents operate.

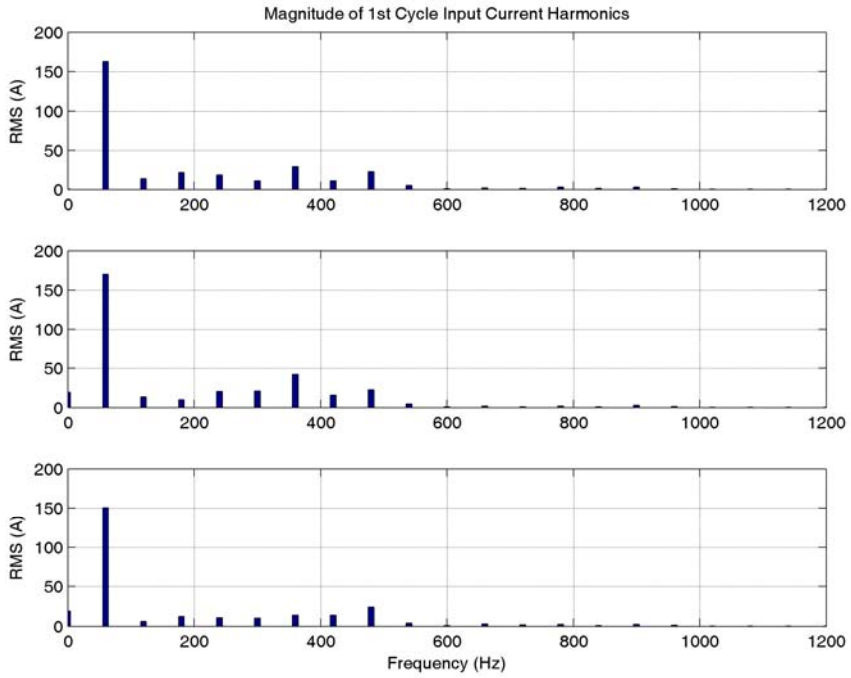

Fig. 7.7 LaGrange compensated EAF harmonic content, 1st cycle of data

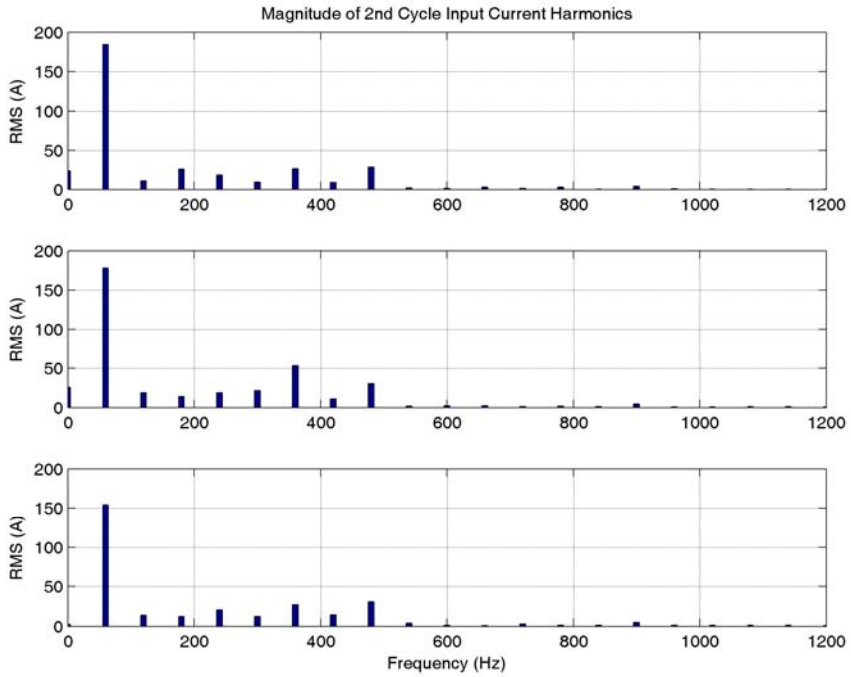

Fig. 7.8 LaGrange compensated EAF harmonic content, 2nd cycle of data

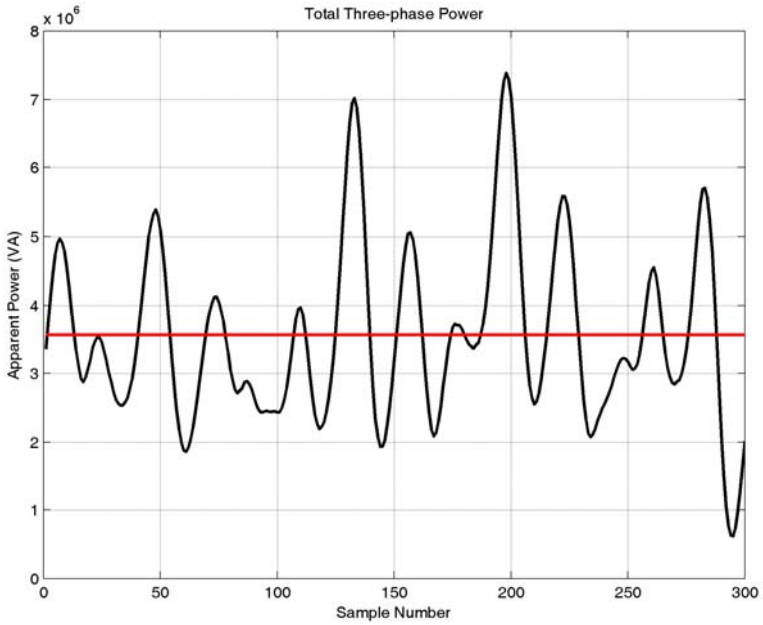

Fig. 7.9 Total active power with LaGrange compensation; EAF rating is 4 MVA

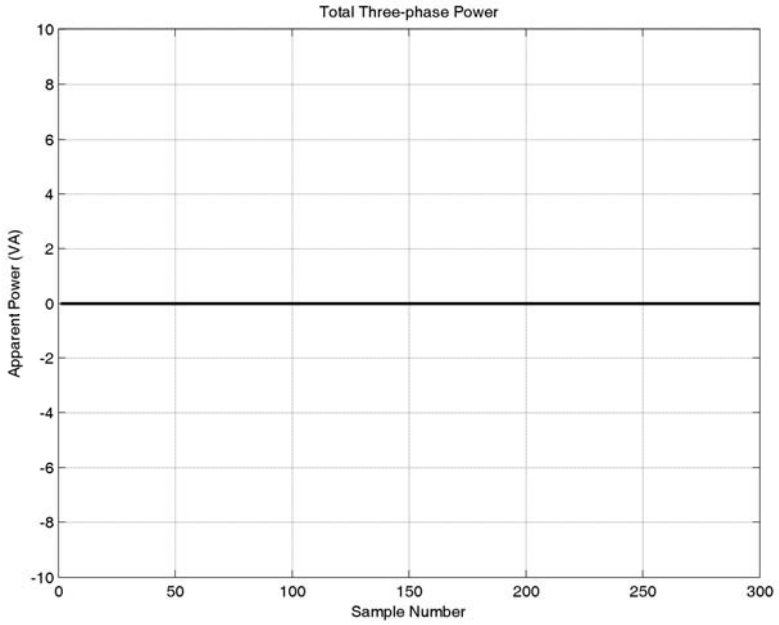

Fig. 7.10 Total inactive power with LaGrange compensation

7.3 – Evaluation of results

The information presented graphically as harmonic bar charts in Figs. 7.3 – 7.8 clearly indicate that the LaGrange minimization technique as applied to one of the data sets captured from an operating EAF significantly reduce the harmonic content of the input current waveform as compared to the *dq*-theory method of compensation. Also, again visually, the LaGrange method appears to provide some improvements over the uncompensated input current waveform harmonics. These data can be quantified by use of the Total Harmonic Distortion (THD) as a figure of merit.

There are several ways of computing THD. [58] The method selected, which is preferred for use with power system analysis, defines THD as:

$$THD = \frac{\sqrt{\sum_{h=2}^{\infty} I_h^2}}{I_1} \tag{7-5}$$

where I is the current magnitude of the harmonic whose number is h; under this harmonic numbering scheme, I_1 is current due to the fundamental frequency. I_0 is the DC component, which is not used in the computation of THD. For the case at hand, the maximum value of h is 75, as the

input data set has 150 data values per cycle. It is noted that it is technically possible to view this system in frequency domain, *i.e.*, as harmonic content, only because we are looking *a posteriori* at data that is considered to be a single cycle.

THD information for each of the captured data sets in presented in Tables 7.1 – 7.4. The THD values computed are for three cases of the same input data waveform: (1) The uncompensated case, (2) The case as compensated by the dq-theory method, and (3) The case as compensated by the LaGrange minimization method. A total of eight (8) data sets were captured during the field work, each of two (2) nominal 60 Hz cycles. One data set, number three (3), was corrupt as downloaded from the monitor and is not included in the analysis.

7.4 – Harmonic content of *dq*-theory compensation

It is immediately observed that the THD of the dq-theory compensated waveforms are much higher than those of the uncompensated waveform. At first glance, this result is counterintuitive; the avowed goal of compensation is to reduce harmonics, not to increase them. The explanation is relatively straightforward.

The *dq*-theory method operates by removing that portion of the current waveform that is caused by reactive power in the load. For must loads, including EAFs, the bulk of the reactive current component is in the fundamental frequency. The operation of the THD calculation, as described by (7-5), has the magnitude of fundamental frequency current in the denominator of the expression. It follows directly that if the magnitude of the fundamental is reduced and other components remain unchanged that the value of the THD is going to increase.

The LaGrange minimization method also reduces the magnitude of the fundamental of current, but it also reduces the magnitude of the upper harmonics. The exact amount of the reduction is dependent on the particular waveform and the degree of unbalance of the system. For this reason, the THD values of the LaGrange technique are lower than those seen from the *dq*-theory method.

7.5 – Conclusions from results

The following conclusions can be drawn, or reasonably extrapolated, from the tabulated THD computations:

1. In every case the application of the *dq*-theory compensation technique results in an input waveform with higher average harmonic content than the uncompensated case.

2. In every case the application of the LaGrange minimization developed herein results in an input waveform with lower average harmonic content than the *dq*-theory compensated case.
3. In some cases, the LaGrange minimization results in an input waveform with a lower average harmonic content than the uncompensated case.
4. For the cases presented, an insignificant amount of real power is required to affect the reduction of harmonic content in the input current waveforms.

The final conclusion is that EAF compensation using the LaGrange minimization approach has significant advantages over compensation techniques based on *dq*-theory. It is noted that the particular cases presented are from specific measured data. While these may lead one to suspect that there is a general method that will result in a desirable outcome, this is, in and of itself, not a proof. Next, a proof will be undertaken that will resolve any theoretical concerns about the applicability of the LaGrange method.

Table 7.1 THD computations for data sets one (1) and two (2)

Data Set No. 1 *(Clean_dataset1.csv)*			
Condition	Phase	1st Cycle	2nd Cycle
Uncompensated	A	17.26%	13.35%
	B	27.02%	32.25%
	C	20.99%	50.98%
	Average	21.76%	32.19%
dq-compensated	A	40.23%	53.82%
	B	36.71%	70.31%
	C	55.78%	86.62%
	Average	44.24%	70.25%
LaGrange compensated	A	25.65%	27.01%
	B	22.39%	30.73%
	C	29.64%	46.88%
	Average	25.89%	34.87%

Data Set No. 2 *(Clean_dataset2.csv)*			
Condition	Phase	1st Cycle	2nd Cycle
Uncompensated	A	48.44%	21.64%
	B	31.35%	33.56%
	C	36.37%	17.17%
	Average	38.72%	24.12%
dq-compensated	A	288.26%	41.99%
	B	102.53%	36.23%
	C	78.82%	86.20%
	Average	46.24%	54.81%
LaGrange compensated	A	46.24%	27.42%
	B	31.76%	25.48%
	C	32.86%	24.14%
	Average	36.95%	25.68%

Table 7.2 THD computations for data sets four (4) and five (5)

Data Set No. 4 *(Clean_dataset4.csv)*			
Condition	Phase	1st Cycle	2nd Cycle
Uncompensated	A	27.63%	33.02%
	B	20.85%	28.29%
	C	19.82%	22.77%
	Average	22.77%	28.03%
dq-compensated	A	166.91%	63.35%
	B	56.22%	146.01%
	C	51.55%	49.20%
	Average	91.56%	86.19%
LaGrange compensated	A	23.84%	26.59%
	B	18.10%	22.57%
	C	20.15%	28.36%
	Average	20.70%	25.84%

Data Set No. 5 *(Clean_dataset5.csv)*			
Condition	Phase	1st Cycle	2nd Cycle
Uncompensated	A	9.40%	11.58%
	B	21.48%	11.95%
	C	18.49%	16.37%
	Average	16.46%	13.30%
dq-compensated	A	35.39%	35.76%
	B	40.73%	25.19%
	C	47.14%	49.45%
	Average	46.24%	36.80%
LaGrange compensated	A	20.47%	22.19%
	B	18.82%	14.81%
	C	23.14%	20.75%
	Average	20.81%	19.25%

Table 7.3 THD computations for data sets six (6) and seven (7)

Data Set No. 6 *(Clean_dataset6.csv)*			
Condition	Phase	1st Cycle	2nd Cycle
Uncompensated	A	18.59%	18.70%
	B	14.67%	26.18%
	C	19.85%	18.74%
	Average	17.70%	21.21%
dq-compensated	A	60.20%	53.21%
	B	26.46%	32.02%
	C	62.58%	72.29%
	Average	49.75%	52.51%
LaGrange compensated	A	24.56%	20.75%
	B	16.36%	17.27%
	C	20.71%	19.90%
	Average	20.54%	19.31%

Data Set No. 7 *(Clean_dataset7.csv)*			
Condition	Phase	1st Cycle	2nd Cycle
Uncompensated	A	39.99%	37.40%
	B	11.55%	16.33%
	C	59.32%	69.85%
	Average	36.95%	41.19%
dq-compensated	A	76.48%	78.88%
	B	85.05%	62.01%
	C	111.22%	108.50%
	Average	46.24%	83.13%
LaGrange compensated	A	44.48%	43.56%
	B	36.35%	36.55%
	C	48.98%	54.24%
	Average	43.27%	**44.78%**

Table 7.4 THD computations for data set eight (8)

Data Set No. 8 *(Clean_dataset8.csv)*			
Condition	Phase	1st Cycle	2nd Cycle
Uncompensated	A	35.04%	25.00%
	B	56.88%	65.50%
	C	30.08%	37.58%
	Average	40.67%	42.69%
dq-compensated	A	112.39%	79.74%
	B	70.89%	87.72%
	C	137.17%	72.29%
	Average	106.82%	132.20%
LaGrange compensated	A	31.43%	28.75%
	B	35.67%	40.89%
	C	24.97%	34.81%
	Average	30.69%	34.82%

7.6 – Theoretical equivalence of the *dq0* and LaGrange methods under balanced conditions

The values selected for the demonstration plot of Fig. 6.2 were selected arbitrarily. The apparent correspondence of the results of the *dq0* method and the LaGrange minimization method causes one to wonder if the two methods are actually mathematically equivalent when the voltages and currents are each part of a balanced system. The following rigorous proof was undertaken to resolve this question.

Consider a balanced three phase voltage set defined by the following equations:

$$\begin{aligned} v_A &= V_m \cos(\omega t) \\ v_B &= V_m \cos(\omega t - \frac{2\pi}{3}) \\ v_C &= V_m \cos(\omega t + \frac{2\pi}{3}) \end{aligned} \tag{7-6}$$

with currents similarly defined as:

$$
\begin{aligned}
i_A &= V_m \cos(\omega t + \phi) \\
i_B &= V_m \cos(\omega t - \frac{2\pi}{3} + \phi) \\
i_C &= V_m \cos(\omega t + \frac{2\pi}{3} + \phi).
\end{aligned}
\tag{7-7}
$$

In the above expressions v_i and i_i represent the instantaneous voltage and currents respectively. The angular frequency, in radians per second is given by ω, while the time, in seconds, is given by t. The power factor angle, in radians, is given by ϕ. It should be noted that the voltage is not phase shifted, *i.e.*, the reference angle for phase A of the voltage set is arbitrarily set to be zero. This has no effect on the generality of the proof as the entire set can be rotated by any fixed amount without modifying the validity of the calculations.

To begin the proof, the first step is to determine the reactive power by using the *dq0* method. Toward this end, convert the given voltage and current values to a two-phase system using the Clarke transformation as defined by (5-21):

$$
\begin{aligned}
V_{dq0} &= \left[\mathrm{T_C}\right] V_{abc} \\
I_{dq0} &= \left[\mathrm{T_C}\right] I_{abc}.
\end{aligned}
\tag{7-8}
$$

Performing the matrix multiplication for each of the phase voltages and currents and then reducing the resulting equations by the use of trigonometric identities gives the following values in the *dq0* reference frame:

$$
\begin{aligned}
v_d &= V_m \sqrt{3} \cos(\omega t) \\
v_q &= V_m \sqrt{3} \sin(\omega t) \\
v_0 &= 0 \\
i_d &= I_m \sqrt{3} \cos(\omega t + \phi) \\
i_q &= I_m \sqrt{3} \sin(\omega t + \phi) \\
i_0 &= 0.
\end{aligned}
\tag{7-9}
$$

Complex power is given by:

$$
\begin{aligned}
s &= vi^{\dagger} = (v_d + jv_q)(i_d - ji_q) \\
s &= (v_d i_d + v_q i_q) + j(v_q i_d - v_d i_q) \\
s &= p + jq.
\end{aligned} \tag{7-10}
$$

Using (7-9) in (7-10) and reducing by the use of trigonometric identities gives the well-known result:

$$p = 3V_M I_M \cos\phi, \tag{7-11}$$

while reactive power, q, is given by:

$$q = -3V_M I_M \sin\phi. \tag{7-12}$$

As an aside, it is noted that this is also the results of the same derivation as would be obtained by using the phasor method.

Using the LaGrange minimization method, the active power, P_A, is given by:

$$P_A = i_{Aa} v_a + i_{Ab} v_b + i_{Ac} v_c. \tag{7-13}$$

In this relationship the values of current are determined by use of the LaGrange minimization relationship, originally presented as (6-10) and reproduced here for convenience:

$$\begin{bmatrix} i_{Aa} \\ i_{Ab} \\ i_{Ac} \end{bmatrix} = \frac{(v_a i_a + v_b i_b + v_c i_c)}{v_a^2 + v_b^2 + v_c^2} \begin{bmatrix} v_a \\ v_b \\ v_c \end{bmatrix}. \tag{7-14}$$

Using equations (7-6), (7-7), in (7-14) and then substituting the current values into (7-13) gives the following value for P_A:

$$P_A = 3V_M I_M \cos\phi. \tag{7-15}$$

Equations (7-11) and (7-15) are observed to be equal, indicating that the values produced by the LaGrange minimization method is identical to that produced by the *dq0* method or phasor methods when the input voltages and currents are a balanced set.

It was observed, from Fig. 6.5, that under balanced input conditions the passive power was zero. These data were based on arbitrarily selected values for the inputs but now it can be shown that the result is generally true.

The passive current is given by the following expression, first presented as (6-9), reproduced here for convenience:

$$\begin{bmatrix} i_{Pa} \\ i_{Pb} \\ i_{Pc} \end{bmatrix} = \begin{bmatrix} i_a \\ i_b \\ i_c \end{bmatrix} - \frac{(v_a i_a + v_b i_b + v_c i_c)}{v_a^2 + v_b^2 + v_c^2} \begin{bmatrix} v_a \\ v_b \\ v_c \end{bmatrix}. \tag{7-16}$$

Allowing total passive to be the sum of the products of the individual phase voltages and currents,

$$P_P = i_{Pa}v_a + i_{Pb}v_b + i_{Pc}v_c \tag{7-17}$$

and carrying out similar substitutions as before*, viz.*, using (7-6) and (7-7) in (7-16) and then substituting the current values into (7-17) gives the value of P_P as:

$$P_P = 0. \tag{7-18}$$

The symbolic evaluation of these equations was performed first by hand, then by the use of *Mathematica* 7. [59] The printouts from this software are included in Appendix J for reference.

The purpose of the forgoing proof is to demonstrate that under balanced input conditions the LaGrange minimization method will produce identically the same results as the *dq0* or phasor methods. It is when conditions are not balanced, as in Electric Arc Furnaces, that the LaGrange method offers advantages over methods that assume balance of the input conditions.

7.7 – Current balance in measured data

It was previously noted that the $dq0 \leftrightarrow abc$ transformations are fully revisable as long as all components are used for the transformations. As will be demonstrated, the "0" component is not used in the STATCOM compensation scheme for an EAF, which presents an immediate obstacle to accuracy in the face of a severely unbalanced system. Fig. 7.11 is presented to illustrate the relative magnitude of the phase and the neutral currents at the input to an operating EAF; refer to Appendix K for a listing of the software used to generate this plot.

It is immediately obvious from the plot that the magnitude of the neutral current is significant and that if this level of current remains uncompensated then a STATCOM cannot faithfully deliver accurate compensating currents. The presented data set is one of those captured at the subject 4 MW copper EAF; all other captured data sets exhibit the same relative unbalance.

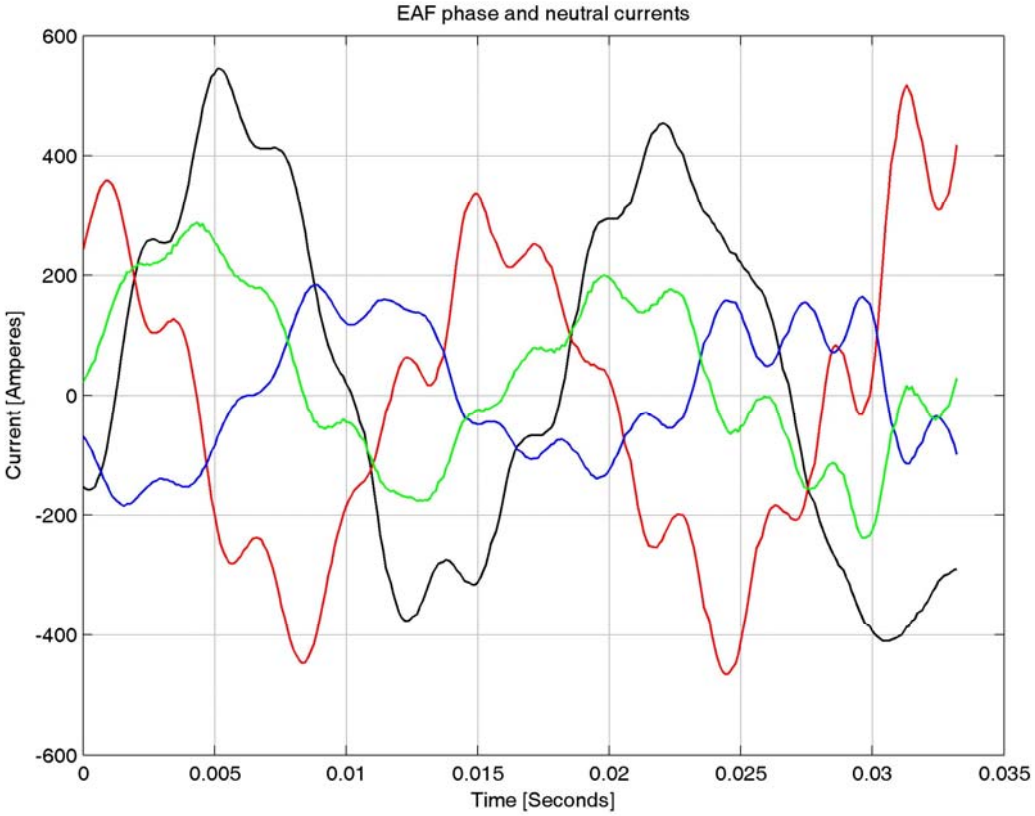

Fig. 7.11 Typical EAF phase and neutral currents

8 – An operating EAF STATCOM

8.1 – Introduction

In order to truly compare and contrast the LaGrange minimization method with the *dq0* method it is necessary to apply both compensation techniques to an operating EAF with an existing compensating Static Compensator (STATCOM). Inasmuch as EAFs are generally operated for profit on a 24 hour per day, 7 day per week, basis it is unlikely to expect that the operator of such equipment would be willing to allow 'experimental' work with their primary source of income. The next best thing would be to locate a working STATCOM-compensated EAF and to perform the following sequence:

1. Obtain all EAF and STATCOM design information, specifications, control and compensation information, and relevant information about the electrical supply system.
2. Construct a model in software to duplicate the physical system and the compensation arrangement.
3. Measure real-time voltage and current data from selected points in the actual operating STATCOM-compensated EAF system.
4. Apply the data to the software model.
5. Verify that the results of the software model match the real-world data with reasonable faithfulness.
6. Apply the LaGrange method to the software model.
7. Compare and contrast the result with data obtained in Item 3 above.

Toward this end a company was located that was willing to sign a non-disclosure agreement with NC State University that would allow full access to their facility for measurement and documentation purposes; the subject company agreed to provide all original documentation for their complete installation, including all available design documents for the EAF and STATCOM.

After the non-disclosure documents were executed site visits were conducted to gather data to construct the model. While all physical information was available and was freely given an obstacle was encountered with respect to the algorithms that were used in the compensating STATCOM. The problem was that the STATCOM manufacturer regards the software as propriety information and will not release *any* information regarding software to either the facility owner or to any third party.

Unfortunately, without information about the existing compensation strategy it is not possible to create a software model to faithfully reproduce the operation of the existing physical system.

Faced with the above roadblock, the decision was taken to model a physical system identically matching the subject facility and to assume a compensation scheme that would work for both the *dq0* and LaGrange methods. Since it was no longer possible to accurately model the actual existing system it made little sense to capture real data; the decision was taken to use a high-accuracy model of the EAF arcs to generate the data for the model. The sequence stated above was modified to the following:

1. Obtain all EAF and STATCOM design information, specifications, and relevant information about the electrical supply system.
2. Construct a model in software to duplicate the physical equipment arrangement; the software package selected was *PSCad*. [60]
3. Construct a software arrangement using a compensation strategy based on the *dq0* approach.
4. Locate a realistic, real-time, EAF arc model.
5. Apply the EAF model as a load to the software model.
6. Verify that the results of the software model are consistent with available data from similar compensation schemes.
7. Apply the LaGrange method to the software model.
8. Compare and contrast the result with data obtained in Item 6 above.

The above was accomplished; the following sections of this chapter detail subject system configuration, the design of the software STATCOM, and the validation process that was used to demonstrate the accuracy of the model.

At this juncture, the questions might well be asked, "Why go to all the trouble of creating a STATCOM model in its entirety? Why not just use one of the many models that are available as a part of the individual software packages?" The answer is that there is just not sufficient internal information available about the operational details of STATCOM models that are included with software packages. These models are essentially 'black boxes', where input data is provided and output information is generated; there is no documented way to access the internal operation of the model, in particular, the phase-to-phase behavior of the STATCOM. By generating a STATCOM model completely from fundamental components we achieve the multiple goals of (1) knowing exactly how the model functions, (2) being able to individually control all the internal functions of the model, and (3) being able to extract detailed information from within the model with the knowledge

that the extracted information truly represents the quantities that we seek. We start this task with a look at the various large components that comprise the overall system.

8.2 – Overall configuration of subject EAF and STATCOM

The subject facility is essentially in the scrap metal business, where steel is taken into a scrap yard, sorted, and then introduced into an EAF where it is melted and then extruded into steel stock. The physical capacity of the EAF basin is approximately 75 tons; the electrical rating is 33 MW, compensated by a STATCOM-based system installed in 2003. The entire plant is supplied by the electric utility *via* a dedicated transmission line operating at the 112.5 kV level. A local utility substation transforms the transmission line voltage to 12.47gndY/7.2 kV, which is the delivery voltage for the plant.

Like all EAF installations, the facility is extremely disruptive to the surrounding electrical grid; the facility is equipped with a compensating STATCOM to moderate the effects of the EAF. The STATCOM is rated at 20 MVA; it is connected directly across the delivery supply at the 12.5 kV level. A block diagram of the entire plant is shown in Fig. 8.1.

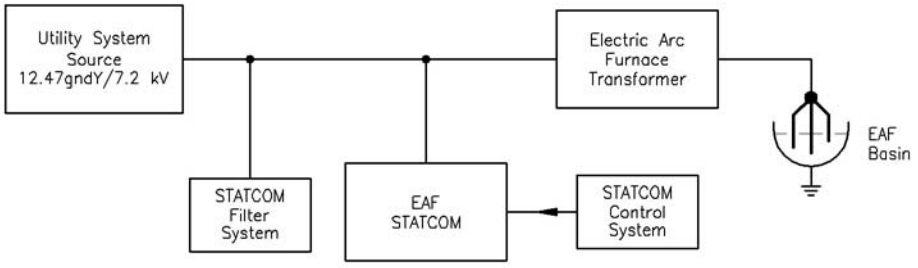

Fig. 8.1 Overall plant block diagram

8.3 – Utility source modeling

Modeling of the facility begins at the utility system source, the concept being to include not only an accurate representation of the source impedances but also a representation of the harmonic content of the source. In order to determine the harmonic content of the unloaded utility source a harmonic analyzer was used to capture data at an instant when the EAF was not on-line. These data were then used to generate a model of the utility source that contained all significant harmonic values. In order to keep number of the individual higher frequency sources manageable, the decision was

taken to include only those harmonics that contributed at least 0.10% to the magnitude of the actual voltage waveform; this resulted in a model with a fundamental component plus ten sources to represent the harmonic content.

Data was captured from the facility from phase A at the 277 Volt level. A spot check indicated that the other two phases were, except for the angle difference, essentially of the same magnitude. The voltage waveform harmonic content as measured at the 277 Volt level was translated into equivalent sources to match the plant delivery voltage of 12.47gndY/7.2 kV by allowing the actual measured RMS voltage (288.4 V) to be equivalent to the line-to-neutral voltage (7.2 kV) of the plant Medium Voltage (MV) system; the assignment of the upper harmonics is then a simple multiplier assigned to each of the measured harmonic magnitudes. The values and angles thus obtained are presented in Table 8.1 for Phase A. The other two phase magnitudes are not presented, the magnitudes being identical to those for Phase A. The harmonics having magnitudes large enough to be included are highlighted in yellow. The raw data used for these calculations is presented as Appendix L.

The next item of concern in creating an accurate utility system model is the determination of the source impedances for the system. Fortunately this information was available from the electric utility in the form of transmission line fault currents and transformer data from the plant substation. The following is provided.

At the 100 kV bus: 8,167 A 3-phase or 4,382 A line-to-gnd

At the 12.47 kV bus: 10,845 A 3-phase

Substation transformer: 36 MVA, %Z = 11.99%; X/R = 24.807

Looking first at the substation transformer the base ratings are as follows:

$$S_{Base} = 36 \text{ MVA}$$
$$V_{Base} = 12.47 \text{ kV}$$
$$I_{Base} = \frac{S_{Base}}{V_{Base} \cdot \sqrt{3}} = \frac{\left(36x10^{6}\right)}{12.47x10^{3} \cdot \sqrt{3}} = 16,668 \text{ A} \qquad (8\text{-}1)$$
$$Z_{Base} = \frac{V_{Base}^{2}}{S_{Base}} = \frac{\left(12.47x10^{3}\right)^{2}}{\left(36x10^{6}\right)} = 4.3195 \Omega.$$

The magnitude of the actual impedance is:

$$Z_{Act} = \%Z \cdot Z_{Base} = (0.1199) \cdot 4.3195 = 0.5179 \Omega.$$

Using the given X/R ratio, the components of the impedance are calculated to be:

$$R_{Act} = \sqrt{\frac{Z_{Act}^2}{\left(\frac{X}{R}\right)^2 + 1}} = 0.0208\Omega$$

$$X_{Act} = 24.807 R_{Act} = 0.51748\Omega. \tag{8-2}$$

The inductance associated with X_{Act} is determined to be:

$$L = \frac{X_{Act}}{2\pi f} = \frac{0.51748}{2 \cdot \pi \cdot 60} = 0.00137\text{H}. \tag{8-3}$$

At this point a simplification is made by observing that, based on the value of the base current computed in (8-1) and the stated value of available fault current, it is unlikely that ignoring substation transformer line-side impedances will have significant effect on the accuracy of the utility system model. For this reason no additional corrections are made to the system impedances and the values determined in (8-2) and (8-3) are used in the system model.

The X/R ratio provided by the electric utility 'feels' to be a bit high, so some effort was made to independently verify this value. A range of values for the X/R ratios of utility transformers is available from an IEEE standard. [61] The relevant plot is presented as Fig. 8.2 which indicates that the utility-provided information is indeed in the correct range for transformers in this size range.

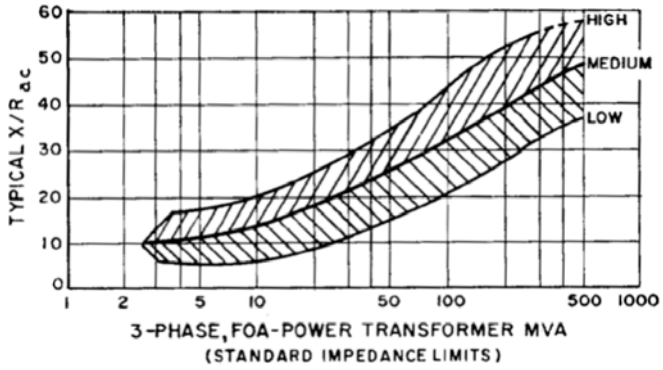

Fig. 8.2 Typical transformer X/R ratios

A complete model of the utility system is shown in Fig. 8.3. A switching arrangement was also included so that the utility model could produce either a pure sine wave at 60 Hz or the

approximation of actual existing conditions; the ability to turn off the harmonic content was useful during the design and validation of the STATCOM portion of the model. The model is arranged so that by proper operation of switches S_A and S_B the model can either deliver a pure sine wave or a sine wave distorted by a very close approximation of the harmonic content actually available on site. The voltage waveform outputs from the utility system model are presented in Fig. 8.4. A close look at the upper waveform will show the voltage waveform distortion; quantitatively, the overall voltage waveform has a Total Harmonic Distortion (THD) of 2.09%.

It is common to modify the X/R ratio of a system that includes an EAF to reflect the true value of the impedance looking back into the Point of Common Coupling (PCC) between the EAF system and the utility system. [62-63] In the present arrangement, the impedance looking back in the utility system is known as data has been provided by the electric utility company. The impedance of the EAF itself is determined dynamically by the *PSCad* simulation program, so the PCC impedance is not a direct issue. It is mentioned at the present time to call attention to the fact that the overall impedance looking back into the PCC is much lower than the 24:1 value provided by the utility company. In the sequel, when it is demonstrated that the real power fluctuation under a *dq0* strategy is much greater than under a LaGrange strategy, it will become obvious that the reduced X/R ratio presented by the cited references will have a direct effect on the level of observed flicker.

Table 8.1 Utility source voltage harmonic content

Utility Source Voltage Harmonic Content						
Harmonic	Measured Frequency (Hz)	Nominal Frequency (Hz)	Voltage Magnitude (Vrms)	Adjusted Voltage Magnitude (kVrms)	% Vrms	Voltage angle (°)
DC	0	0	0.06	0	0.02	0
1	59.96	60	288.38	7.2	99.99	0
2	119.92	120	0.03		0.01	112
3	179.88	180	0.66	0.016	0.23	169
4	239.85	240	0.02		0.01	50
5	299.81	300	4.80	0.12	1.66	50
6	359.77	360	0.02		0.01	89
7	419.73	420	1.23	0.031	0.43	-177
8	479.69	480	0.05		0.02	-149
9	539.65	540	0.30	0.007	0.10	129
10	599.62	600	0.03		0.01	54
11	659.58	660	2.56	0.064	0.89	158
12	719.54	720	0.02		0.01	122
13	779.50	780	1.91	0.048	0.66	168
14	839.46	840	0.05		0.02	112
15	899.42	900	0.33	0.008	0.11	104
16	959.38	960	0.05		0.02	-178
17	1019.35	1020	0.83	0.021	0.29	-146
18	1079.31	1080	0.02		0.01	120
19	1139.27	1140	0.33	0.008	0.11	-121
20	1199.23	1200	0.03		0.01	121
21	1259.19	1260	0.05		0.02	-90
22	1319.15	1320	0.02		0.01	-8
23	1379.12	1380	0.27		0.09	-9
24	1439.08	1440	0.02		0.01	41
25	1499.04	1500	0.16		0.05	8
26	1559.00	1560	0.02		0.01	117
27	1618.96	1620	0.03		0.01	79
28	1678.92	1680	0.03		0.01	-167
29	1738.88	1740	0.28	0.007	0.10	129
30	1798.85	1800	0.02		0.01	136
31	1858.81	1860	0.20		0.07	130

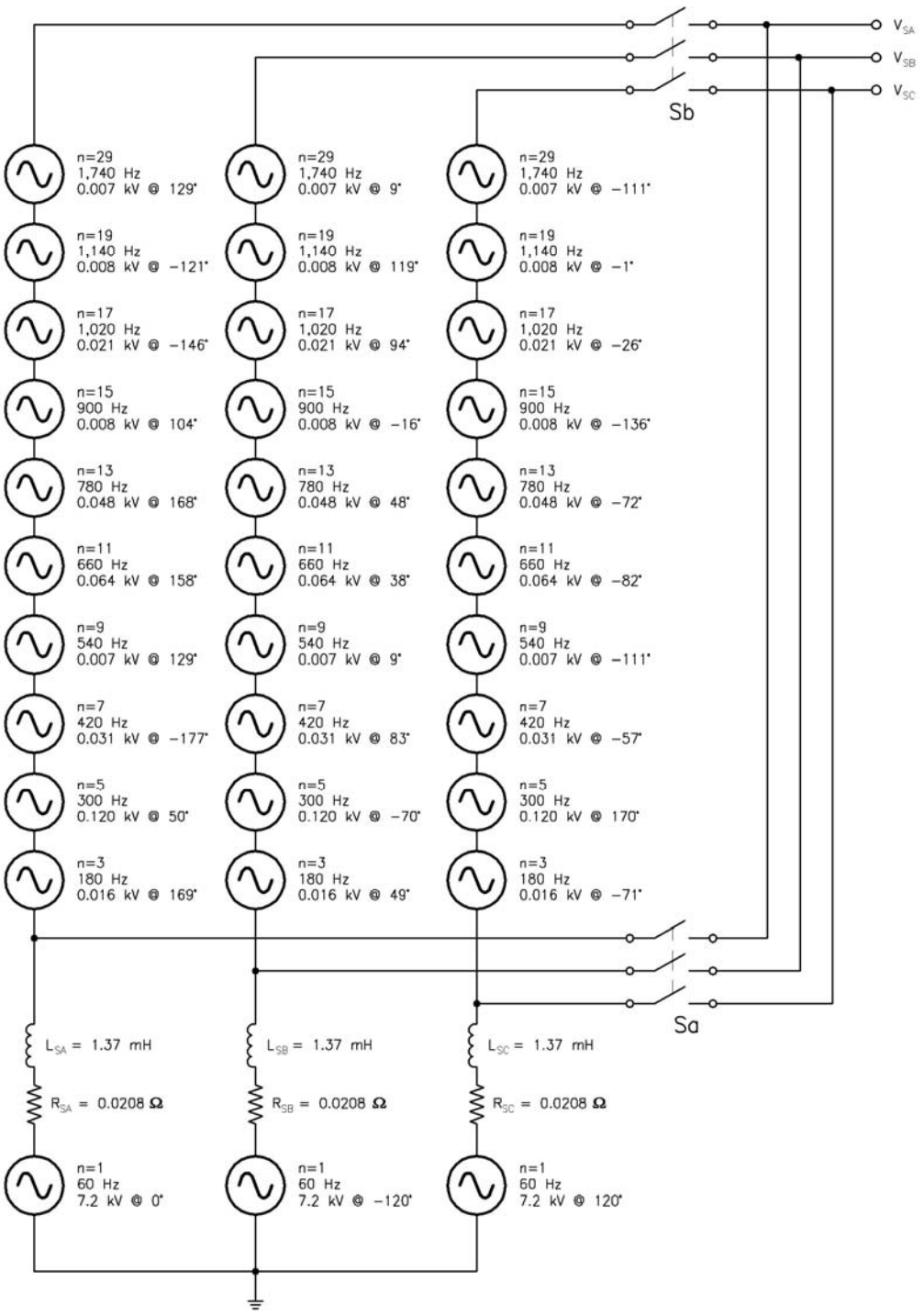

Fig. 8.3 Utility source connections diagram

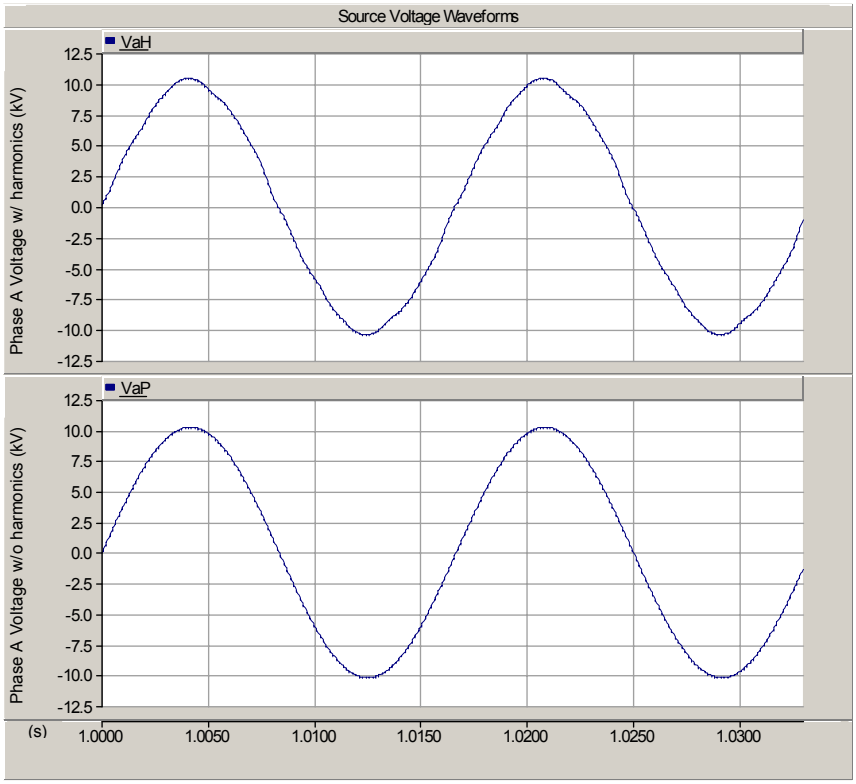

Fig. 8.4 Model voltages without (bottom) and with (top) harmonic content

8.4 – STATCOM modeling

The subject EAF is compensated by an ABB brand name STATCOM, for which full documentation has been made available; because of the level of detail available about the physical structures it is possible to model the STATCOM itself with great accuracy. From the point of view of topology, the STATCOM is a Neutral-Point-Clamped (NPC) Pulse Width Modulated (PWM) Inverter connected directly across the 12.47 kV line supplying the EAF transformer. The arrangement and operation of a NPC STATCOM is well understood, having being introduced by [64] in 1981.

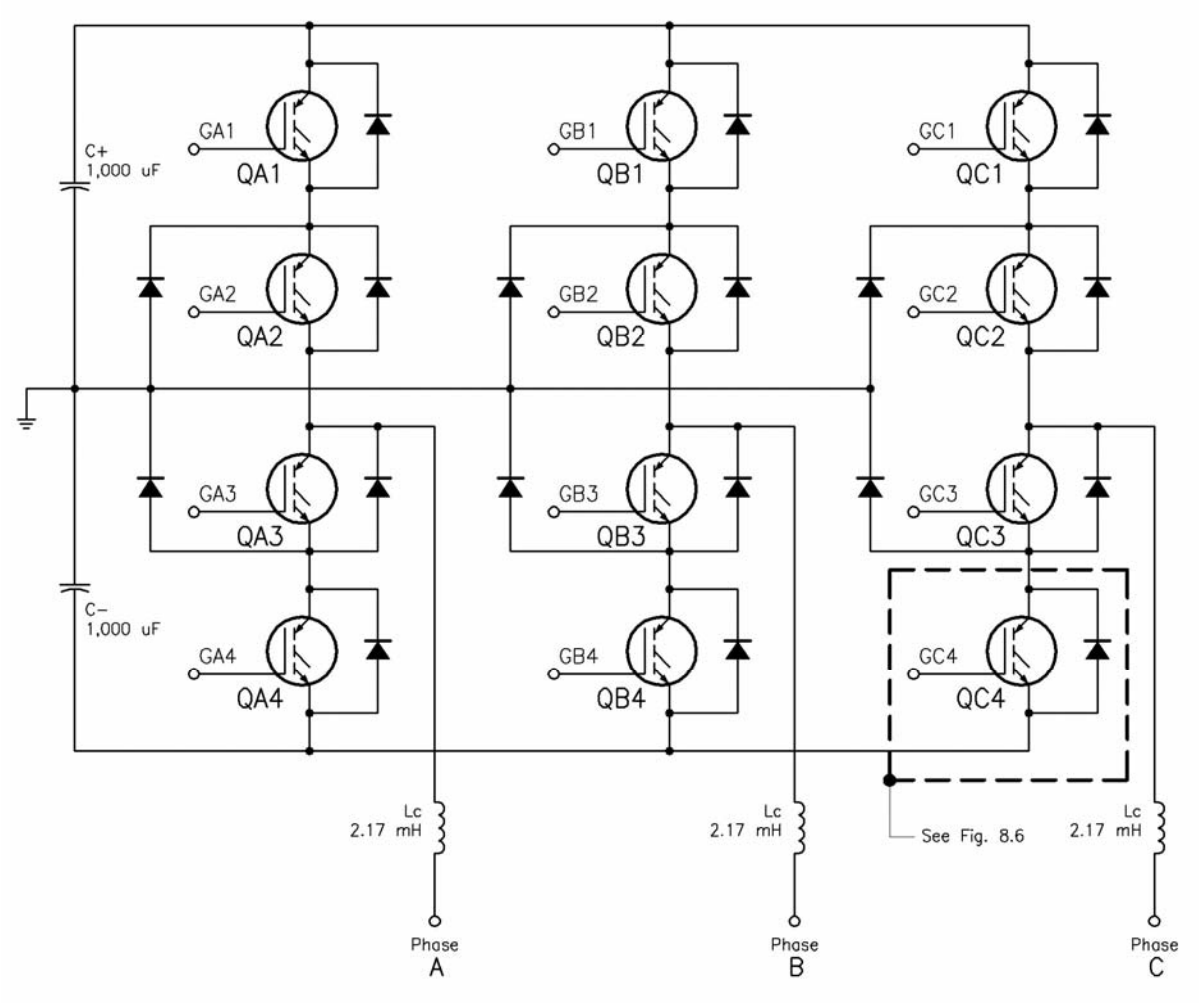

Fig. 8.5 Complete STATCOM as modeled

In the actual installation, minimum changes to the STATCOM topology have been made by the equipment manufacturer as compared to the arrangement described by the reference. The most significant modification that has been made is in the use of multiple devices in series to accommodate the voltage levels present in the system. A complete diagram of the STATCOM model is shown in Fig. 8.5; an enlargement showing the actual contents of one of the Insulated Gate Bipolar Transistors (IGBTs) presented as Fig. 8.6.

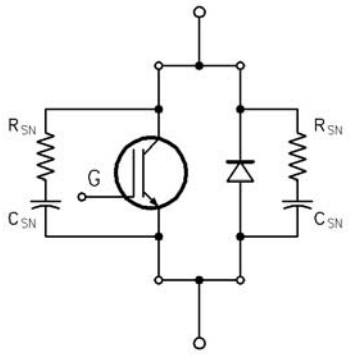

Fig. 8.6 Enlarged diagram of a typical modeled IGBT

The enlarged diagram of a typical modeled IGBT and diode as shown in Fig. 8.6 is the arrangement of the devices as used by the *PSCad* modeling software. In this detail, the electronic devices are ideal; the values of the individual resistive and capacitive components are as follows:

$$R_{SN} = 5{,}000\ \Omega$$
$$C_{SN} = 0.05\mu\text{F}.$$

With respect to the R and C values, it is noted that the series combination of these components is actually in parallel for the particular STATCOM topology. This connection implies that the equivalent impedance for the combination could be used, thus simplifying the arrangement somewhat. The values given are those initial values that closely approximate the device characteristics of the actual components. The decision was made to keep the components separate so that, if necessary, individual changes could be made in the IGBTs and diodes should this prove advantageous to the model; in the sequel, this was not actually necessary.

PSCad offers a technique of device gating that they refer to as "interpolated switching." The basic concept behind interpolated switching and firing control is that the turn-on and turn-off of a controlled device is not strictly tied to the step-time of the active model, *i.e.*, the actual switching event in somewhere between the normal discrete time points of the simulation. The advantage of such switching is that it significantly improves the accuracy of the device model without unduly increasing the simulation time. Without interpolated switching it would be necessary to reduce the time-step to a very small value in order to accurately model the turn-on or turn-off the devices – which would significantly slow the run-time of the overall simulation. In the present simulation full

advantage has been taken of the *PSCad* interpolation algorithm and integrated firing control for all solid state devices.

Gate control for a STATCOM is extremely critical and it is, arguably, the most complex issue encountered in making a complete system function as desired. Unfortunately, gating and compensation strategy are the two pieces of the overall plant puzzle that are missing in the present model design. Because this information was not available from the STATCOM manufacture a gating scheme was devised that was appropriate the NPC VSI. The overall gating concept is based on [64], in its essence a standard Pulse Width Modulation (PWM) scheme, with a reference input and a carrier input. The main differences in the way the PWM is accomplished in the NPC VSI lie in the fact that this topology has a three-level output which requires two separate carriers.

An example of the overall operation of the PWM is shown in Figs. 8.7 and 8.8. In this example, only one phase is shown; the two carriers, C_U and C_L, are shown in black, the reference waveform, R_A, is shown in blue, and the output waveform, V_A, is shown in red. The carrier frequency in this example plot is 600 Hz, selected to be deliberately low to better display the PWM output waveform of V_A. The carrier waveform is generated in the demonstration example by a simple voltage source at the carrier frequency of 600 Hz; the source voltage is shifted up and down by the direct addition of a displacement voltage to form the two carriers. The relationship that governs the output is the following:

$$\begin{aligned} &\text{if:} && R_A \geq C_U \; then \; V_A = V+ \\ &\text{or if:} && R_A \leq C_U \; then \; V_A = V- \\ &\text{else:} && V_A = 0. \end{aligned} \tag{8-4}$$

In the example, the reference, V_R, is a 60 Hz waveform with approximately 20% distortion added for the purpose of demonstrating the resolution of the system. The example plots clearly demonstrate the three-level PWM waveform and show the waveforms generated by this modulation scheme. In practice, the PWM waveform is smoothed by passing the load current through an inductance; all that then remains is to filter the carrier frequency from the final waveform. The three-phase physical realization of the gating model that is based on (8-4) is shown in Fig. 8.8. In this detail a master STATCOM enable line is included, S_C, so that the STATCOM can be turned on and off for demonstration purposes.

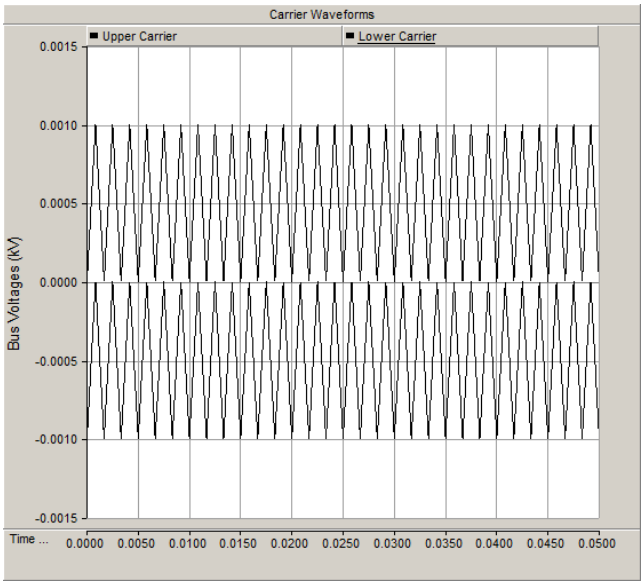

Fig. 8.7 Example carrier for use with demonstration NPC VSI

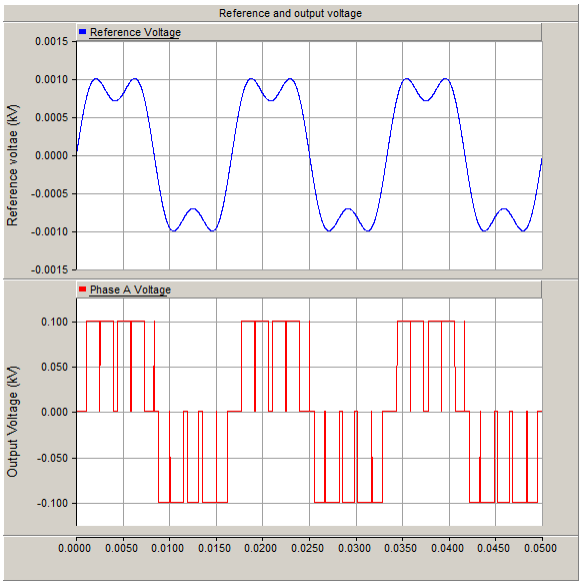

Fig. 8.8 Example of demonstration reference waveform and resultant PWM waveform

The generation of the carrier waveforms is somewhat more involved in the actual model that it is in the demonstration waveform. In a working STATCOM it is necessary to synchronize the carrier waveforms with the line across which the STATCOM is connected. If these waveforms are

not closely coordinated there will be large levels of current that circulate between the STATCOM and the utility source. The synchronization is accomplished in practice by the use of a Phase Locked Loop (PLL) that is locked to the line frequency. The PLL used in the model takes three inputs, the line voltages for phases A, B, and C, and produces a best estimate of the angle of the input waveforms. The output of the PLL is multiplied by a constant that increases the frequency to the carrier frequency. In the present case the desired carrier frequency is 1,500 Hz yielding a multiplier of 25.

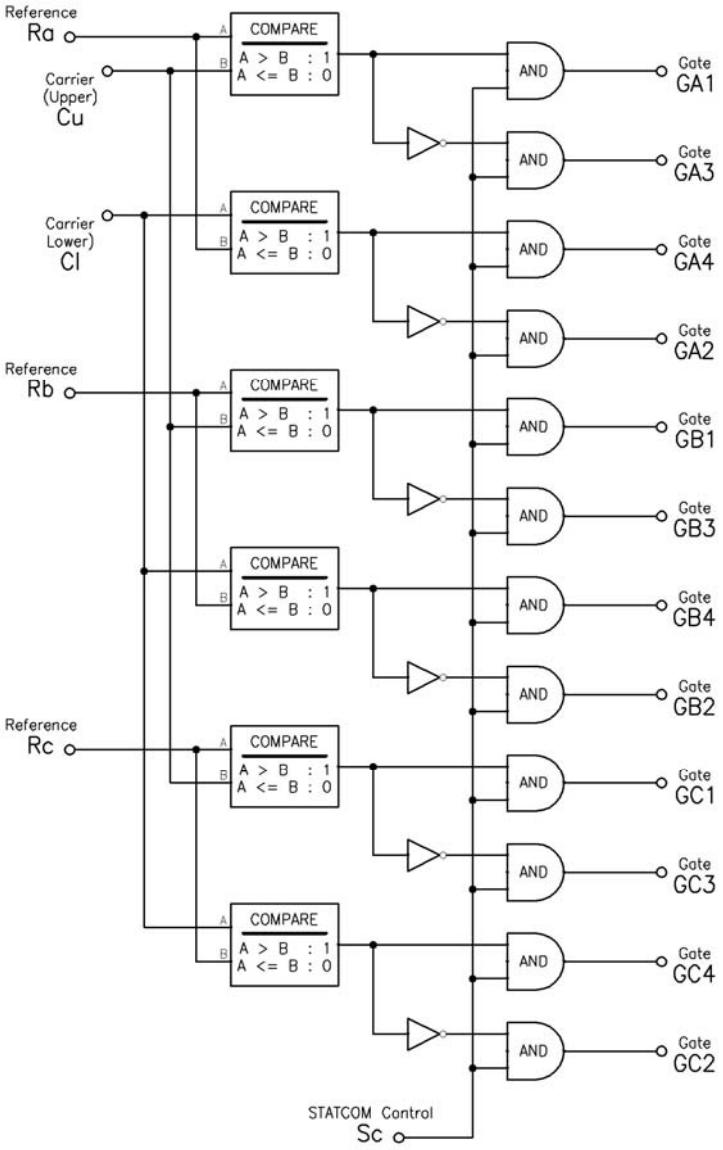

Fig. 8.9 STATCOM gating circuit diagram

The output of the multiplier, 25θ, is then conditioned by an 'angle resolver.' The angle resolver simply guarantees that the modified value of θ, which grows without limit during the simulation, is always between 0° and 360°. All that remains is to shift the waveforms to generate the upper and lower carriers, C_U and C_L. This is accomplished by the use of two programmable transfer function blocks, one arranged to shift the waveform up and the other to shift the same waveform down. It should be noted that the carriers and the reference waveform are both arranged such that an output of unity represents the full output of the STATCOM. The value of the reference voltages, R_A, R_B, and R_C, are scaled to a value appropriate to the actual voltages in the control section.

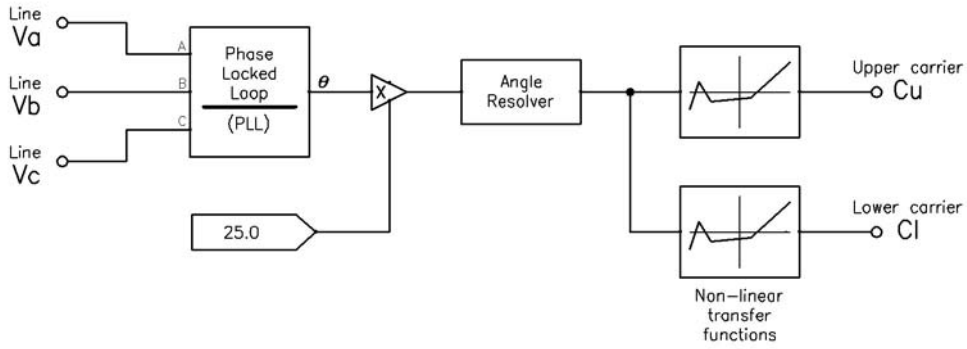

Fig. 8.10 STATCOM carrier generation

Compensation by STATCOM is based on the ability of the system to inject a desired value of current; the control consists of a simple Proportional-Integral (PI) controller. The arrangement of a single phase is shown in Fig. 8.10; there are two other identical arrangements for the other two phases. In operation, the control system takes a takes a value of the actual STATCOM line current and compares it with the desired STATCOM current; the desired current is determined by the overall compensation scheme which is described elsewhere. The method used is a straightforward Proportional-Integral (PI) control scheme but the values are modified by the voltage drop across the series inductor (see Fig. 8.4). This voltage drop is determined by using the fundamental relationship between inductor voltage and current, $e = L\dfrac{di}{dt}$, where the derivative is taken by the sT block and

the inductance (2.17 mH) is multiplied by this value. The results of the operations are summed along with the output of the PI sections.

The values of current that are actually measured by the system are in the base *PSCad* units, *i.e.*, kV and kA. As noted earlier, the carrier waveforms are based on a peak value of 1 Volt which means that the final reference value generated by the control scheme must be scaled by the value of the peak line-to-ground voltage. This value is the nominal line voltage, 7,200 V multiplied by $\sqrt{2}$.

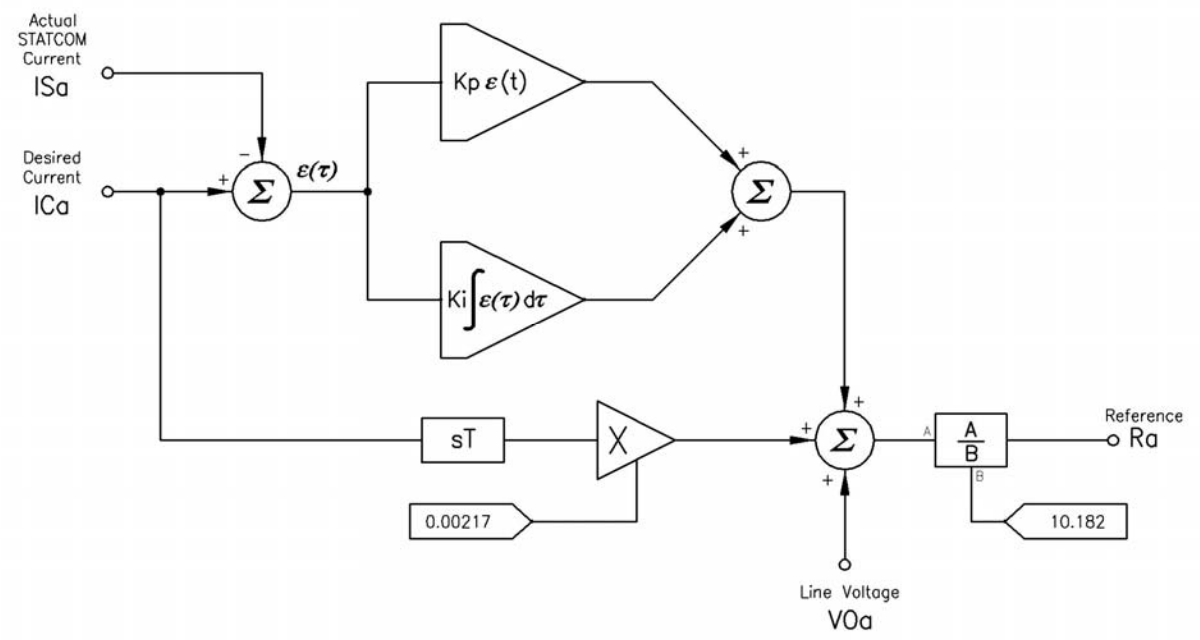

Fig. 8.11 STATCOM control diagram

The final part to the overall STATCOM configuration is a filter to reduce the carrier frequency from the output voltage waveform. The filter, shown in Fig. 8.12, has been constructed to duplicate the values of the filter in place at the subject facility. The documentation for the filter indicates a reference of "H-25 Filter Reactor." This nomenclature is interpreted to mean that the filter is a 25th harmonic type, *i.e.*, the central frequency is 1,500 Hz, a value that matches the carrier frequency of the STATCOM. A brief check using the basic relationship for a LC filter,

$$f_o = \frac{1}{2\pi\sqrt{LC}}$$

indicates that the frequency center frequency is 1,516.5 Hz. This value is close enough to the carrier frequency to confirm our earlier interpretation of the labeling. No effort was expended to determine bandwidth, *Q*, dampening factor or other details of the filter as it is a given part of the system; however, a Bode diagram was created so that the overall filter characteristics can be easily visualized.

The Bode plot was generated based on the circuit arrangement and the component values as shown in the filter schematic diagram, with the resulting transfer function being:

$$Z(s) = \frac{V(s)}{I(s)} = \frac{s^2 R_F L_F C_F + s L_F + R}{s(s L_F C_F + R_F C_F)} \tag{8-5}$$

A very quick calculation reveals that the insertion power lost in the filter, over all three phases is approximately 250 kW when the STATCOM is operational and about 25 kW when the STATCOM is off; these values closely match the values observed during the operation of the model. In the actual *PSCad* circuit, the filter is switched so that it can be easily removed from the circuit; in all subsequent discussion and the presentation of STATCOM waveforms the filter is switched into the circuit.

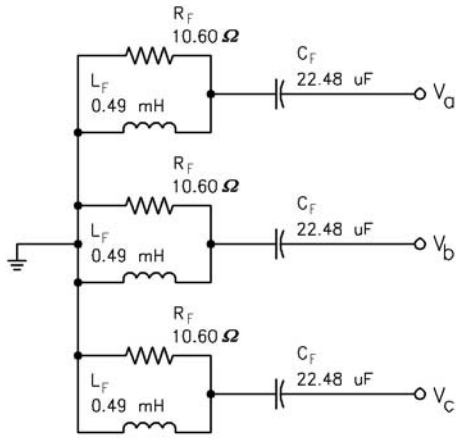

Fig. 8.12 STATCOM filter

Once the individual parts to the STATCOM are assembled all that remains is to determine the value of the control constants, *viz.*, K_P and K_I, devise a validation strategy, and then confirm the proper operation of the model. Upon a successful validation of STATCOM operation the standard *dq0* compensation method can be compared and contrasted with the LaGrange minimization technique.

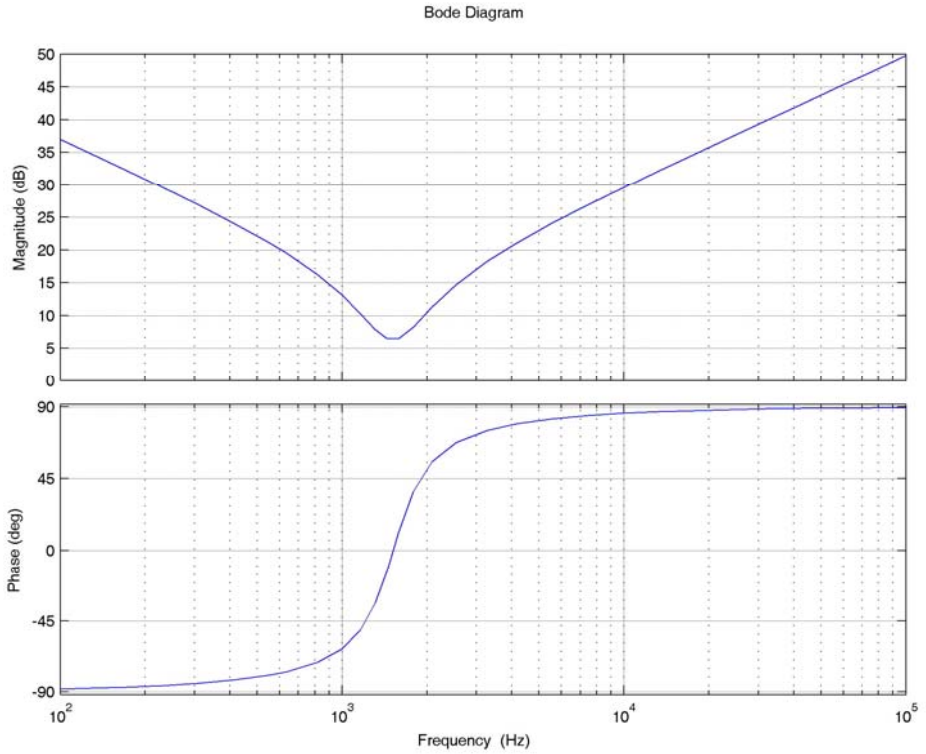

Fig. 8.13 Bode plot of STATCOM filter

8.5 – STATCOM validation

Arguably, the best method of validating the operation of a STATCOM involves directing the equipment to deliver inductive reactive power and capacitive reactive power at the rating of the equipment and then switching back and forth between the types of reactive power. An observation of the voltage, current, and power waveforms during the switching interval will prove the operation of the system; but first, a scheme must be derived that will allow an input to the system in the form of a positive or negative reactive power; the control scheme will translate this value into a reference voltage that is then applied to the various circuits as previously described.

Starting with equation (4-3), reproduced here for reference as (8-6),

$$\begin{aligned} S &= VI^{\dagger} = (V_d + jV_q)(I_d - jI_q) \\ S &= P + jQ \\ P &= V_d I_d + V_q I_q \\ Q &= (V_q I_d - V_d I_q), \end{aligned} \tag{8-6}$$

Putting the expression into matrix form gives:

$$\begin{bmatrix} P \\ Q \end{bmatrix} = \begin{bmatrix} V_d & V_q \\ V_q & -V_d \end{bmatrix} \begin{bmatrix} I_d \\ I_q \end{bmatrix}.$$

Inverting the matrix and solving for I_d and I_q gives:

$$\begin{bmatrix} I_d \\ I_q \end{bmatrix} = \frac{1}{V_d^2 + V_q^2} \begin{bmatrix} V_d & V_q \\ V_q & -V_d \end{bmatrix} \begin{bmatrix} P \\ Q \end{bmatrix}. \tag{8-7}$$

Because the STATCOM cannot provide real power, on a steady state basis, without an external active power source the value of P in (8-7) is zero. Making this substitution and solving for I_d and I_q gives:

$$I_d = \frac{V_q Q}{V_d^2 + V_q^2} \tag{8-8}$$

and

$$I_q = \frac{-V_d Q}{V_d^2 + V_q^2}\,. \tag{8-9}$$

The two expressions are reduced to block diagram form as shown in Fig. 8.14 and applied directly to the STATCOM model. In practice the desired value, Q*, is programmed to change at a particular time in the simulation to provide validation of proper STATCOM operation.

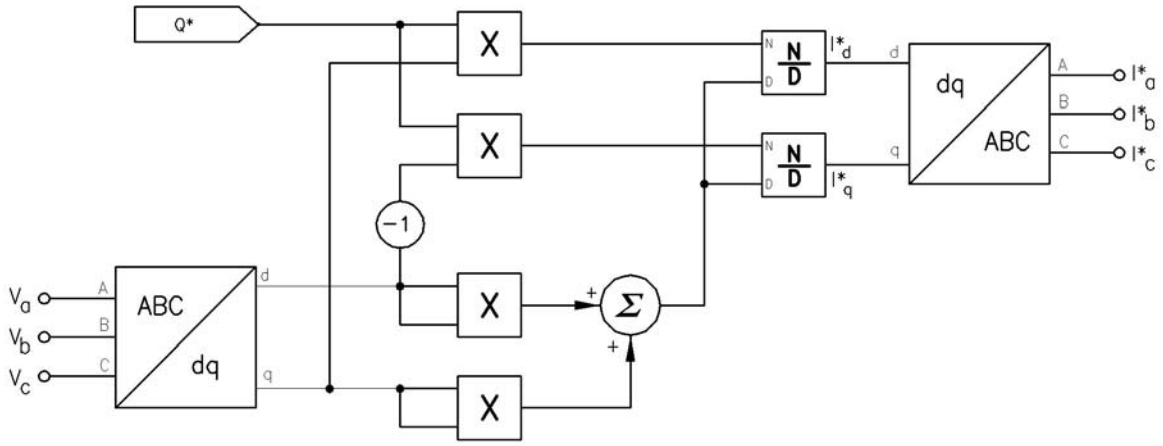

Fig. 8.14 Desired STATCOM output block diagram

The output of the circuit to drive the STATCOM to provide a specific reactive power output is fed into the input of the control circuit shown in Fig. 8.11, where it is identified as IC_A^*. Again note that the control diagram is only one of three phases; the other two inputs are from the 'B' and 'C' phase outputs of the $dq \rightarrow abc$ converter block.

The details of the validation process are as follow: First, the STATCOM is connected across the AC line; a pure sine wave is used for validation purposes. Then, at time $t = 0.10$ s, the STATCOM is turned on by raising the gate enable, control line S_C in Fig. 8.9, to a Logical '1'. At this time the STATCOM begins to deliver the requested reactive power, 20 MVA, to the line. Next, at time $t = 0.50$, the STATCOM is commanded to change the power from 20 MVA to -20 MVA. This first test is shown in Fig. 8.14.

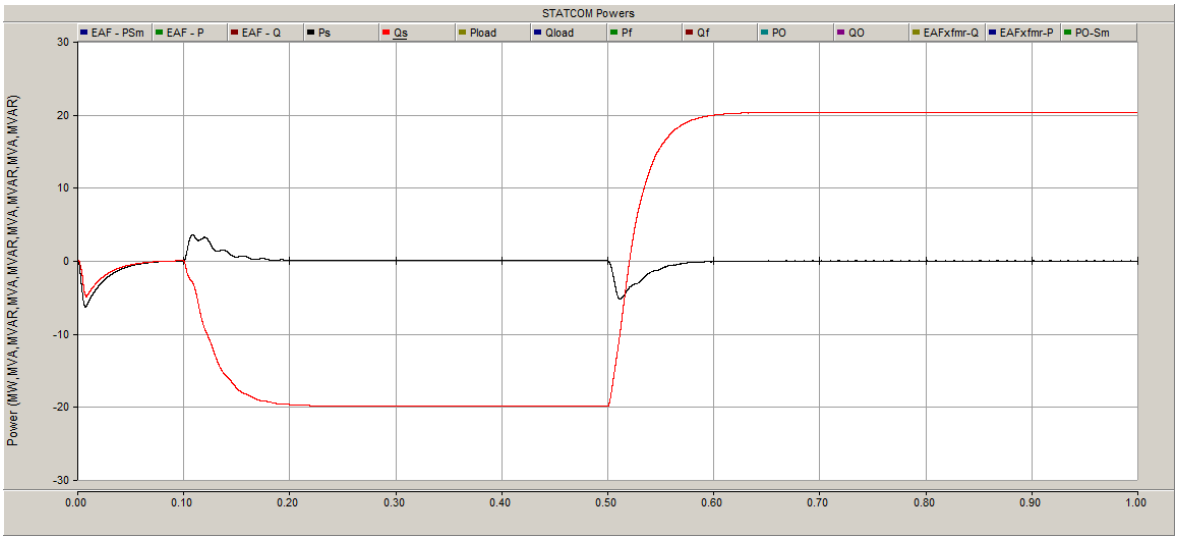

Fig. 8.15 STATCOM validation: Positive to negative reactive power transition

The power transition shown in Fig. 8.15 is derived from a three-phase Watt/VAR meter connected to the output of the STATCOM. Power flow through the meter is positive when the power is flowing away from the STATCOM, thus the positive value indicates that reactive power is being delivered; the command to actually deliver this power is a negative number.

In looking at the graph, the black trace is real power; the red trace is reactive power. The points of interest are the initial connection, $0 < t \le 0.1$s, when the STATCOM capacitors are charging; power out of the STATCOM is positive, so this is a negative value. The mid-range of the graph, $0.1 < t < 0.5$, the STATCOM is delivering the scheduled reactive power, 20 MVA, to the line. At time $t = 0.5$, the STATCOM is programmed to change from negative to positive reactive power. As can be seen, the transition is smooth, with the STATCOM producing -20 MVA after the transition interval.

The plot shows that the transition occurs in around 6 cycles but this is slightly misleading as the Watt/VAR meter is a three-phase device that averages the total power over one cycle. A better idea of the speed of the transition can be seen by looking at the voltage and current plots at the instant of transition as provided in Fig. 8.16. In this plot, the voltage waveform is in black; the current waveform is red. In order to plot the two waveforms at approximately the same visual magnitude, the current waveform has been scaled by a factor of eight.

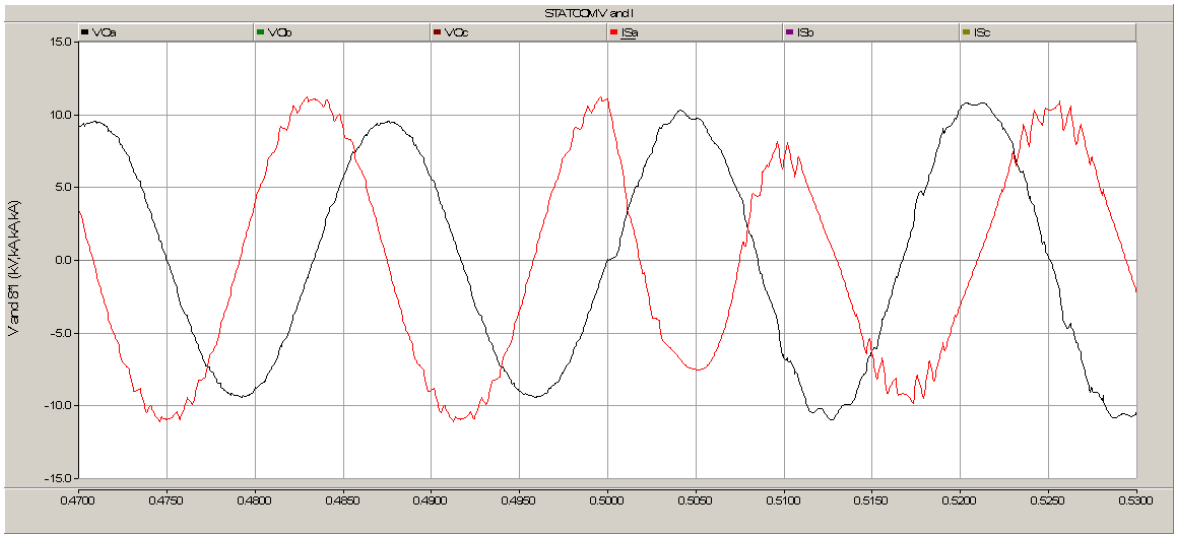

Fig. 8.16 STATCOM validation: Positive to negative voltage and current waveforms

In Fig. 8.15, which is plotted over the interval $0.1 \le t \le 1.0$, the instant of transition, $t = 0.5$, is the center of the plot. It can be clearly seen that the current waveform, which has been lagging the voltage waveform, shifts to a leading waveform in around a half of one cycle.

The reverse transition, from negative to positive reactive power is shown in Figs. 8.17 and 8.18. Again, it can be seen that the transition between the two reactive power delivery conditions is both fast and smooth.

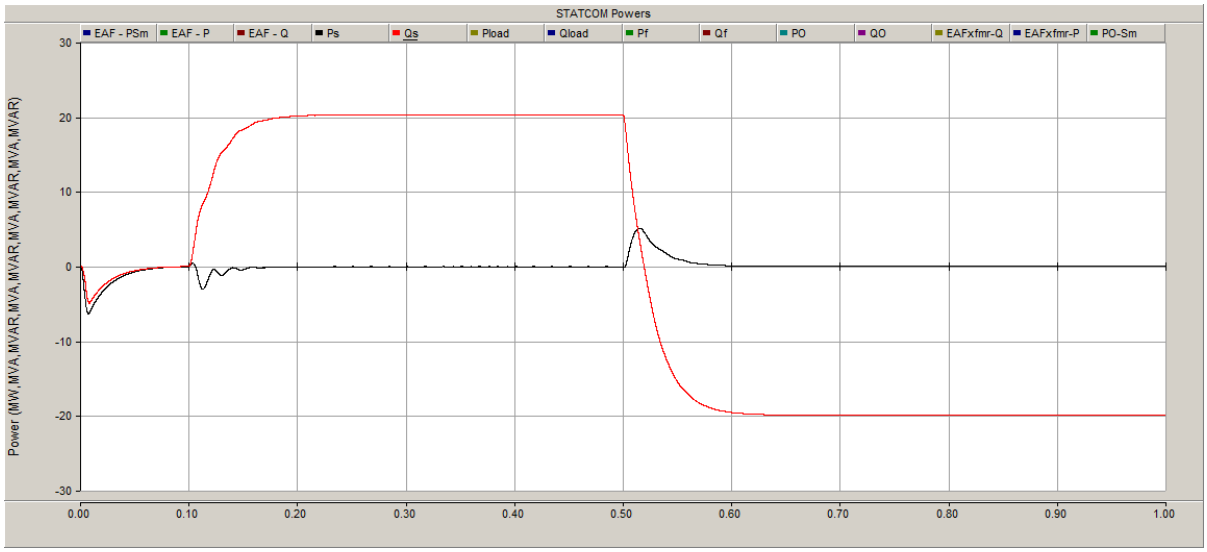

Fig. 8.17 STATCOM validation: Negative to positive reactive power transition

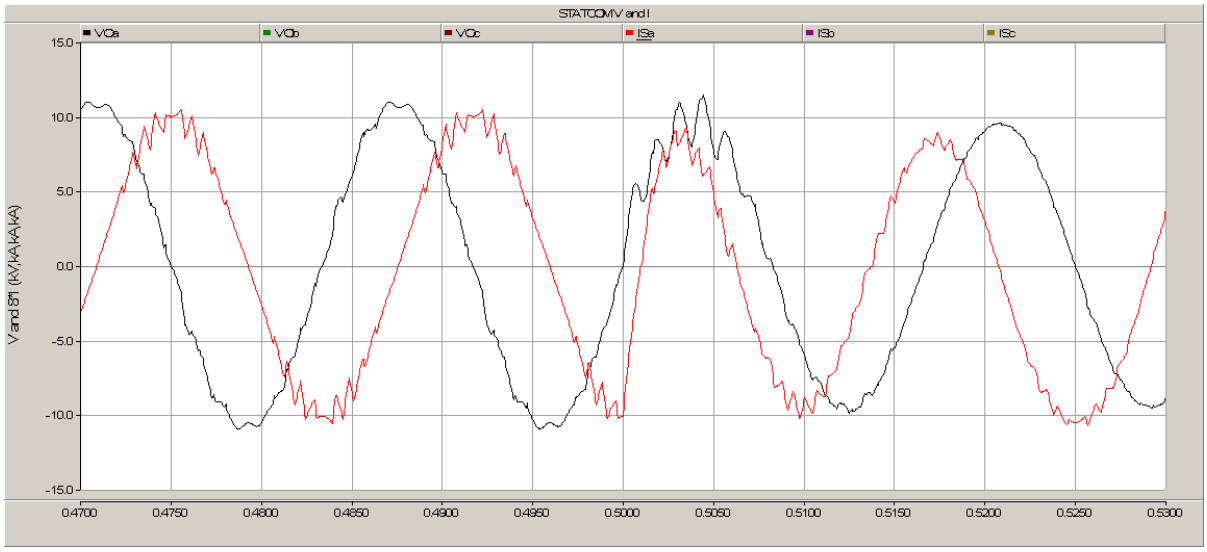

Fig. 8.18 STATCOM validation: Negative to positive voltage and current waveforms

With respect to the validation, a summation of the results is in order:

1. The STATCOM model will deliver either rated reactive capacitive or reactive inductive power to the line.
2. The transition between capacitive reactive to inductive reactive powers or *vice versa* is smooth.
3. The transition time for the current waveform between the two power extremes is fast, within about ½ of one cycle.
4. The real power delivered by the STATCOM is zero.
5. The calibration of the STATCOM is accurate, *i.e*., an input value of 20 MW, either positive or negative, actually delivers very close to the programmed value.

Based upon the above validation the STATCOM model is deemed to perform as designed; the next step is to provide a load for the combined utility-STATCOM system that approximates the load of an actual 33 MW Electric Arc Furnace.

9 – An Electric Arc Furnace Model

9.1 – Introduction

When the decision was taken to use modeled data rather that data captured from an operating EAF it was with the knowledge that there were many accurate arc models available and that there was one in particular that was ideally suited to the task at hand; that particular model was known to be available from the publishers of the previously referenced *PSCad* software package. The EAF model as described by an on-line document, included in Appendix M for reference, is intended to demonstrate the versatility and accuracy of the *PSCad* software by combining a power system, an EAF, a STATCOM compensator, and an IEC Flickermeter into a single model. The model is configured to demonstrate how the flicker generated by an EAF can be mitigated by the use of a STATCOM. This configuration, at least in its concept, is of the same general topology as the present system so, at the onset this seemed to be a very good place to obtain an EAF model; in the sequel, it turns out to be not so nearly ideal.

The *PSCad* EAF model is freely offered by the publishers of *PSCad*; it is furnished as a complete demonstration program and includes the source *FORTRAN* [65] code for the EAF component and the IEC Flickermeter. The demonstration package is identified as a 'beta' version and is not actively supported by the publisher; it was made available as a courtesy and was much appreciated.

Upon deployment of the model it was discovered that there were certain operational features that would make the model unsuitable for the intended purpose. Some of these were known *a priori*, as indicated below, and others were discovered during the course of the development. Briefly, the problems were the following:

1. The STATCOM model is not a neutral point clamped configuration. This was a known feature of the model.
2. The STATCOM model uses a control method that is not consistent with LaGrange compensation. Specifically, the control technique uses a *dq0* transformation which is to be totally avoided when using the LaGrange compensation scheme. This was a known feature of the model.
3. The EAF in the model uses a generation scheme that is described in a referenced publication. While the referenced document had been used to obtain the basic EAF

equations, the technique used by the EAF model is different from that described by the paper. This was unknown, but was ultimately unimportant to the final results.

4. The EAF model uses the same arc parameters for each of the three phases of the arc, resulting in an EAF load with no neutral current. This was unknown.
5. Other than several comments in the *FORTRAN* code, the model is undocumented. This was unknown.
6. The IEC Flickermeter is not compliant with IEC-61000-15-4, the flickermeter standard. [18] This was unknown but is not important in that flicker evaluation is not a consideration of the present work.

Use of the EAF model STATCOM was never considered an option, because of the topology and control, so initial work involved the development of the NPC STATCOM as described in the previous chapter. Upon completion and validation of this model the EAF model, as received from the publisher, was applied to the model. The result of this was that there was absolutely no difference in the *dq0* method and the LaGrange method. This was a very unsettling result, as it had been previously shown theoretically that the LaGrange method would produce superior control of harmonic content of the input waveforms. A detailed review of the model revealed that it was in fact a balanced model which produces no 'zero' values from the *dq0* transformations. It was previously mathematically proven that under balanced conditions the *dq0* method and the LaGrange method produce identical results. The next step became one of developing an EAF model that would produce the requisite neutral currents.

It is at this point that the lack of documentation of the model became a significant issue. Without documentation is was difficult to determine exactly how the model generated the very non-linear values of an electric arc. Significant time and effort was dedicated to 'reverse engineering' the code, including communications with individuals that were involved with the initial creation of the model, all to no avail. Ultimately, it was not possible to determine the exact operation of the model and the decision was taken to write a model that would satisfy the needs of the test protocol.

The model as provided is allegedly based on the publication, "A harmonic domain computational package for nonlinear problems and its application to electric arcs" [66] but it quickly became apparent that the model did not use the harmonic domain technique to generate the arc data. It did seem, however, that the two equations referenced in the advertising document are used in the generation process. There are many EAF models available, as previously referenced, but the present

model produces acceptable results, except for the difficulties previously indicated; the decision was made to use the same equations to develop a model that would have the following characteristics:

1. The model must be a single phase model that can be inserted into a circuit in any combined arrangement.
2. The model must allow easy definition of the parameters that control the electric arc characteristics.
3. The model must be independent of any other similar models, *i.e.*, the outputs must not be related in a way that would reduce the neutral currents that are seen in real-world EAFs.
4. The model must respond to changing characteristics of the circuit into which it is inserted, *i.e.*, the model cannot be driven by a simple voltage waveform.
5. The solution method for the defining equations must be both fast and accurate.

The equations referenced in [66] are the following:

$$\begin{aligned} k_1 \cdot r^n + k_2 r \frac{dr}{dt} &= \frac{k_3}{r^{m+2}} \cdot i^2 \\ v &= \frac{k_3}{r^{m+2}} \cdot i. \end{aligned} \tag{9-1}$$

In this expression, i is the current through the arc, v is the voltage across the arc, and r, is the arc radius in cm. The reference does not provide any clues to the physical meaning to the variables, *k1*, *k2*, and *k3*; these values must be determined experimentally. The values *m* and *n* are selected as based on information from the reference. After a comparison of several solution methods the modified Euler method, occasionally called Heun's method [67] was selected. The main reason for this selection is that intermediate values as would be needed in, for example, a Runge-Kutta solution, are not required. Note that data in a *PSCad* model is only available at discrete points; intermediate data points, if needed for a model, must be interpolated, introducing both time delays and inaccuracies that are not justified by the increased accuracy of the solution method. The modified Euler method is a second-order solution method that produces acceptable accuracy in a time frame that does not result in exceptionally long simulations.

9.2 – A *MatLab* validation of the EAF equations

Before the *PSCad* model was created it was thought appropriate to first determine an appropriate solution method and to validate the method with a *MatLab* program. The additional complexities of allowing actual circuit values to modify the variables in (9-1) are not present in the *MatLab* solution, so the solution method can be evaluated without bias. A *MatLab* program was written for this purpose, a source code listing of which is included as Appendix N for reference.

The *MatLab* program is intended to reproduce the results of [66]. As such it drives the equation set of (9-1) with current source that is a pure sine wave at 60 Hz. The program has three separate sections, one to perform the solution using the Euler method, another to perform the solution using the Runge-Kutta method, and a final solution using the modified Euler method. In the source code listing in the appendix all sections except the final modified Euler solution are commented out with the *MatLab* comment character, "%"; by relocating the comment characters the code may be easily used to provide the results from either of the three methods.

In using *MatLab* to solve the equation set as driven by a pure sine wave current source we have the advantage of knowing *a priori* what the current will be at any instant of time. This knowledge is necessary for the Runge-Kutta solution method, either by direct knowledge or by interpolation. In the real-world current through the arc would be determined by circuit constraints and would only be available at intermediate points through interpolation of one type or another. Obviously interpolation takes more time, giving reason to avoid the method if other, speedier, solutions are available.

The *MatLab* simulations demonstrated that all three solution methods gave acceptably accurate results when the equation set was driven with a sine wave. The original Euler method was rejected as it was (correctly) believed that the unpredictable nature of the actual current waveform would lead to erroneous results due to the well-known problems with accuracy of this method. [67] The Runge-Kutta method was rejected because of the problem of obtaining information at times other than at the discrete evaluation points. The method of choice, then, is the modified Euler method. The results of this solution method, using a *MatLab* program, are presented in Figs. 9.1 – 9.3. The current plot is not presented in the series of output from the *MatLab* program since this plot is simply a pure sine wave. The plots that are presented, *viz.*, arc radius, voltage, and voltage *vs.* current, are indistinguishable from the plots presented in [66].

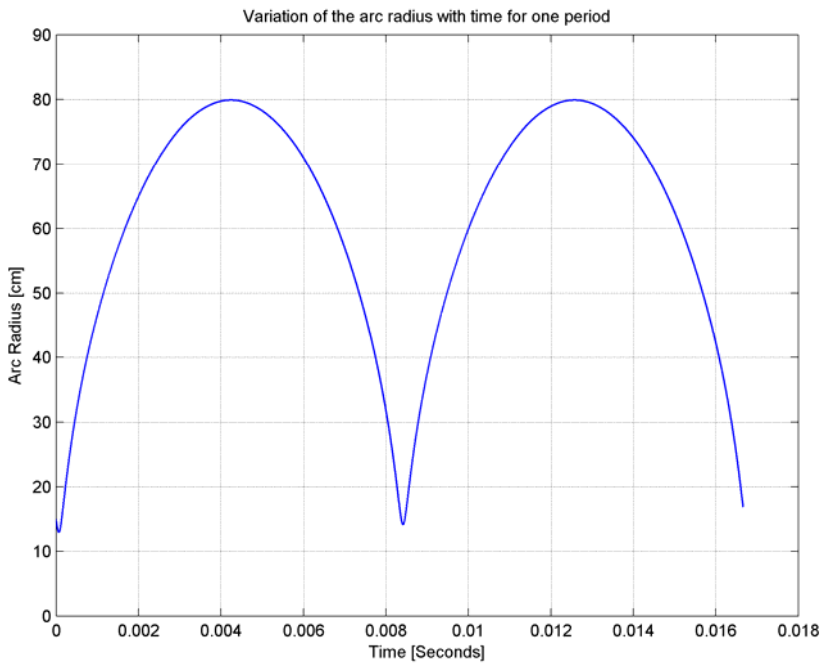

Fig. 9.1 *MatLab* simulation: Arc radius for pure sine wave current source

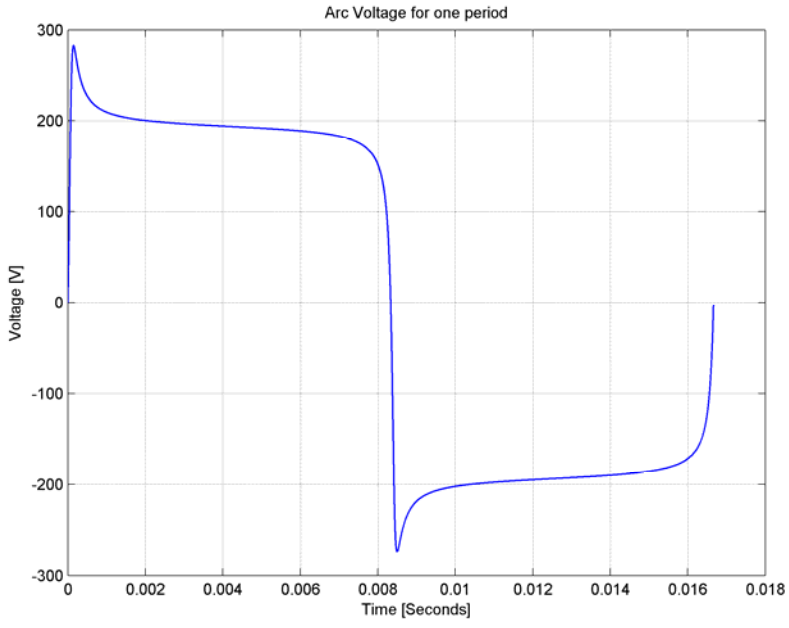

Fig. 9.2 *MatLab* simulation: Arc voltage for pure sine wave current source

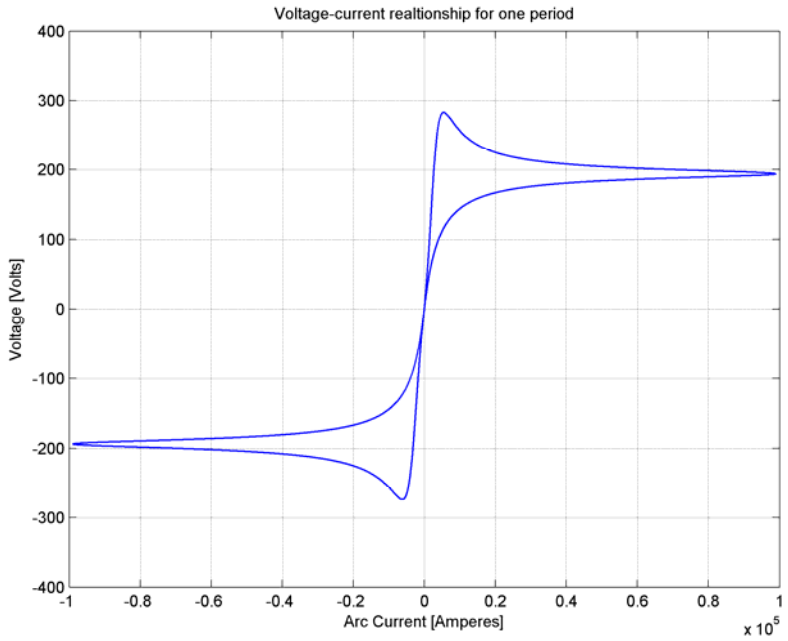

Fig. 9.3 *MatLab* simulation: Arc voltage *vs.* arc current for pure sine wave current source

9.3 – *PSCad* solution to the EAF equations

The next step is to apply the modified Euler solution method, now verified as accurate by a *MatLab* simulation, to the *PSCad* model. This turns out to be a considerably more difficult problem since the EAF model in the *PSCad* simulation will be driven by the actual line voltage rather than by a simple current. Although the simulation is the same, the determination of the discrete evaluation points is must be approached from a completely different direction. The solution method within *PSCad* is probably best explained with the assistance of a flow chart of the overall program. Keep in mind that the flow chart, presented in Fig. 9.4, shows only the computations involved in the actual component; the setup of the component within the *PSCad* structure is a completely different issue and is described in detail later.

The EAF model *FORTRAN* routine begins by the usual housekeeping functions: loading of the 'include' blocks, declaration of variable names, and the setting up of vector locations for the storage of variables that must be passed from one iteration to the next. This is followed by a section for initialization of values for the first pass through the routine. The specific values stored are the arc radius, R_{last}, and the current, I_{last}. This section is not used again as in subsequent iterations the values used will be those determined from the previous iteration.

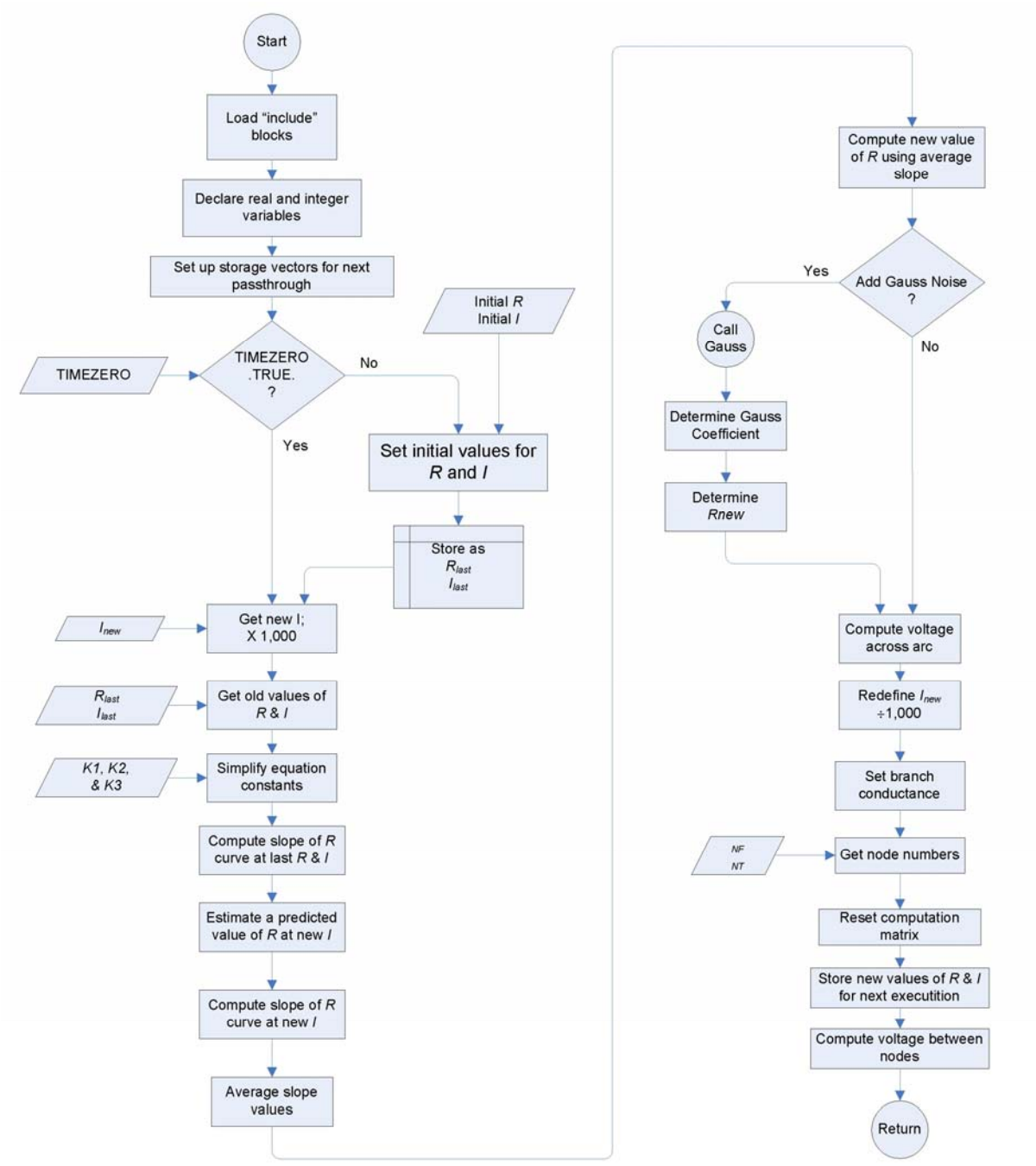

Fig. 9.4 Flow chart of *PSCad* EAF arc model

The next section of code retrieves the new value of current, I_{new}, and the old values of the arc radius and arc current, R_{last} and I_{last}. Note that the value of current that is extracted from the *PSCad* routine must be multiplied by 1,000. The reason is that the actual extracted value is in Amperes (A) while the remainder of the circuit values is in thousands of Amperes (kA) or thousands of Volts (kV). The reason for this is not immediately obvious; it may be an internal issue with the way the current value is extracted from the *PSCad* engine. In any case, extracted current values are Amperes; they must be multiplied by 1,000 to have the final value in kA.

With all the necessary values in hand, the modified Euler method may be applied to determine the next value of arc radius. This computation involves the determination of a slope of the R curve at the last values of R & I; this value is then used to predict a new value of R & I. For part two of the modified Euler method a slope is computed for the R curve at the predicted values of R & I. Next, the two slopes are averaged and then the final arc radius output for the iteration is a value of R based on the averaged slope and the value of the last computed value of R. Once R & I are known, the computation of arc voltage is a simple operation.

Following the application of the modified Euler method, the new current must be divided by 1,000 to return it to the *PSCad* engine. The remainder of the operations is to set the branch conductance for the next iteration, reset the computation matrix, and get node numbers for a direct calculation of the voltage across the arc. The values of R & I are stored for the next iteration and then, the final step, the actual voltage across the arc is computed after which the component subroutine returns control to the main *PSCad* program.

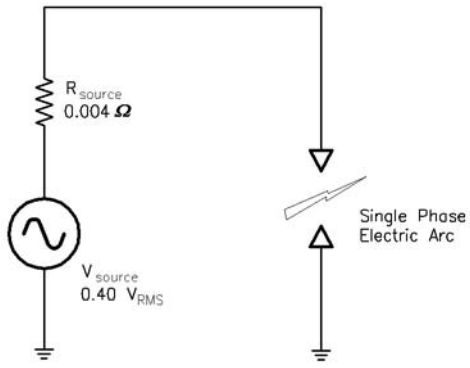

Fig. 9.5 Single phase EAF model test circuit

The single phase EAF model is tested with the circuit as shown in Fig. 9.5. The values used in this circuit are intended to closely approximate the magnitude of the source impedance as used in the final model. The value of the source voltages matches the EAF source voltage in the subject steel plant.

The difference in driving the model with a pure sine wave, as in the *MatLab* simulation, and driving it with a voltage, as in the *PSCad* simulation is obvious from the waveforms as shown in Figs. 9.6 – 9.9. The first major difference noted is in the plot of arc radius, R, *vs*. time, as shown in Fig. 9.6. In the current driven model the arc radius comes to a single sharp minimum value and then increases; in the voltage driven model the value decreases smoothly to a minimum and then remains quite low for a length of time. Note that in both cases the value of arc radius never reaches zero.

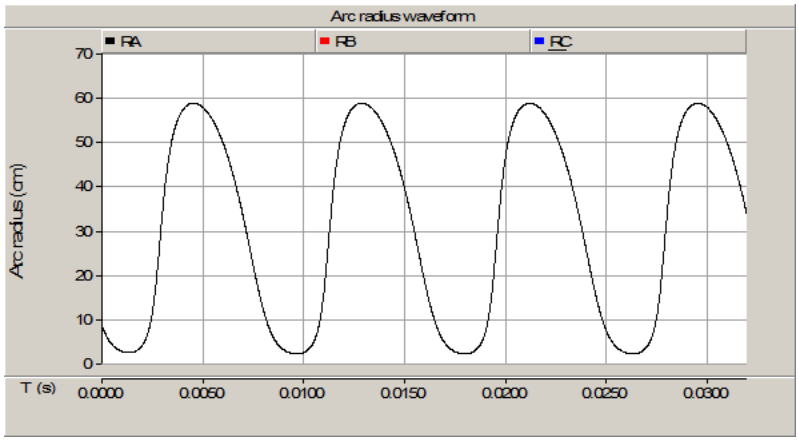

Fig. 9.6 *PSCad* model: arc radius

The driving waveform that is used in the *MatLab* model is a pure sine wave. The *PSCad* model is driven by the actual circuit constraints as based on the voltage supplied to the arc – as limited by circuit impedances – so it is expected that the actual current through the arc would not be sinusoidal. This is in fact the case; the arc current is shown in Fig. 9.7. It is to be noted that the arc current remains at or very near to zero for a considerable length of time. Even though the current through the arc remains near zero and then reverses the arc does not visually appear to extinguish as the plasma remains at the location of the arc until the re-ignition that occurs at the next cycle. Again, it is noted that the arc radius never falls to zero once the arc is established.

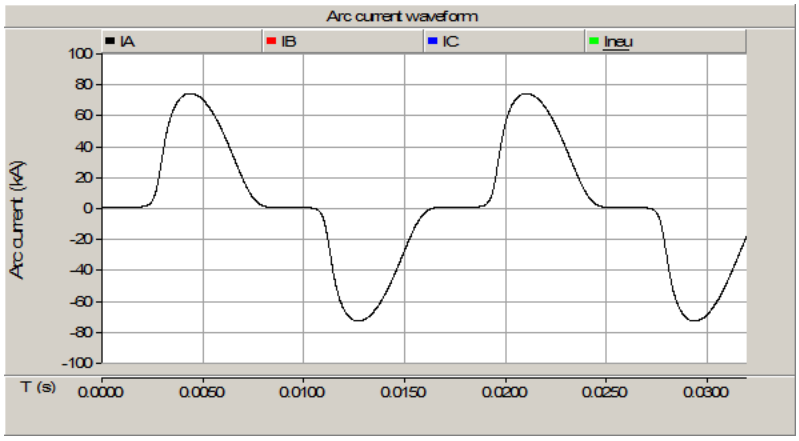

Fig. 9.7 *PSCad* model: arc current

The arc voltage in the *PSCad* model reflects the re-ignition sequence. The voltage increases rapidly after the current zero-crossing, and then drops as current begins to flow through the arc. The voltage across the arc is shown in Fig. 9.8.

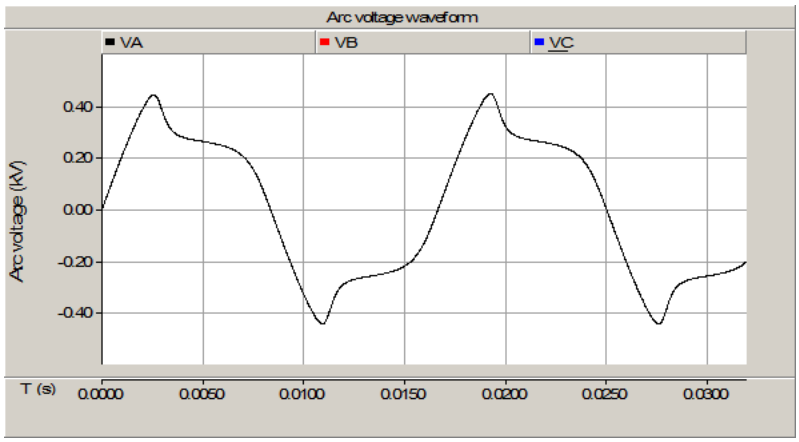

Fig. 9.8 *PSCad* model: arc voltage

The definitive plot for an EAF arc is the current *vs.* voltage plot. This is presented in Fig. 9.9 and demonstrates that the *PSCad* model closely matches the arc characteristics of an actual operating

EAF. In this figure the horizontal axis is current in kA; the vertical axis is in kV x 100. As an aside, it is noted that there does not appear to be a way to present the actual values of the different axes in a P*SCad* x-y type plot.

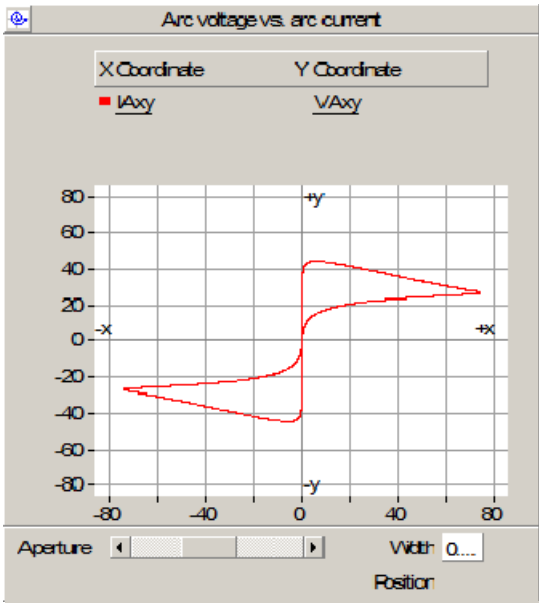

Fig. 9.9 *PSCad* model: arc voltage *vs.* arc current

9.4 – Neutral current from the EAF model

The entire purpose of creating a single phase EAF model is to provide a means to generate neutral currents as are seen in steel plants that utilize EAFs. In order to demonstrate the effectiveness of the EAF model a plot was extracted from the final simulation that compares the *dq0* compensation to the LaGrange method. Fig. 9.10 shows that the individual phase currents combine to yield neutral current that flows in the system and that contributes to the '0' component of the *dq0* compensation scheme.

In Fig. 9.10, the Phase A current is black, the Phase B current is red, and the Phase C current is blue; the neutral current is green. The line voltage in the plot is the utility source, 12.47gndY/7.2 kV; the currents are the utility line currents. The plot is generated at a time before the compensation is engaged, so the total power to the arc is 23 MW with a reactive power of 18 MVA. As can be seen from the plot, the total power is, like a real EAF, not equally distributed to the individual phases.

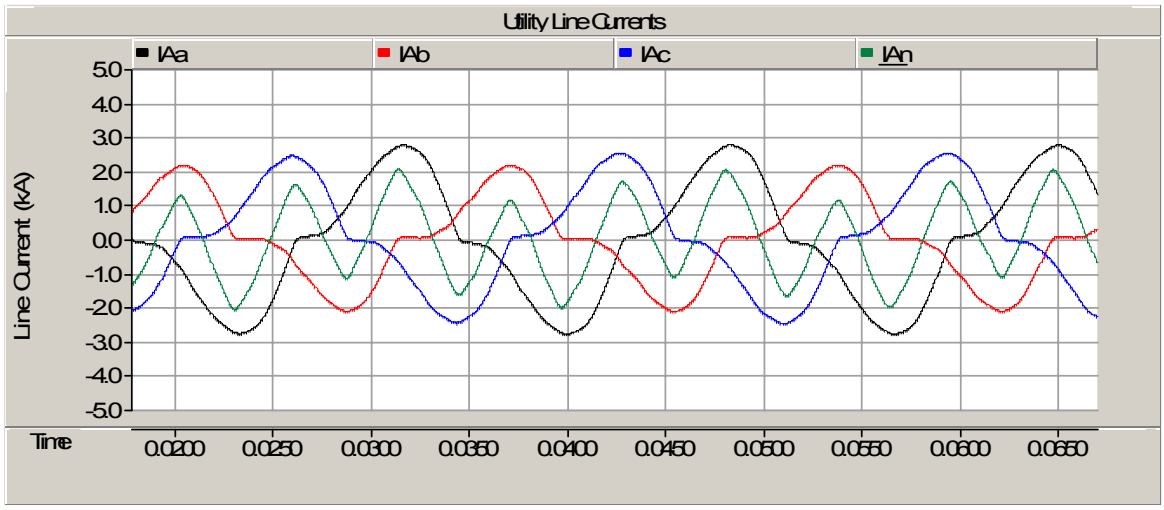

Fig. 9.10 Utility line current for three EAF models connected in wye

9.5 – The addition of Gauss noise

There are two major characteristics of an electric arc that are important from the modeling point of view, (1) the non-linear nature of the arc's voltage *vs*. current characteristic and (2) the stochastic nature of the arc itself. The first has been modeled quite effectively by the equations of [66]; the second can be approached by introducing Gaussian noise to the model.

In an effort to make the model more realistic *FORTRAN* code has been generated to add Gaussian noise to the model. The particular approach taken is to allow the noise to act on the arc radius, R; the resultant current and voltage then necessarily include the effects of the noise, the same method as used by the original three-phase EAF model provided by [60]. Although the original version of the three-phase model is not documented the method was determined to be the same as was used in [68] and in fact appears to be taken, for the most part, line-for-line from this source. The root source of the method was determined to be [69]. The flow chart for the addition of Gaussian noise is presented in Fig. 9.11.

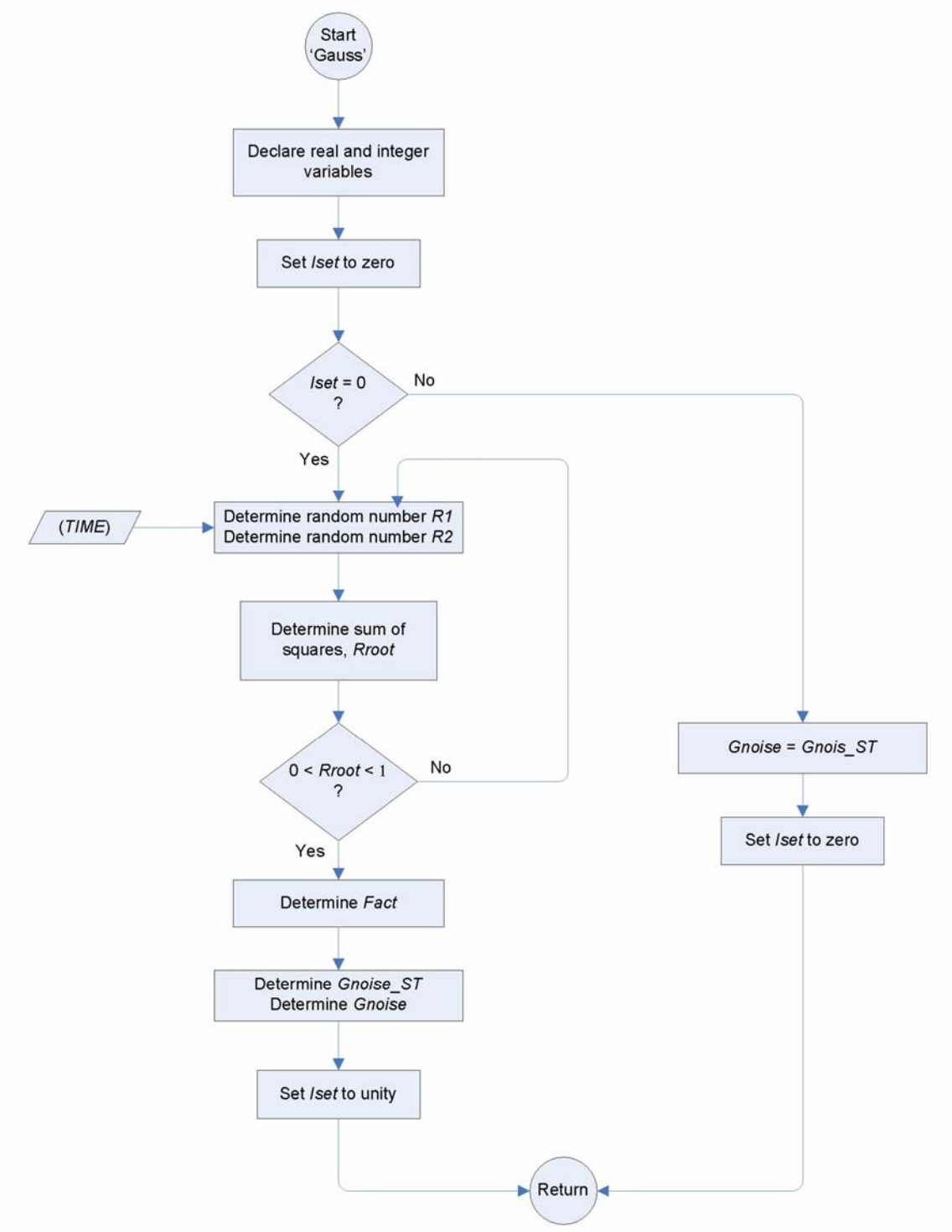

Fig. 9.11 Flow chart of Gauss noise addition to EAF model

In operation, the Gauss addition subroutine actually computes *two* values that are used to adjust the arc radius even though only one of the values is actually used each time the routine is called. The routine keeps track of the number of times that it is called and computes a pair of values every other time it is called. The actual calculation depends first on the generation of a pair of random numbers. The seed number to generate the random numbers is the *TIME* variable from *PSCad*. These numbers are conditioned so that the final random number is greater than zero but less than one. The actual Gauss factor is generated by using the equation from [69]:

$$F_{act} = \sqrt{\frac{-2\log(R_{root})}{R_{root}}} \tag{9-2}$$

Note that under the inequality conditions set by the testing of variables that the value of R_{root} is guaranteed to be less than one, so the logarithmic expression $\log(R_{root})$ will always be negative; the multiplication by -2 will thus always result in a positive term under the radical. The two Gauss noise values are computed by multiplying the Gauss factor determined above by the random numbers previously determined. One is used immediately and is returned to the calling program; the other is stored and on the next iteration it is used for the returned value. Once the value of the Gauss factor is returned to the calling program it is multiplied by the desired Standard Deviation and then applied to the value of the arc radius that was determined by the modified Euler method.

While the addition of Gaussian noise is necessary for a realistic EAF model, it is not actually used in the present work, being only included to make the single phase arc model more realistic and useful. In the present work we are only concerned with the delivery of power to the arc and the harmonic content of the input waveform; the addition of noise would only complicate this analysis as it would have to be removed by filters before useful power and harmonic data could be obtained. It is expected that the major usefulness of the noise feature of the model will be in flicker analysis, where the random nature of the arc is a significant contributing factor to the flicker phenomena.

9.6 – A *PSCad* implementation

One of the features that make *PSCad* so valuable as a simulation tool is the ability to create custom components that can meet specialized requirements. While this ability is available, the actual creation of a custom component is not a simple process. While it is not the goal of the present work to be a primer of *PSCad*, it is appropriate that a few notes should be provided to assist future

researchers in duplicating the single-phase arc model described herein; toward that end detailed listings and screen shots are provided in Appendices O and P. The following section will detail the three major sections of *PSCad* that deal with the creation of a new component; also, these same sections are used should it be desired to modify an existing component. These sections are accessed by right-clicking a component and then selecting 'Edit Definition' from the drop down menu that will appear.

Graphic: This tab allows the creation of a graphic symbol to represent the component. The only item important in the graphic is the names assigned to the nodes that will connect the component to the circuit into which the component is inserted. The actual shape and arrangement of the component is totally unimportant to the way the component is integrated into the *PSCad* solution.

Parameters: This tab provides a mechanism to allow values to be input into the component model. These parameters can be individual values that are used in the computations associated with the component, different configurations for the component, or spaces where custom names can be assigned to various internal values within the component. In the present model the following parameter values are provided under the basic 'Configuration' heading.

Is the component grounded?	Yes/no
Add Gauss noise?	Yes/no
Enter model parameters:	*k1*, *k2*, *k3*, *m*, *n*, initial arc length

A heading was created called 'Outputs.' Under this heading the internal variables V_{arc}, I_{arc}, and R_{arc} are displayed with provisions for adding an external variable name to each. This is an important feature as it allows internal values to be extracted from the model. The feature of allowing the user to assign names is vital when more than one instance of the model appears in a single simulation. A further section called 'Gauss noise' was created to allow the user to input the standard deviation of the Gauss noise to be applied. This section is not visible if 'no' is selected under the 'Add Gauss noise' parameter above.

Script: The Script tab offers three sections, *FORTRAN*, Branch, and Computations. The *FORTRAN* section calls the *.f* (or *.for*) *FORTRAN* source code that defines the component. In this section internal and external variables are defined so that they can be accessed by the *PSCad* engine. In the present model the name of the called program is *EAF.f*; it contains both the main source code that defines the electric arc and the subroutine that is used for the generation of Gauss noise.

The second part of this tab is the 'Branch' section. In this section the actual connections that relate the graphic to the model are defined. In this particular model there is a selection that allows the arc model to be used either as a grounded element or as a free-floating element that can be connected between any two nodes.

The third part of the 'Script' tab is the 'Computations' section. This section is provided as a place to define global calculations that may be used by any other section of the model. For example, this section might be used to define a degrees-to-radians conversion. In the present work it is not used; it is mentioned only for technical completeness.

As one of the goals of the present work is to provide sufficient information so that the model can be easily recreated by others, a complete listing of all the above sections, as well as the *FORTRAN* source code, are provided in the Appendices.

9.7 – A *RSCad* validation

It was previously noted that EAFs are large electrical loads and that it would be unlikely that a steel mill would interrupt its product (and profit) stream to allow experimental work to be done on their STATCOM. It is for that reason that a simulation on a real-time platform has value in demonstrating that a new method will function properly in the real-world. A Real Time Digital Simulator (RTDS) is available and the EAF model software was modified to run on that platform. This work was performed by Saman Babaei, a PhD graduate student in the Electrical Engineering Department at NC State University. The results of the simulations are not to be considered a part of the present work and are presented only to demonstrate that EAF model can be operated in a real-time environment.

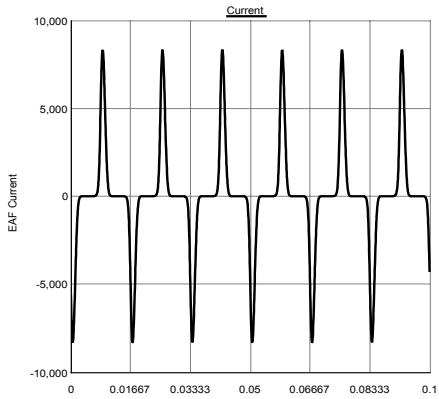

Fig. 9.12 *RSCad* model: arc current

Fig. 9.12 shows the arc current through the *RSCad* model, followed by Fig. 9.13, the arc voltage, and Fig. 9.14, the arc voltage *vs.* arc current plot. It is noticed that there are differences in the plots as the values in the RTDS system do not correspond to those in the *MatLab* and *PSCad* versions. It is recognized that the parameter values have not been correlated; the purpose for providing the plots is to demonstrate that the modified Euler solution will also function with the *RSCad* software. There are additional comments in the Conclusions and future work section regarding the desirability of additional real-time simulations.

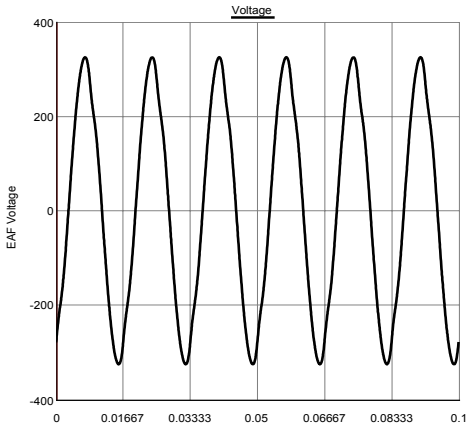

Fig. 9.13 *RSCad* model: arc voltage

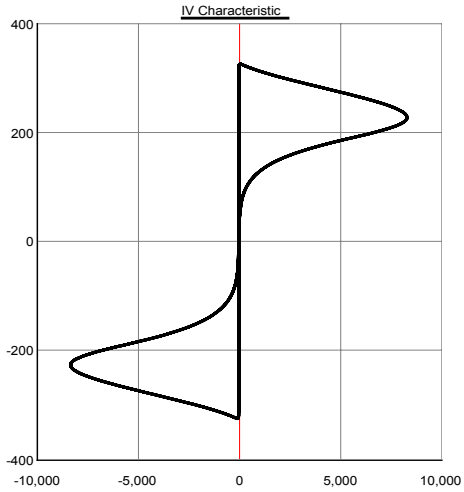

Fig. 9.14 *RSCad* model: arc voltage *vs.* arc current

10 – A comparison of *dq0* and LaGrange compensation strategies

10.1 – Introduction

With both a validated STATCOM model and an accurate arc model it is now possible to perform an equitable comparison of the *dq0* and LaGrange compensation schemes. The theory of the two schemes was presented earlier, along with results that were derived by assuming that the compensation schemes were 'perfect', *i.e.*, there were no losses or other real-world issues involved. In applying the methods to a real, albeit modeled, system it is necessary to first develop the necessary structure to apply for both of the two methods. The development will begin with the traditional *dq0* method.

10.2 – Development of the *dq0* method for application to STATCOM compensation

The basis of the *dq0* compensation method was presented by Akagi in [55]. The method directs the STATCOM to provide to provide the reactive power needed by the load, effectively removing the requirement that the utility source provide the reactive component of complex power. In development, the method begins with the solution of the solution of the matrix equation to determine the direct and quadrature values of current, I_d and I_q as presented earlier as equation (8-7) and reproduced here as equation (10-1) for convenience:

$$\begin{bmatrix} I_d \\ I_q \end{bmatrix} = \frac{1}{V_d^2 + V_q^2} \begin{bmatrix} V_d & V_q \\ V_q & -V_d \end{bmatrix} \begin{bmatrix} P \\ Q \end{bmatrix}. \tag{10-1}$$

The goal is to direct the STATCOM to deliver a current that effectively removes the reactive power, so the desired value of Q is simply the negative of the reactive component, *i.e.*, $-Q$. The STATCOM cannot deliver real power on a continuous basis without an external energy source, which is not provide in the present case, so the STATCOM must be directed to deliver a value of $P = 0$. From (8-6) we have the relationship for Q in terms of the direct axis and quadrature axis load voltages and load currents:

$$Q = V_q I_d - V_d I_q. \tag{10-2}$$

Using P=0 and the negative of (10-2) in equation (10-1) gives:

$$\begin{bmatrix} I_d^* \\ I_q^* \end{bmatrix} = \frac{1}{V_d^2 + V_q^2} \begin{bmatrix} V_d & V_q \\ V_q & -V_d \end{bmatrix} \begin{bmatrix} 0 \\ (V_d I_q - V_q I_d) \end{bmatrix}. \tag{10-3}$$

In equation (10-3) the values voltages, I_d^* and I_q^* are the desired values of direct and quadrature current that must be subtracted from the load current by the STATCOM in order to deliver the negative value of the reactive power under the constraint that the real power remains zero. Performing the matrix multiplication gives the following explicit values for I_d^* and I_q^* :

$$\begin{aligned} I_d^* &= \frac{V_q (V_d I_q - V_q I_d)}{V_d^2 + V_q^2} \\ I_q^* &= \frac{V_d (V_q I_d - V_d I_q)}{V_d^2 + V_q^2}. \end{aligned} \tag{10-4}$$

The values determined in (10-3) are incorporated into circuit elements as shown in Fig. 10.1, the negative of which is inserted directly into the STATCOM model as the desired output current. It is important to an understanding of the overall concept of the LaGrange method to notice that the transformation blocks used in the diagram are the *dq0* $\rightarrow$ *abc* and *abc* $\rightarrow$ *dq0* blocks*, i.e.*, the blocks have the "zero" element even though it is not used. In the transformation from the three-phase system to the two-phase system the zero component is not used; in the re-transformation from the two phase system back to the three phase system the value of the zero element is physically set to 0. It is at this specific location in the strategy that the loss of a degree of freedom previously mentioned occurs.

At this point it might be well to point out the reasons that the zero component cannot be used in the *dq0* approach. There are three outputs from the Clarke transformation, two related to two-phase waveform – these are 90° out of phase with each other – and a third component that is simply a single phase waveform that represents the part of the original *abc* set that is not balanced. The zero value is not tied to the two-phase waveforms; it changes from instant-to-instant as the degree of balance changes. Should there be both a voltage and a current waveform, as in the present case, there is indeed power in the zero component, but there is no way to determine (on an instantaneous basis)

the relationship between the two waveforms. It is for this reason that real and reactive instantaneous single phase power cannot be determined from the *dq0* approach.

It is fairly obvious that the total amount of power – either real or reactive – is small, as the voltage waveforms are generally well balanced, resulting in a relatively small zero component for voltage. As power is the product of these quantities, the result is that net power is also small. The same cannot be said of the current waveform. As we have observed from the captured data, the unbalance of the current is significant and results in a significant amount of current that cannot be compensated using the *dq0* approach.

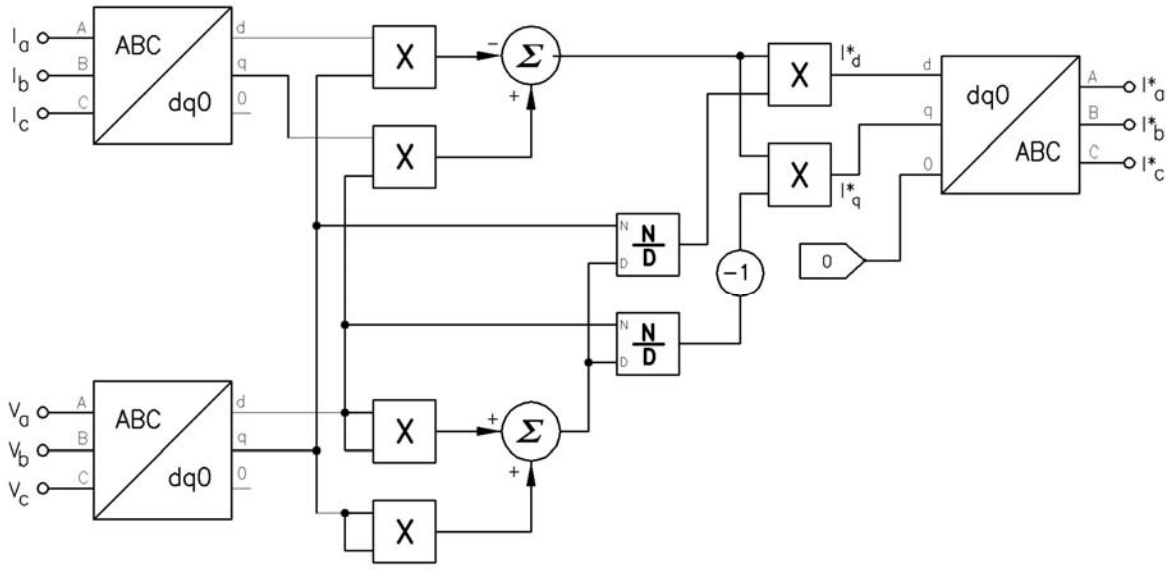

Fig. 10.1 Reactive power compensation using the *dq0* method

10.3 – Development of the LaGrange method for application to STATCOM compensation

The basis of the of the removal of passive currents by the LaGrange method was previously described and culminates with the passive currents in ABC format presented as equation (6-9), presented here for convenience as equation (10-5):

$$\begin{bmatrix} i_{Pa} \\ i_{Pb} \\ i_{Pc} \end{bmatrix} = \begin{bmatrix} i_a \\ i_b \\ i_c \end{bmatrix} - \frac{(v_a i_a + v_b i_b + v_c i_c)}{v_a^2 + v_b^2 + v_c^2} \begin{bmatrix} v_a \\ v_b \\ v_c \end{bmatrix}. \tag{10-5}$$

This matrix equation expressed the passive current required by the load; it is expanded in equation set (10-6) to show the individual desired passive phase currents. Again, the currents identified as the 'desired' currents are those that we wish the STATCOM to subtract from the actual load currents. It is recognized that it would be simpler to change the signs in control block rather than later, but this notation was selected to maintain a similar presentation of both the LaGrange and *dq0* compensation techniques. The diagram that embodies the application of the equation set (10-6) is shown in Fig. 10.2.

$$\begin{aligned} i_a^* &= i_a - v_a \frac{(v_a i_a + v_b i_b + v_c i_c)}{v_a^2 + v_b^2 + v_c^2} \\ i_b^* &= i_b - v_b \frac{(v_a i_a + v_b i_b + v_c i_c)}{v_a^2 + v_b^2 + v_c^2} \\ i_c^* &= i_c - v_c \frac{(v_a i_a + v_b i_b + v_c i_c)}{v_a^2 + v_b^2 + v_c^2} \end{aligned} \tag{10-6}$$

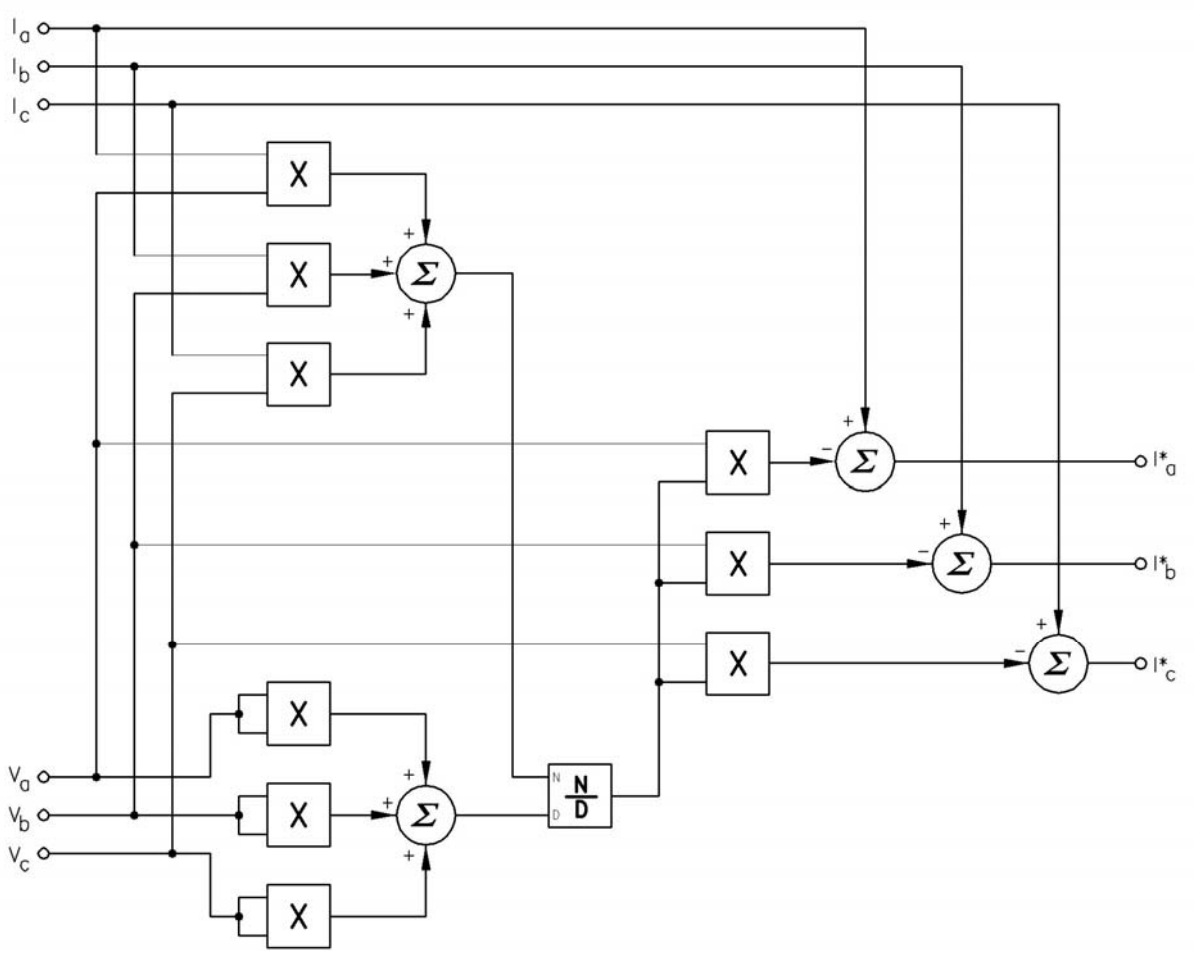

Fig. 10.2 Reactive power compensation using the LaGrange method

10.4 – Relative complexity of the LaGrange method

As mentioned previously, the physical equipment needed to implement LaGrange compensation is identical to that required for the implementation of the *dq0* method. There are, however, some computational differences in the two methods. The following is a brief comparison of the fundamental operations required to implement the two schemes.

The *dq0* scheme embodies three instances of the Clarke transformation: two to transfer the input current and voltage into *dq0* space and a third instance to re-transform back to *abc* space. Each operation of the Clarke transformation requires nine multiplication operations and six addition

operations. Each of the other operations that appear in the scheme is individually indicated on the diagram shown in Fig. 10.1.

The LaGrange compensation embodies no closed blocks similar to the Clarke transformation; all operations are individual and are shown on the diagram in Fig. 10.2. In computing the total number of operations required by the LaGrange method the three part additions are counted as two single additions. The relative number of operations required by each method is presented for comparison purposes in Table 10.1.

Table 10.1: Comparison of operations: *dq0 vs.* LaGrange

	dq0 Method	LaGrange Method
Additions	2	7
Subtractions	1	0
Multiplications	33	9
Divisions	2	1
Totals	38	17

A comparison of the computational efficacy of the two methods is not quite so straight-forward as it might appear. There are many variables to consider in determining the basis of comparison, for example, instructions, clock cycles, number of gates required, number of transistors required, chip area, chip cost, dissipated power, *etc.* Without detailed information about the specific platform upon which the computations are to be performed it is not possible to quantify a comparison between the two approaches. Suffice it to present, based on the fact that the total number of operations required to implement the LaGrange solution is less than half the number required to implement the *dq0* solution, that if a system is capable of generating *dq0* solutions there will be no operational impediments to performing the calculations required for the LaGrange approach.

10.5 – A *PSCad* validation

Before moving onward with the comparison of the *dq0* and LaGrange compensation methods with the EAF model, it is instructive to see how the STATCOM behaves with the two compensation

schemes with a simple inductive load that is sized to match the rating of the STATCOM. Although the *PSCad* model itself does not truly have a 'rating' the individual components that comprise the model are based on the components in the physical STATCOM used at the subject steel mill; the rating of that equipment is 20 MVA which is the reactive power that will be taken from the line before the STATCOM, with the two compensation strategies, will be applied.

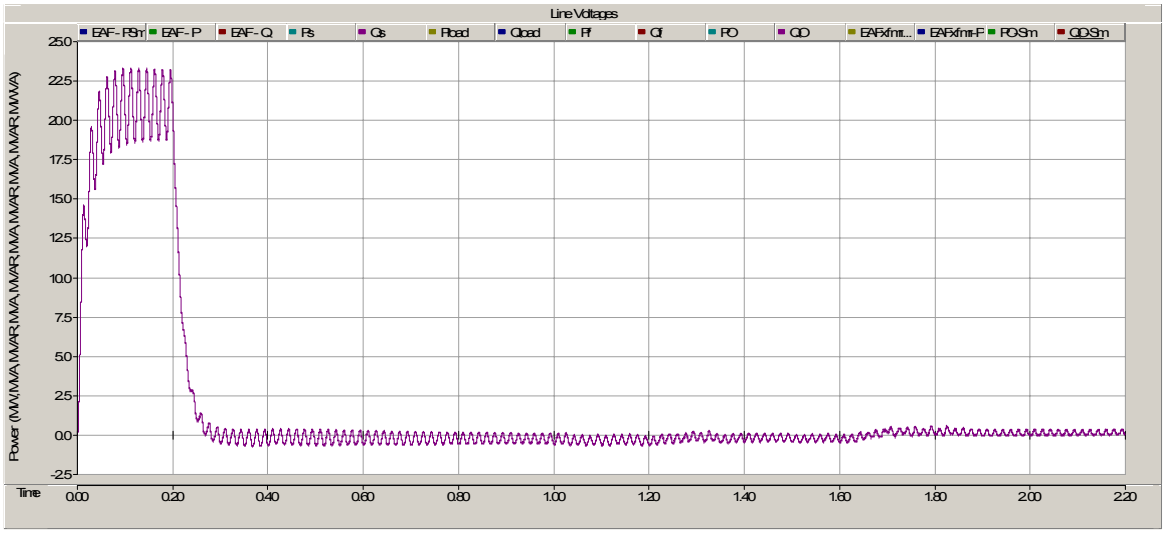

Fig. 10.3 Utility reactive power with *dq0* and LaGrange compensation schemes

The reactive power delivered by the utility system is shown in Fig. 10.3 under three different conditions. The first interval, $0 \le t < 0.2$, seconds shows the delivered power with no compensation; in this time interval the gate drivers to the STATCOM IGBTs are forced to zero. At time $t = 0.2$ the gate drivers are energized with the modification scheme selected to be *dq0* compensation. From $0.2 \le t < 1.2$ the compensation scheme remains the *dq0* method. At time $t = 1.2$ the scheme is switched by a timer within the *PSCad* STATCOM model to the LaGrange method. From time $1.2 \le t \le 2.2$ the compensation scheme remains LaGrange; this same timing is also used for the remaining comparison plots.

It will be observed that, as expected, the line delivered power drops by 20 MVA when the STATCOM is first energized. After the switch to LaGrange is made at $t = 1.2$ the delivered power remains at essentially zero as was predicted by the LaGrange derivation. Note that there is a slight

DC offset component to both of these waveforms that gradually drops to zero as the simulation progresses. The next step is use the exact same configuration with the previously described single-phase EAF model connected in wye. The particular parameters used for the EAF model in the simulation are presented in Table 10.2.

Table 10.2: Single-phase EAF model parameters

	Phase A	Phase B	Phase C
m	0	0	0
n	2	2	2
k1	4,000	4,100	3,900
k2	2.00	2.05	1.95
k3	12.5	13.0	12.0

The EAF operates at approximately 350 Volts, a value close to the voltage of the furnace in the subject steel mill. The transformers that drive the EAF from the 12.47 kV line are essentially the same as those that are used in the physical installation except that three individual transformers are used instead of a single phase version at the plant. The transformers in the *PSCad* simulation are connected in wye instead of the delta configuration at the actual facility. The reason for the shift is that the *PSCad* software uses the traditional model for determination of neutral currents in a delta connection system. In the actual physical arrangement, as shown by the plots of Chapter 5, there is neutral current that flows between the utility system and the furnace; the use of individual transformers allows this current to be directly measured.

Fig. 10.4 shows the result of the two compensation strategies as applied to the 33 MW single-phase EAF model. It is this plot that demonstrates the true value of the LaGrange compensation strategy over the *dq0* method where there is unbalance among the load phase currents. As with the plot before, the *dq0* strategy is used in the interval $0.2 \le t < 1.2$; LaGrange is used for the interval $1.2 \le t \le 2.2$.

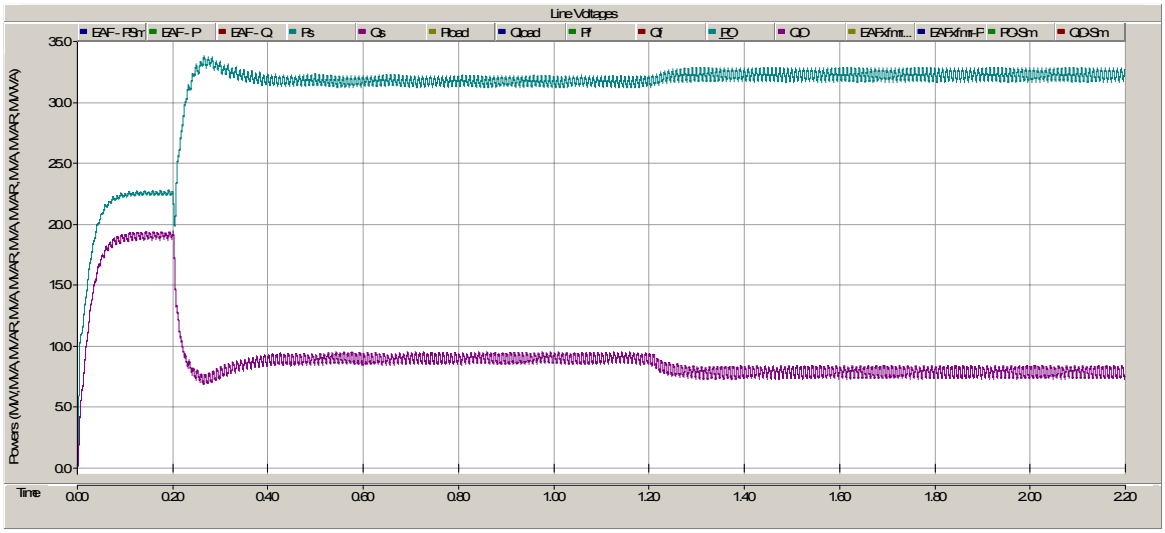

Fig. 10.4 Utility powers for EAF with *dq0* and LaGrange compensation schemes

The LaGrange compensation has the ability to direct the STATCOM to compensate for the unbalance currents that would be a part of the '0' value of the *dq0* scheme; as previously noted the '0' value in the re-transformation is set to zero (see Fig. 10.1) and is thus not included in the compensation. Fig. 10.5 presents the same information except that in this plot the real and reactive powers have been smoothed over a one cycle interval so that the improvement in performance can be more clearly seen. In looking at this plot it can be seen that the power delivered by the utility line has been increased by around 500 kW; the reactive power delivered by the utility line has been reduced by 1 MVA. From the relative power point of view, the delivered power using the LaGrange approaches increased by 1.6 % over the *dq0* method. It is again emphasized that the only change that has been made in the two sections of the plot is in the compensation scheme, *i.e.*, software. There have been no physical changes made between the two plot segments.

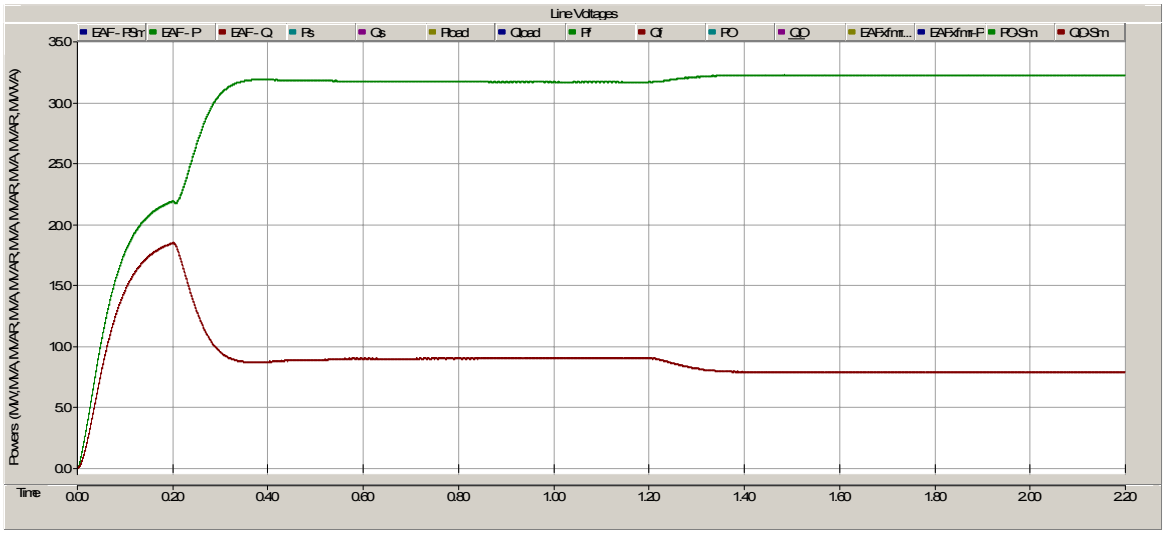

Fig. 10.5 Smoothed utility powers for EAF with *dq0* and LaGrange compensation schemes

A compressed vertical axis view is shown of the comparison in Fig. 10.6. In this view the vertical axis has been limited to the values between approximately 31.0 and 32.5 MW or MVA. In this unsmoothed view it can be seen that not only does the level of power delivered to the EAF increase but the power appears to be more stable. The implication is that LaGrange compensation would not only increase the power delivered to the arc but also make the arc more stable, implying a reduced level of flicker. Previously referenced publications [62-63] demonstrated that due to the low effective X/R ratio of at EAF system the real power fluctuation is a significant contributor to the flicker phenomena. As an aside, it was previously noted that a validated IEC 61000-4-5 compliant [18] flickermeter is not available as a part of the *PSCad* software system; the writing of such a model is beyond the scope of the present work and is left as a future research activity.

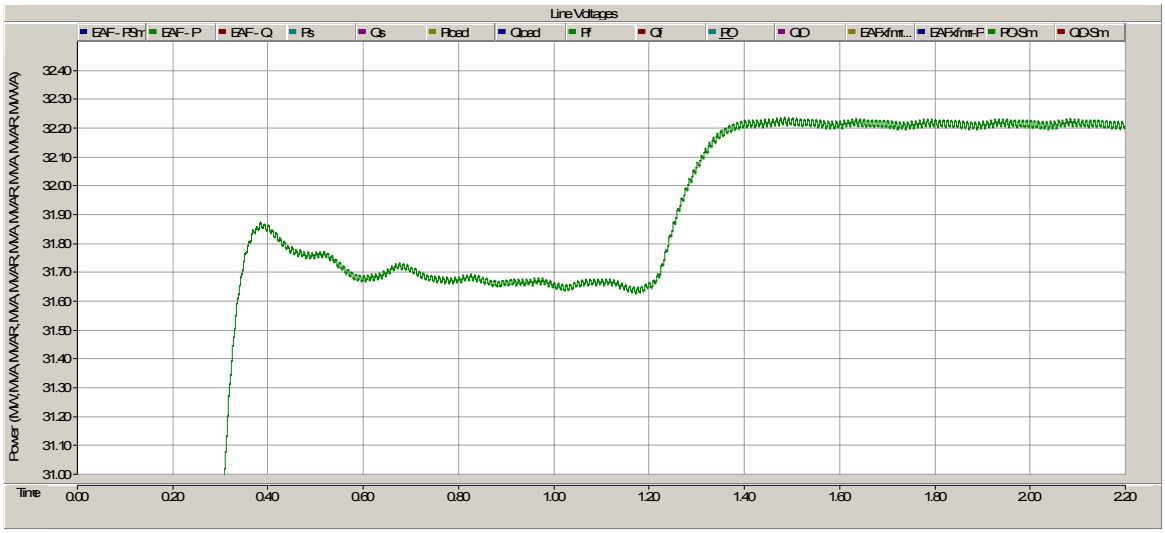

Fig. 10.6 Detail of utility powers for EAF with *dq0* and LaGrange compensation schemes

There are several other plots that are of interest in the comparison of the *dq0* and LaGrange compensation schemes. One such plot involves the real and reactive powers that are actually delivered to the arcs of the EAF. In the actual utility/furnace configuration there is not much real resistance so it is logical that the arcs would consume essentially all of the real power delivered by the utility supply. The reactive power that is consumed by the arc should be relatively independent of the compensation technique, *i.e.*, it should not make a great deal of difference to the arc reactive power whether the compensation scheme is *dq0*, LaGrange, or, for that matter, a static capacitor bank. These considerations are both reflected in Fig. 10.7, which shows arc powers under the two compensation schemes. Again observe that real power to the arc increases upon application of the LaGrange compensation strategy.

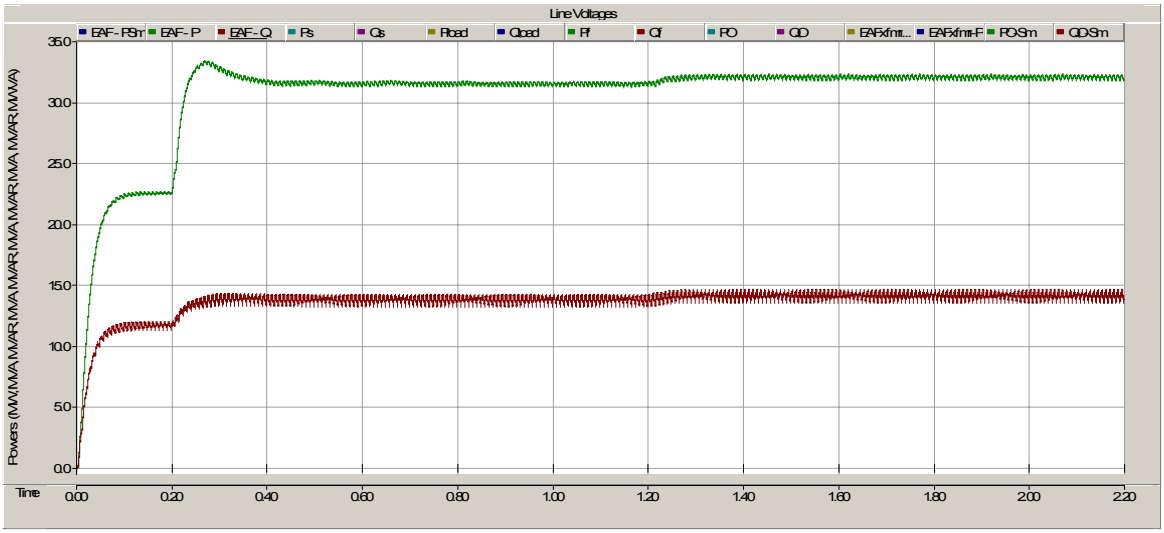

Fig. 10.7 Detail of arc powers for EAF with *dq0* and LaGrange compensation schemes

Another plot that comes to mind is a comparison of the output of the STATCOM itself under the two compensation arrangements, a feature of particular interest being the real power delivered by the STATCOM. It was previously noted that a STATCOM cannot deliver real power without a separate power source and that the real power delivered under both the *dq0* scheme and the LaGrange schemes is zero. This is now demonstrated by the plot of Fig. 10.8, which shows real and reactive STATCOM powers. Note that in this Figure the increase in STATCOM delivery of reactive power mirrors the reduction of reactive power delivered by the utility line as shown in earlier plots.

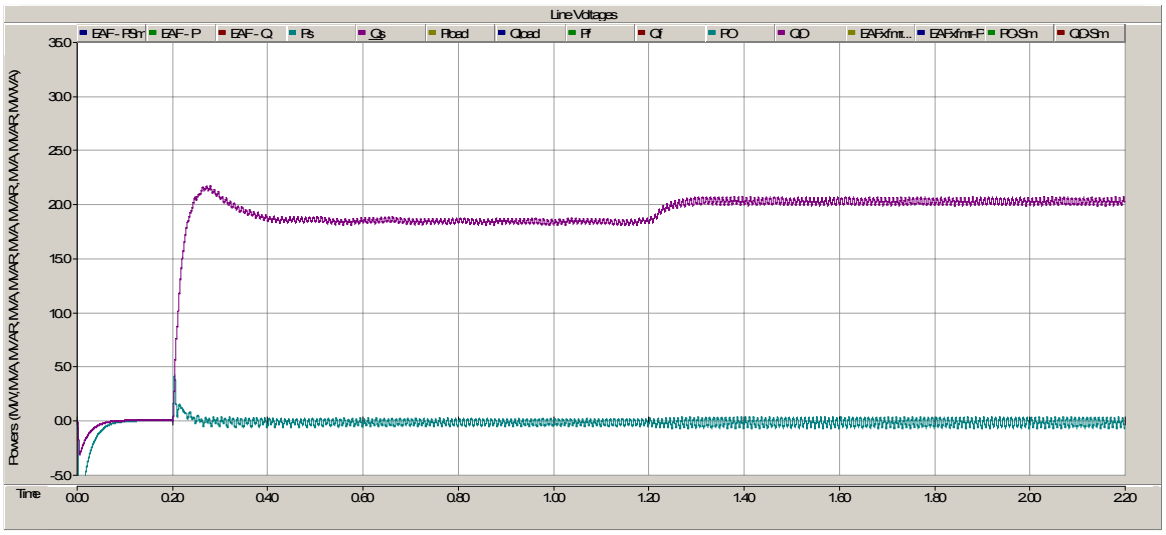

Fig. 10.8 STATCOM real and reactive power outputs

An additional point of interest in the comparison of the two compensation schemes is the behavior of the DC bus under the different operation methods. Fig. 10.9 shows the behavior of the DC bus as the compensation scheme changes from *dq0* to LaGrange. Again, keep in mind that there are no changes within the STATCOM model when the system switches between *dq0* and LaGrange compensation modes.

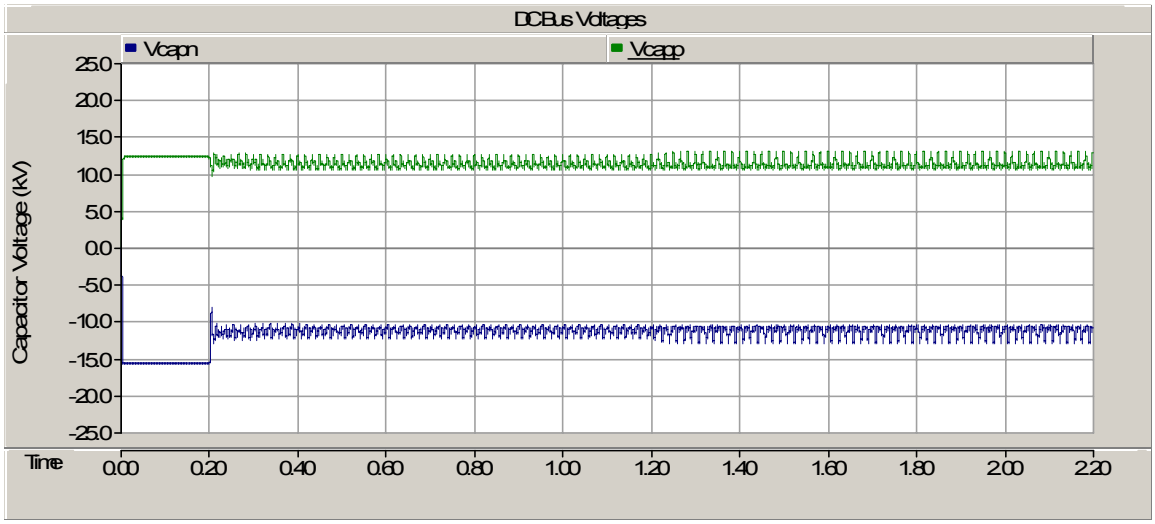

Fig. 10.9 STATCOM DC bus with *dq0* and LaGrange compensation schemes

Visually, the DC bus appears to be changed only slightly during the transition from the *dq0* to the LaGrange compensation scheme. A look at the harmonic content will show that there is an increase in the 60 Hz fundamental component and a slight increase in the 2nd harmonic content. The DC component remains essentially constant, as can be seen in Fig. 10.10.

The minimal changes in the overall harmonic content of the DC bus does not affect the operation of the STATCOM with respect to improving energy delivery to the EAF. As an aside, note that there is no active DC bus control in the simulations, either for the *dq0* or the LaGrange compensations.

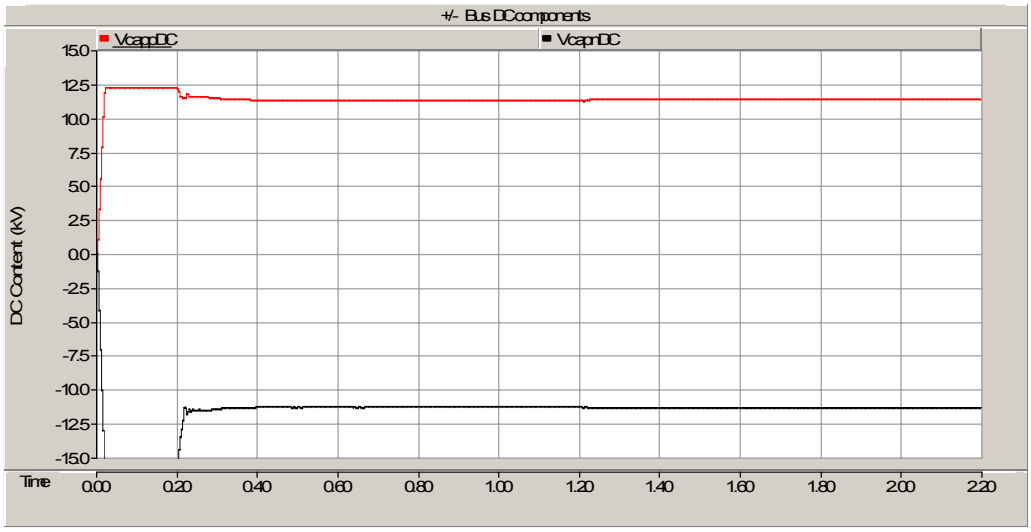

Fig. 10.10 STATCOM bus DC content for *dq0* and LaGrange compensation

Another item of consideration is the magnitude of the input current waveform. Visually, the waveform appears to have less magnitude but it is quite difficult to discern real differences of a complex waveform visually. A plot of the harmonic content of the input waveform reveals that in fact the magnitude of the fundamental has been reduced by use of the LaGrange technique as compared to the *dq0* method; a plot showing this change is presented as Fig. 10.11. The harmonic content of the odd harmonics, through the 13th is presented in Fig. 10.12. As can be seen from this plot there are relatively minor reductions in line harmonic content as compared with the drop in the fundamental content as previously presented.

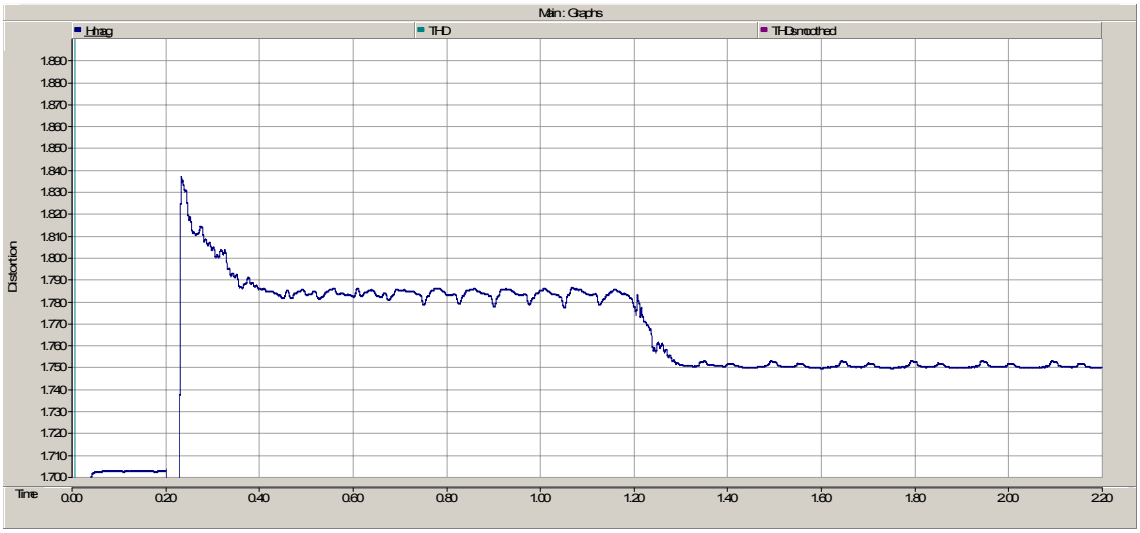

Fig. 10.11 Utility input current fundamental component for *dq0* and LaGrange compensation

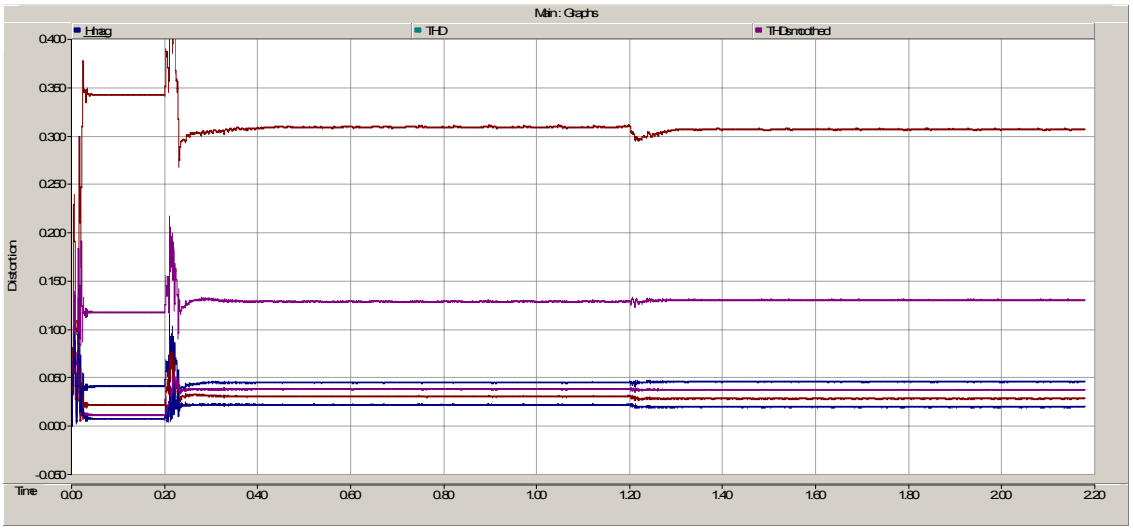

Fig. 10.12 Utility input current harmonic content for 3rd, 5th, 7th, 9th, 11th, and 13th harmonics

It was noted in Fig.10.6 there are variations in real power input in the *dq0* compensation strategy that do not appear in the LaGrange method strategy. The implication is that, since the X/R ratio of the system at the PCC is so low, the real power fluctuations will have a significant impact on

the voltage level of the input utility line. To take a closer look at this, Fig. 10.13 was created to show a detail of the Phase A utility line source.

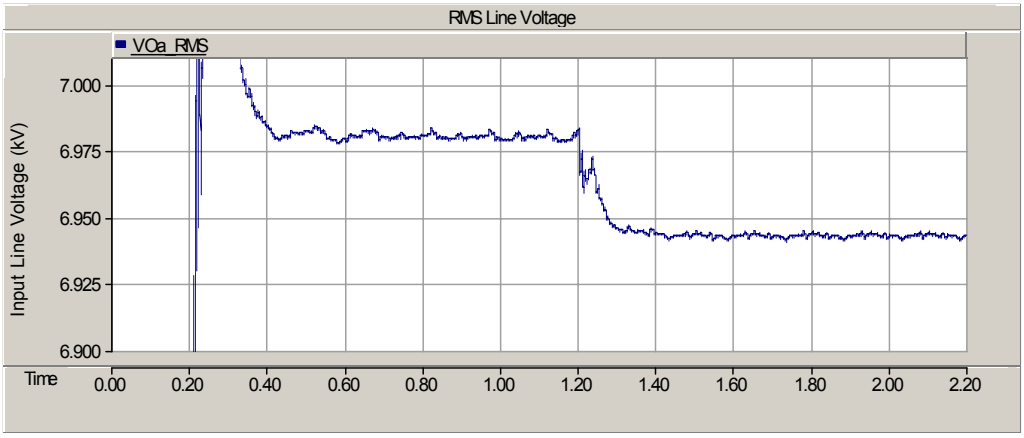

Fig. 10.13 Utility Phase A input RMS voltage for *dq0* and LaGrange compensation

It is observed that the RMS voltage during *dq0* appears to be much more irregular than during LaGrange compensation. The fact that the line voltage actually drops while the power increases is due to the low X/R ratio being acted on by an increased level or real power. While it is always risky to estimate flicker from the visual appearance of a waveform it is noted in passing that, based on the steadier power delivery under the LaGrange approach that the overall level of flicker will probably also be lower.

A final item that is of interest is to examine the input line currents under the three conditions of operation established for the model, *viz.* (1) no compensation, (2) *dq0* compensation, and (3) LaGrange compensation. Fig. 10.14 shows the transition from no compensation to *dq0* compensation that occurs at time $t = 0.2$ s.

It is observed that at the transition between no-compensation and *dq0* compensation the input current waveforms become more irregular. This is due to the action of the STATCOM, which must draw current from the utility lines as needed to compensate for the non-linearity of the EAF arcs.

Fig. 10.15 presents the transition between the *dq0* compensation scheme and the LaGrange method, which occurs at time $t = 1.2$. At this transition the current waveforms become even more irregular. As the LaGrange compensation scheme provides the STATCOM with the ability to

compensate for currents that were not previously compensated it is to be expected that the input current waveforms would exhibit more irregularity. A plot captured at the transition time between *dq0* and LaGrange schemes showing the neutral current only is presented as Fig. 10.16; the voltage waveforms are duplicated in this figure for comparison purposes.

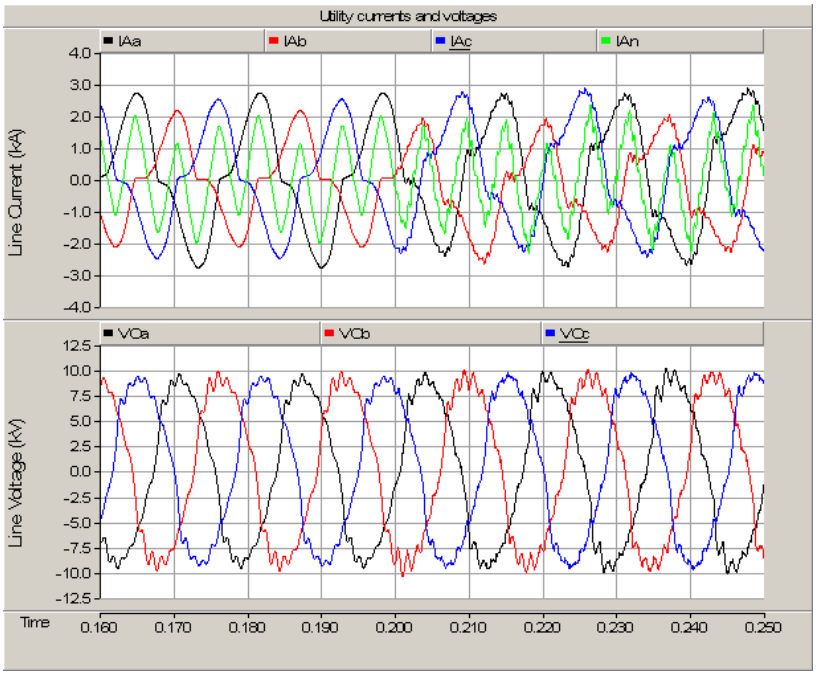

Fig. 10.14 Utility currents and voltages at *dq0* startup

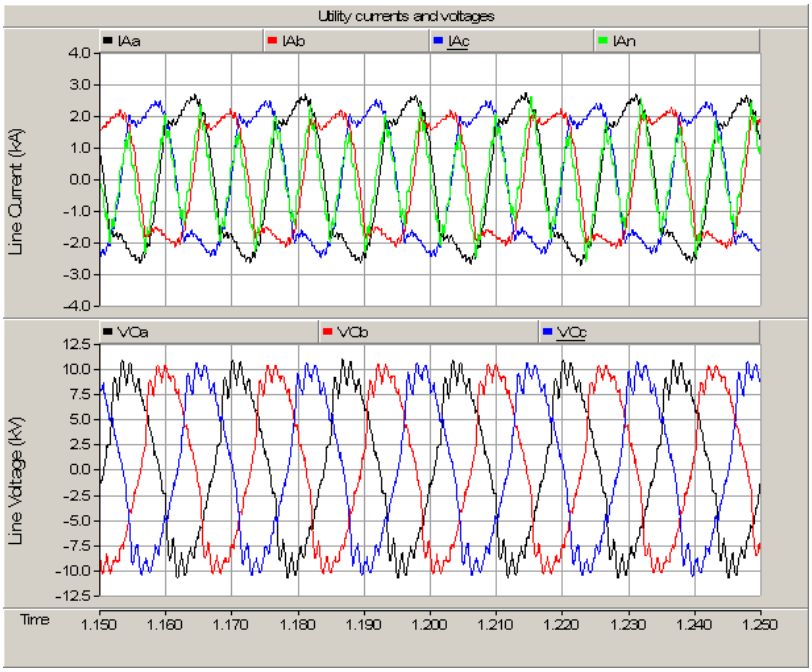

Fig. 10.15 Utility currents and voltages at LaGrange startup

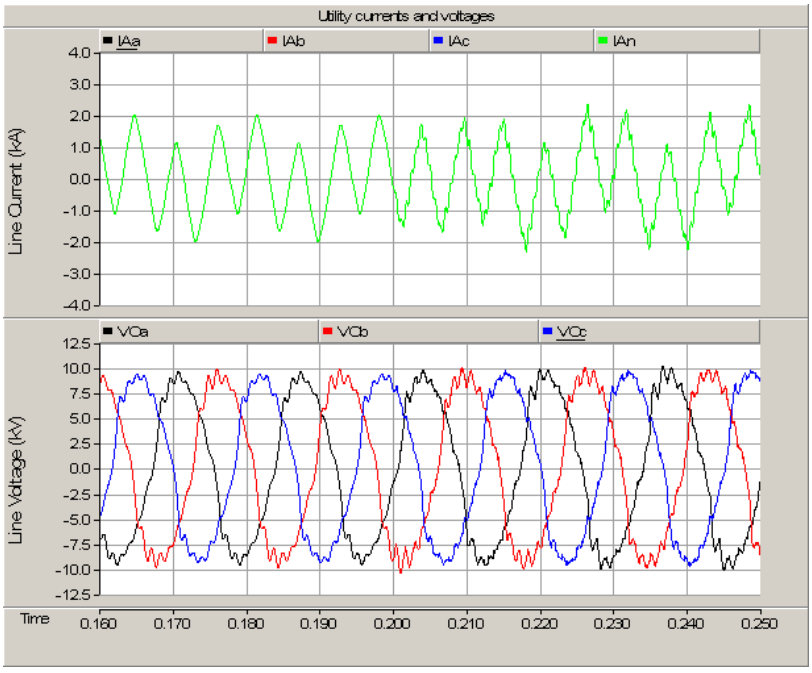

Fig. 10.16 Neutral current at LaGrange startup

11 – Conclusions and future work

11.1 – Conclusions

The following conclusions may be drawn from the present work:

1. The Clarke transformation, as embodied in the widely used *dq0* compensation scheme is a valid method in cases where the system is balanced. In cases where the system loads are *not* balanced phase-to-phase, as in Electric Arc Furnaces, use of the *dq0* scheme results in uncompensated currents that reduce the amount of energy that is delivered to the EAF arcs. It is noted that the '*0*' component of the *dq0* compensation scheme cannot be used to determine the total amount of reactive power to be compensated.
2. The LaGrange compensation scheme provides a minimized desired compensation current that can be delivered by a STATCOM. Compensation by the LaGrange method is independent of input waveforms or of balance of current or voltages between or among the phases.
3. Compensation of an EAF STATCOM by the LaGrange method delivers more energy to the EAF arcs than compensation by the *dq0* method.
4. Compensation of an EAF STATCOM by the LaGrange method delivers more consistent power to the EAF arcs than compensation by the *dq0* method.
5. Compensation of an EAF STATCOM by the LaGrange method reduces the magnitude of the input current waveform.
6. Compensation of an EAF STATCOM by the LaGrange method reduces the variability of the real power delivered to the arc.
7. Under balanced conditions the compensation delivered by the LaGrange method and the *dq0* methods are identical.
8. The real power delivered by a STATCOM under either the *dq0* or LaGrange techniques is zero over a complete cycle.
9. Physically, the equipment used by the LaGrange technique is identical to that used by the *dq0* method. The only changes needed to implement this scheme in a working STATCOM compensated system are modifications to the software.
10. Computationally, the LaGrange technique requires fewer mathematical operations than does the *dq0* method.

11.2 – Future work

The present work has developed the LaGrange minimization technique into a generalized compensation scheme for Electric Arc Furnaces. The advantages of the method over the present *dq0* approach are many and the implementation costs are nominal. Further work is required in several areas:

1. The method should be applied to an actual operating EAF in order to quantify real benefits. It is appreciated that an application of the method will require the interruption of a profit stream at an industrial facility and, as such, is not to be lightly undertaken. A joint effort between a STATCOM manufacturer and a steel producer will be necessary to provide this outcome. Simulation using a Real Time Digital Simulator (RTDS) would provide additional validation of the approach prior to making modifications to a physical installation.
2. It is not theoretically clear how unbalance currents appear on the line side of a delta-delta transformer. It is apparent that these currents exist – they were measured as a part of the data-gathering portion of this work – and that they are uncompensated by the *dq0* compensation scheme. It is known that the utility system, invariably a grounded wye configuration, is connected to the EAF basin through multiple paths of the grounded electrical system at the plant. It is suspected that the magnetic coupling of the close proximity, high current, arcs in the EAF are behaving as a zig-zag transformer, providing a return path for zero sequence currents around the EAF transformer. This superstition is unsupported by present data and is a rich area for future work.
3. Based on the appearance of the *dq0* compensated and the LaGrange compensated power waveforms, it would seem that the LaGrange method is more stable. A standard-validated flickermeter is not a part of the *PSCad* software package. The code for such a device should be written, validated, and applied to the present compensation scheme to confirm that the method also improves the mitigation of flicker generated by an EAF.

References

[1] C. L. Fortescue, "Method of Symmetrical Co-Ordinates Applied to the Solution of Polyphase Networks," *American Institute of Electrical Engineers, Transactions of the,* vol. XXXVII, pp. 1027-1140, 1918.

[2] J. Dolezal*, et al.*, "Topologies and control of active filters for flicker compensation," in *Industrial Electronics, 2000. ISIE 2000. Proceedings of the 2000 IEEE International Symposium on*, 2000, pp. 90-95 vol.1.

[3] C. Schauder, "STATCOM for compensation of large electric arc furnace installations," in *Power Engineering Society Summer Meeting, 1999. IEEE*, 1999, pp. 1109-1112 vol.2.

[4] H. Chong*, et al.*, "Design of an Ultra-Capacitor Energy Storage System (UESS) for Power Quality Improvement of Electric Arc Furnaces," in *Industry Applications Society Annual Meeting, 2008. IAS '08. IEEE*, 2008, pp. 1-6.

[5] Z. Zhang*, et al.*, "Flicker analysis and methods for electric arc furnace flicker (EAF) mitigation (a survey)," in *Power Tech Proceedings, 2001 IEEE Porto*, 2001, p. 6 pp. vol.1.

[6] R. Grunbaum*, et al.*, "STATCOM, a prerequisite for a melt shop expansion-performance experiences," in *Power Tech Conference Proceedings, 2003 IEEE Bologna*, 2003, p. 6 pp. Vol.2.

[7] V. Staudt, "Fryze - Buchholz - Depenbrock: A time-domain power theory," in *Nonsinusoidal Currents and Compensation, 2008. ISNCC 2008. International School on*, 2008, pp. 1-12.

[8] A. Smith, *An inquiry into the nature and causes of the wealth of nations*. Dublin,: Whitestone, 1776.

[9] J. Korp*, et al.*, "Conductance and temperature measurement system for a 1500 deg.C metallurgy slag," in *Electronic Instrument Engineering Proceedings, 2004. APEIE 2004. 2004 7th International Conference on Actual Problems of*, 2004, pp. 178-182.

[10] "Commentary - Understanding Electric Arc Furnace Operations," EPRI Center for Materials Production, Pittsburgh, PA1997.

[11] "Understanding Electric Arc Furnace Operations For Steel Production," Center for Metals Production, Pittsburgh, PA1987.

[12] H. B. Cary and S. C. Helzer, *Modern welding technology*, 6th ed. Upper Saddle River, N.J.: Pearson/Prentice Hall, 2005.

[13] "Arc Furnace Power Delivery Scoping Study," Center for Metals Production, Pittsburgh, PA1984.

[14] J.-C. Baurnert*, et al.*, "Dynamic modeling of the electric arc furnace process using artificial neural networks," *La Revue de Metallurgie-CIT,* pp. 839-849, 2002.

[15] H. Zhennan*, et al.*, "Development of AC Electric Arc-Furnace Control System Based on Fuzzy Neural Network," in *Mechatronics and Automation, Proceedings of the 2006 IEEE International Conference on*, 2006, pp. 2459-2464.

[16] N. G. Bliss*, et al.*, "Neural networks for the high voltage EAF," in *Fifth European Electric Steel Congress*, Paris, 1995, pp. 240-247.

[17] R. Horton*, et al.*, "A Time-Domain AC Electric Arc Furnace Model for Flicker Planning Studies," *Power Delivery, IEEE Transactions on,* vol. 24, pp. 1450-1457, 2009.

[18] *Electromagnetic compatibility (EMC) - Part 4: Testing and measurement techniques - Section 15: Flicker - Functional and design specifications*, IEC Standard 61000-4-15, 2003.

[19] H. Mokhtari and M. Hejri, "A new three phase time-domain model for electric arc furnaces using MATLAB," in *Transmission and Distribution Conference and Exhibition 2002: Asia Pacific. IEEE/PES*, 2002, pp. 2078-2083 vol.3.

[20] MATLAB version 7.4.0.287 (R2007a). Natick, Massachusetts: Mathworks, 2007

[21] A. D. Poularikas and S. Seely, *Signals and systems*. Boston: PWS Engineering, 1984.

[22] T. Wu*, et al.*, "A new frequency domain method for the harmonic analysis of power systems with arc furnace," in *Advances in Power System Control, Operation and Management, 1997. APSCOM-97. Fourth International Conference on (Conf. Publ. No. 450)*, 1997, pp. 552-555 vol.2.

[23] J. G. Mayordomo*, et al.*, "A new frequency domain arc furnace model for iterative harmonic analysis," *Power Delivery, IEEE Transactions on,* vol. 12, pp. 1771-1778, 1997.

[24] L. F. Beites*, et al.*, "Harmonics, interharmonics and unbalances of arc furnaces: a new frequency domain approach," in *Harmonics And Quality of Power, 1998. Proceedings. 8th International Conference on*, 1998, pp. 1071-1078 vol.2.

[25] F. Chen*, et al.*, "Function space valued Markov model for electric arc furnace," *Power Systems, IEEE Transactions on,* vol. 19, pp. 826-833, 2004.

[26] J. J. Grainger and W. D. Stevenson, *Power system analysis*. New York: McGraw-Hill, 1994.

[27] W. H. Hayt*, et al.*, *Engineering circuit analysis*, 6th ed. Boston: McGraw-Hill, 2002.

[28] J. W. Nilsson and S. A. Riedel, *Electric circuits*, 8th ed. Upper Saddle River, N.J.: Pearson/Prentice Hall, 2008.

[29] J. J. Cimino, "Desiderata for controlled medical vocabularies in the twenty-first century," *Methods Inf Med,* vol. 37, pp. 394-403, Nov 1998.

[30] J. J. Cimino, "In defense of the Desiderata," *J Biomed Inform,* vol. 39, pp. 299-306, Jun 2006.

[31] H. Akagi*, et al.*, *Instantaneous power theory and applications to power conditioning*. Hoboken, NJ: Wiley-Interscience/ John Wiley & Sons, 2007.

[32] E. Clarke, *Circuit analysis of A-C power systems*. New York: J. Wiley & sons, 1943.

[33] R. H. Park, "Two-Reaction Theory of Synchronous Machines Generalized Method of Analysis - Part I," *American Institute of Electrical Engineers, Transactions of the,* vol. 48, pp. 716-727, 1929.

[34] R. H. Park, "Two-Reaction Theory of Synchronous Machines Generalized Method of Analysis - Part II," *American Institute of Electrical Engineers, Transactions of the,* vol. 52, pp. 352-354, 1933.

[35] S. Fryze, "Moc, rzeczywista, urojona i pozorna w obwodach elektrycznych o przebiegach odksztalconych prądu i napięcia, (Active, reactive, and apparent powers in electric circuits with distorted voltages and currents, in Polish language)," *Przegląd Elektrotechniczny,* vol. XIII, no. 7 & 8, pp. 193-203 & pp. 193-203, 1931.

[36] S. Fryze, "Wirk-, Blind- und Scheinleistung in elektrischen Stromkreisen mit nich-sinusförmigem Verlauf von Strom und Spannung, (Active, and-active, and apparent power in electrical circuits with nonsinusoidal time functions of current and voltage, in German language)," *ETZ-A Elektrotech. Z.,* vol. 53, no. 25, pp. 596-599, 625-627,700-702, 1932.

[37] F. Buchholz, *Das Begriffsystem Rechtleistung, Wirkleistunc, totale Blindleistung, (The systematic of maximal power, active power, and total non-active power, in German language)*. München: Selbstverlag, 1950.

[38] M. Depenbrock, "The FBD-Method, A Generally Applicable Tool For Analyzing Power Relations," in *Harmonics in Power Systems., ICHPS V International Conference on*, 1992, pp. 135-141.

[39] M. Depenbrock, *Wirk und blindleistungn periodischer ströme in ein- u. mehrphasensystemen mit periodischn spannungen beliegiger kurvenform (Active and non-active powers of periodic*

currents in single and multi-conductos systems with periodic voltages of arbitrary time function, in German language), 1979.

[40] M. Depenbrock, "The FBD-method, a generally applicable tool for analyzing power relations," *Power Systems, IEEE Transactions on,* vol. 8, pp. 381-387, 1993.

[41] M. Depenbrock*, et al.*, "A concise assessment of original and modified instantaneous power theory applied to four-wire systems," in *Power Conversion Conference, 2002. PCC Osaka 2002. Proceedings of the*, 2002, pp. 60-67 vol.1.

[42] M. Depenbrock*, et al.*, "A theoretical investigation of original and modified instantaneous power theory applied to four-wire systems," *Industry Applications, IEEE Transactions on,* vol. 39, pp. 1160-1168, 2003.

[43] R. V. Churchill and J. W. Brown, *Complex variables and applications*, 4th ed. New York: McGraw-Hill, 1984.

[44] H. K. M. Paredes*, et al.*, "A comparative analysis of FBD, PQ and CPT current decompositions - Part II: Three-phase four-wire systems," in *PowerTech, 2009 IEEE Bucharest*, 2009, pp. 1-6.

[45] H. K. M. Paredes*, et al.*, "A comparative analysis of FBD, PQ and CPT current decompositions - Part I: Three-phase, three-wire systems," in *PowerTech, 2009 IEEE Bucharest*, 2009, pp. 1-8.

[46] P. Tenti and P. Mattavelli, "A time-domain approach to power term definitions under non-sinusoidal conditions," in *Sixth international workshop on power definitions and measurements under non-sinusoidal conditions*, Milano, Italy, 2003, pp. 1-10.

[47] T. Furuhashi*, et al.*, "A study on the theory of instantaneous reactive power," *Industrial Electronics, IEEE Transactions on,* vol. 37, pp. 86-90, 1990.

[48] A. O. M. Saleh*, et al.*, "M - to N-phase transformer models in phase co-ordinates," *Generation, Transmission and Distribution, IEE Proceedings C,* vol. 132, pp. 41-48, 1985.

[49] F. P. Marafao*, et al.*, "Critical evaluation of FBD, PQ and CPT current decompositions for four-wire circuits," in *Power Electronics Conference, 2009. COBEP '09. Brazilian*, 2009, pp. 49-57.

[50] W. Z. Gandhare and D. D. Lulekar, "Analyzing Electric Power Quality in Arc Furnaces," in *International Conference on Renewable Energy and Power Quality (ICREPQ'07)*, Sevilla, Spain, 2007.

[51] C. C. Chesney and C. F. Scott, "Early History of the A-C System in America," *American Institute of Electrical Engineers, Transactions of the,* vol. 55, pp. 228-235, 1936.

[52] D. G. Holmes and T. A. Lipo, *Pulse width modulation for power converters : principles and practice*. Hoboken, NJ: John Wiley, 2003.

[53] L. Brand, *Vector analysis*. New York,: Wiley, 1957.

[54] J. J. Craig, *Introduction to robotics : mechanics and control*, 2nd ed. Reading, Mass.: Addison-Wesley, 1989.

[55] H. Akagi*, et al.*, "Instantaneous Reactive Power Compensators Comprising Switching Devices without Energy Storage Components," *Industry Applications, IEEE Transactions on,* vol. IA-20, pp. 625-630, 1984.

[56] D. E. Kirk, *Optimal control theory; an introduction*. Englewood Cliffs, N.J.,: Prentice-Hall, 1970.

[57] R. L. Boylestad, *Introductory circuit analysis*, 3d ed. Columbus, Ohio: Merrill, 1977.

[58] D. Shmilovitz, "On the definition of total harmonic distortion and its effect on measurement interpretation," *Power Delivery, IEEE Transactions on,* vol. 20, pp. 526-528, 2005.

[59] Mathematica 7 version 7.0.0. Champaign, Illinois: Wolfram Research, Inc., 2008

[60] PSCAD version 4.2.1. Winnipeg, Manitoba, Canada: Manatoba HVDC Research Centre, 2006

[61] *IEEE Application Guide for AC High-Voltage Circuit Breakers Rated on a Symmetrical Current Basis*, IEEE Std C37.010-1999, 1999 (R2005).

[62] Z. Li*, et al.*, "EAF voltage flicker mitigation by FACTS/ESS," in *Power Systems Conference and Exposition, 2004. IEEE PES*, 2004, pp. 372-378 vol.1.

[63] Z. Li*, et al.*, "Mitigation of EAF Induced Problems," in *Power Systems Conference and Exposition, 2006. PSCE '06. 2006 IEEE PES*, 2006, pp. 1448-1453.

[64] A. Nabae*, et al.*, "A New Neutral-Point-Clamped PWM Inverter," *Industry Applications, IEEE Transactions on,* vol. IA-17, pp. 518-523, 1981.

[65] FORTRAN 95 version 5.40. Rochester Hills, Michigan: Absoft Corporation, 1998

[66] E. Acha, *et al.*, "A harmonic domain computational package for nonlinear problems and its application to electric arcs," *Power Delivery, IEEE Transactions on,* vol. 5, pp. 1390-1397, 1990.

[67] R. L. Burden, *et al.*, *Numerical analysis*, 2d ed. Boston, Mass.: Prindle, Weber & Schmidt, 1981.

[68] The Fortran Company. 2012. [Web page]. Available: http://www.fortran.com/gauss_random.html

[69] R. Fox, Gatland, I., Roy, R., Vemuri, G., "Fast, accurate algorithm for numerical simulation of exponentially correlated colored noise," *Physical Review A,* vol. 38, no. 11, pp. 5,938-5,940, 1988.

Appendices

Appendix A – *MatLab* source code – V & I plots


```
%*************************************************************************
%
%                        V_and_I_plots.m
%
%   This program extracts data from waveforms captured at Kobe-Weiland
%   on March 9, 2009 and plots measured voltage and current waveforms.
%
%*************************************************************************
%
% Clean slate
%
clear all      % clear workspaces
clc            % clear screen
close all      % close any open files
double all;    % use double precision for all data
%
%*************************************************************************
%
%   Read data files and populate allocate variable matrix
%
D = csvread('Clean_dataset8.csv');  % Data file is in same directory with
%                                     this program.  There are 7 working
%                                     files.
%
%-------------------------------------------------------------------------
%
%   extract vectors from dataset
%
for i=1:300
    t(i)=D(i,1);    % Time in Seconds
    Ia(i)=D(i,2);   % Phase A instanteneous measured current
    Ib(i)=D(i,3);   % Phase B instanteneous measured current
    Ic(i)=D(i,4);   % Phase C instanteneous measured current
    Va(i)=D(i,5);   % Phase A instanteneous measured voltage
    Vb(i)=D(i,6);   % Phase B instanteneous measured voltage
    Vc(i)=D(i,7);   % Phase C instanteneous measured voltage
end
%
%---------------- Incorporate CT and PT turns ratios ---------------------
%
%   CT ratio is 400:5 (80:1)
%   PT ratio is 60:1
%
%   The results of these calcuations are that the voltages are in Volts
%   and the currents are in Amperes.
%
Va=Va*60;
Vb=Vb*60;
Vc=Vc*60;
%
Ia=Ia*80;
Ib=Ib*80;
```

Appendix A Continued – *MatLab* source code – V & I plots


```
Ic=Ic*80;
%
%************************ Begin Sccreen Prompts *************************
%
reply='';      % Create empty matirx, then present screen propmt
while isempty(reply)
reply = input('Select desired output:\n   For voltage plot enter "1" \n   For current
plot enter "2"\n   Any other value to end program.\n', 's');
end
%
if reply=='1'% If screen response is 1 execute this section, else skip.
%
%*********************** Begin creen selection 1 ************************
%
%      This section plots out the measured input voltages
%
    subplot (3,1,1); plot (Va,'k','LineWidth',2) % Phase A voltage
    title('Individual Phase Voltages')
    ylabel('\phi A (V)')
    grid on
    hold
    subplot (3,1,2); plot (Vb,'r','LineWidth',2) % Phase B voltage
    ylabel('\phi A (V)')
    grid on
    subplot (3,1,3); plot (Vc,'b','LineWidth',2) % Phase C voltage
    grid on
    xlabel('Sample Number')
    ylabel('\phi C (V)')
end
%
%*************************** End Screen Selection 1 *********************
%
if reply=='2'
%
%*********************** Begin creen selection 2 ************************
%
%      This section plots out the measured input currents
%
    subplot (3,1,1); plot (Ia,'k','LineWidth',2) % Phase A current
    title('Individual Phase Currents')
     ylabel('\phi A (A)')
     grid on
    hold
    subplot (3,1,2); plot (Ib,'r','LineWidth',2)  % Phase B current
     ylabel('\phi B (A)')
     grid on
    subplot (3,1,3); plot (Ic,'b','LineWidth',2)  % Phase C current
    grid on
    xlabel('Sample Number')
    ylabel('\phi C (A)')
end
```

Appendix A Continued – *MatLab* source code – V & I plots


```
%*************************** End Screen Selection 2 **********************
%
% ----------------------------- End Program --------------------------------
%
```

Appendix B – *MatLab* source code – *abc/dq* comparison


```
%
%*************************************************************************
%
%                    ABC_dq_transform_comparison.m
%
%   This program generates a set of 3-phase voltage and current
%   waveforms for comparison with the dq method.
%
%   The zero sequence value, the "0" of the dq0 is not used in this
%   simulation.
%
%*************************************************************************
%
% Clean slate
%
clear all     %   clear workspaces
clc           %   clear screen
close all     %   close any open files
double all;   %   use double precision variables
%
%-------------------------- Define base values ----------------------------
%
% Voltages
%
Va=120;                          % Phase A RMS voltage
Vb=123.6;                        % Phase B RMS voltage
Vc=116.4;                        % Phase C RMS voltage
Vapd=0;                          % Phase A voltage shift in degrees
Vbpd=-118;                       % Phase B voltage shift in degrees
Vcpd=122;                        % Phase C voltage shift in degrees
%
% Currents
%
Ia=5;                            % Phase A RMS current
Ib=4;                            % Phase B RMS current
Ic=6;                            % Phase C RMS current
%
Iapd=0;                          % Phase A current shift in degrees
Ibpd=-122;                       % Phase B current shift in degrees
Icpd=117;                        % Phase C current shift in degrees
PhiDa=-35;                       % Phase A current PF shift in degrees
PhiDb=-35;                       % Phase B current PF shift in degrees
PhiDc=-35;                       % Phase C current PF shift in degrees
%
%-------------------------- Define Constants ------------------------------
%
R2=sqrt(2);                      % Root 2
f=60;                            % Frequency
A=2*pi/3;                        % 120 degree phase shift in radians
DTR=pi/180;                      % Convert degrees to radians
RTD=180/pi;                      % Convert radians to degrees
CT=sqrt(2/3)*[1 -0.5 -0.5; 0 sqrt(3)/2 -sqrt(3)/2]    % Clarke transform
```

Appendix B Continued – *MatLab* source code – *abc/dq* comparison


```
CTI=sqrt(2/3)*[1 0; -0.5 sqrt(3)/2; -0.5 -sqrt(3)/2]  % Inverse Clarke
                                                      % transform
%
%---------------------- Define computed values ----------------------------
%
W=2*pi*f;                       % Omega
T=1/f;                          % Period
t=linspace (0,T,360);           % 1/60 S, 360 degrees
%
% Voltage Phase Shifts
%
Vapr=Vapd*DTR;                  % Phase A voltage shift in degrees
Vbpr=Vbpd*DTR;                  % Phase B voltage shift in degrees
Vcpr=Vcpd*DTR;                  % Phase C voltage shift in degrees
%
% Phase voltages
%
VA=R2*Va*sin(W*t+Vapr);         % Phase A voltage waveform
VB=R2*Vb*sin((W*t)+Vbpr);       % Phase B voltage waveform
VC=R2*Vc*sin((W*t)+Vcpr);       % Phase C voltage waveform
VT=-(VA+VB+VC);                 % Neutral voltage
%
% Current Phase Shifts
%
Iapr=Iapd*DTR;                  % Phase A current shift in degrees
Ibpr=Ibpd*DTR;                  % Phase B current shift in degrees
Icpr=Icpd*DTR;                  % Phase C current shift in degrees
%
% Current Power Factor Phase Shifts
%
PhiRa=PhiDa*DTR;                  % Phase A current shift in degrees
PhiRb=PhiDb*DTR;                  % Phase B current shift in degrees
PhiRc=PhiDc*DTR;                  % Phase C current shift in degrees
%
% Phase currents
%
IA=R2*Ia*sin(W*t+PhiRa+Iapr);     % Phase A current waveform
IB=R2*Ib*sin((W*t)+PhiRb+Ibpr);   % Phase B current waveform
IC=R2*Ic*sin((W*t)+PhiRc+Icpr);   % Phase B current waveform
IT=-(IA+IB+IC);                   % Neutral current
%
% Compute dq values
%
V=[VA; VB; VC];     % Assemble voltage vector
Vdq=CT*V;           % Multiply by Clarke transform
%
I=[IA; IB; IC];     % Assemble current vector
Idq=CT*I;           % Multiply by Clarke transform

Irep=CTI*Idq;       % Preform inverse opeation
%
%------------------------------ Plot results ------------------------------
```

Appendix B Continued – *MatLab* source code – *abc/dq* comparison


```
%
plot (IA,'k','LineWidth',2)       % Total Power
hold
grid on
xlabel('Angle in Degrees')
ylabel('Current, A')
title('Individual Phase Currents')
plot (Irep(1,:),'r','LineWidth',2)         % Passive Power
plot (IB,'k','LineWidth',2)          % Passive Power
plot (Irep(2,:),'r','LineWidth',2)         % Passive Power
plot (IC,'k','LineWidth',2)          % Passive Power
plot (Irep(3,:),'r','LineWidth',2)         % Passive Power
% plot (Pwt,'c','LineWidth',2)        % Active Power
% plot (TOT,'r','LineWidth',2)        % total pwr LaGrange
%
%------------------------ End of Program ---------------------------------
%
```

Appendix C – *MatLab* source code – EAF voltage comparison


```
%
%*************************************************************************
%
%                    Kobe_dq_transform_comparison.m
%
%   This program downloads the Kobe data for phase voltage and current
%   waveforms for comparison with the dq method.
%
%   The plots in black are the orginal data; the plots in red are the data
%   as transformed to dq axis and then back to abc axis.
%
%*************************************************************************
%
% Clean slate
%
clear all     %   clear workspaces
clc           %   clear screen
close all     %   close any open files
double all;   %   use double precision variables
%
%*************************************************************************
%
%   Read data files and populate allocate variable matrix
%
D = csvread('Clean_dataset8.csv');
%
%-------------------------------------------------------------------------
%
%   extract vectors from dataset
%
for i=1:300
    t(i)=D(i,1);
    Ia(i)=D(i,2);
    Ib(i)=D(i,3);
    Ic(i)=D(i,4);
    Va(i)=D(i,5);
    Vb(i)=D(i,6);
    Vc(i)=D(i,7);
end
%
%---------------- Incorporate CT and PT turns ratios ----------------------
%
%   CT ratio is 400:5 (80:1)
%   PT ratio is 60:1
%
VA=Va*60;
VB=Vb*60;
VC=Vc*60;

IA=Ia*80;
IB=Ib*80;
IC=Ic*80;
```

Appendix C Continued – *MatLab* source code – EAF voltage comparison


```
%
%-------------------------- Define Constants ------------------------------
%
R2=sqrt(2);                     % Root 2
f=60;                           % Frequency
A=2*pi/3;                       % 120 degree phase shift in radians
DTR=pi/180;                     % Convert degrees to radians
RTD=180/pi;                     % Convert radians to degrees
CT=sqrt(2/3)*[1 -0.5 -0.5; 0 sqrt(3)/2 -sqrt(3)/2]
CTI=sqrt(2/3)*[1 0; -0.5 sqrt(3)/2; -0.5 -sqrt(3)/2]
% transform
%
%---------------------- Define computed values --------------------------
%
VT=-(VA+VB+VC);                 % Neutral voltage
IT=-(IA+IB+IC);                 % Neutral current
%
%----------------------- Compute dq values ----------------------------
%
V=[VA; VB; VC];      % Assemble voltage vector
Vdq=CT*V;            % Multiply by Clarke transform
%
I=[IA; IB; IC];      % Assemble current vector
Idq=CT*I;            % Multiply by Clarke transform

Irep=CTI*Idq;        % Preform inverse opeation - recreate current
Vrep=CTI*Vdq;        % Preform inverse opeation - recreate current
%
%------------------------- Begin Sccreen Prompts -------------------------
%
reply='';      % Create empty matirx, then present screen propmt
while isempty(reply)
reply = input('Select desired output:\n   For voltage plots enter "1" \n   For current
plots enter "2"\n   Any other value to end program.\n', 's');
end
%
%----------------------- Begin screen selection 1 ------------------------
%
if reply=='1'% If screen response is 1 execute this section, else skip.
%
%      This section plots out the measured input voltages along with
%      voltages as computed from the dq translation/retanslation
%
    subplot (3,1,1); plot (VA,'k','LineWidth',4) % Phase A
    hold
    subplot (3,1,1); plot (Vrep(1,:),'r','LineWidth',2) % Phase A rep
    title('Individual Phase Voltages')
    ylabel('\phi A (V)')
    axis([0 300 -20000 20000])
    grid on
%
    subplot (3,1,2); plot (VB,'k','LineWidth',4) % Phase B
```

Appendix C Continued – *MatLab* source code – EAF voltage comparison


```
    hold
    subplot (3,1,2); plot (Vrep(2,:),'r','LineWidth',2) % Phase B rep
    ylabel('\phi B (V)')
    axis([0 300 -20000 20000])
    grid on
%
    subplot (3,1,3); plot (VC,'k','LineWidth',4) % Phase C
    hold
    subplot (3,1,3); plot (Vrep(3,:),'r','LineWidth',2) % Phase C rep
    grid on
    xlabel('Sample Number')
    ylabel('\phi C (V)')
    axis([0 300 -20000 20000])
end
%
%----------------------- Begin screen selection 2 -------------------------
%
if reply=='2'% If screen response is 2 execute this section, else skip.
%
%      This section plots out the measured input currents along with
%      currents as computed from the dq translation/retranslation
%
    subplot (3,1,1); plot (IA,'k','LineWidth',2) % Phase A
    hold
    subplot (3,1,1); plot (Irep(1,:),'r','LineWidth',2) % Phase A rep
    title('Individual Phase Currents')
    ylabel('\phi A (I)')
    axis([0 300 -500 500])
    grid on
%
    subplot (3,1,2); plot (IB,'k','LineWidth',2) % Phase B
    hold
    subplot (3,1,2); plot (Irep(2,:),'r','LineWidth',2) % Phase B rep
    ylabel('\phi B (I)')
    axis([0 300 -500 500])
    grid on
%
    subplot (3,1,3); plot (IC,'k','LineWidth',2) % Phase C
    hold
    subplot (3,1,3); plot (Irep(3,:),'r','LineWidth',2) % Phase C rep
    grid on
    xlabel('Sample Number')
    axis([0 300 -500 500])
    ylabel('\phi C (I)')
end
%
%--------------------------- End Screen Selection 1 ----------------------
%
%****************************** End of Program *************************
%
```

Appendix D – *MatLab* source code – Comparison of power


```
%
%*************************************************************************
%
%                     Kobe_power_comparison.m
%
%   This program extracts data from the waveforms captured at Keob-Weiland
%   on March 9, 2009, and performs calculations to compare three
%   different power representations.  The calculations are the following:
%
%   1. Total ower as computed by the product of V & I over all phases (FDB)
%   2. Total power as computed using dq-Theory.
%   3. Total ower as computed using LaGrange minimization.
%
%   The program plots the three values in incresing pen-widths so that
%   discrepencies are easily visible.
%
%*************************************************************************
%
% Clean slate
%
clear all     %   clear workspaces
clc           %   clear screen
close all     %   close any open files
double all;   %   use double precision variables
%
%
%*************************************************************************
%
%   Read Kobe data files and populate variable matrix
%
D = csvread('Clean_dataset8.csv');
%
%-------------------------------------------------------------------------
%
%   extract vectors from dataset
%
for i=1:300
    t(i)=D(i,1);        % Time index
    Ia(i)=D(i,2);       % Phase A current
    Ib(i)=D(i,3);       % Phase B current
    Ic(i)=D(i,4);       % Phase C current
    Va(i)=D(i,5);       % Phase A voltage
    Vb(i)=D(i,6);       % Phase B voltage
    Vc(i)=D(i,7);       % Phase C voltage
end
%
%---------------- Incorporate CT and PT turns ratios ----------------------
%
%   CT ratio is 400:5 (80:1)
%   PT ratio is 60:1
%
VA=Va*60;
```

Appendix D Continued – *MatLab* source code – Comparison of power


```
VB=Vb*60;
VC=Vc*60;
%
IA=Ia*80;
IB=Ib*80;
IC=Ic*80;
%
%-------------------------- Define Constants ------------------------------
%
CT=sqrt(2/3)*[1 -0.5 -0.5; 0 sqrt(3)/2 -sqrt(3)/2];    % Clarke transform
CTI=sqrt(2/3)*[1 0; -0.5 sqrt(3)/2; -0.5 -sqrt(3)/2];  % Inverse Clarke
%                                                       %   transform
% ==================== Compute total power - method I ====================
%
PA=VA.*IA;  % Phase A VI
PB=VB.*IB;  % Phase B VI
PC=VC.*IC;  % Phase C VI
Power=(VA.*IA + VB.*IB + VC.*IC);
%
% ==================== Compute total power - method II ====================
%
%------------------------ Generate ABC matrices --------------------------
%
Vabc=[VA; VB; VC];
Iabc=[IA; IB; IC];
%
%--------------------- Determine power using dq method --------------------
%
Vdq=CT*Vabc;        % Determine d & q voltage
Idq=CT*Iabc;        % Determine d & q current
Valpha=Vdq(1,:);    % Separate parts of V and I (for easy identification)
Vbeta=Vdq(2,:);
Ialpha=Idq(1,:);
Ibeta=Idq(2,:);
%
P=Valpha.*Ialpha + Vbeta.*Ibeta;    % Determine Real Power
Q=Vbeta.*Ialpha - Valpha.*Ibeta;    % Determine Reactive Power
%
% ==================== Compute total power - method III ====================
%
%-------------------------- Define Lambda -------------------------------
%
%   Lm=Lambda/2 with Lambda being defined by (X-8)
%
%   Determine active and passive currents
%
for i=1:300
    Lm(i)=(VA(i)*IA(i)+VB(i)*IB(i)+VC(i)*IC(i))/(VA(i)^2+VB(i)^2+VC(i)^2);
    IPa(i)=IA(i)-Lm(i)*VA(i);
    IPb(i)=IB(i)-Lm(i)*VB(i);
    IPc(i)=IC(i)-Lm(i)*VC(i);
    IAa(i)=Lm(i)*VA(i);
```

Appendix D Continued – *MatLab* source code – Comparison of power


```
    IAb(i)=Lm(i)*VB(i);
    IAc(i)=Lm(i)*VC(i);
end
%
% ------------------ Determine total active power -------------------------
%
Piii=(VA.*IAa + VB.*IAb + VC.*IAc);
%
% ============================ End Computations ============================
%
%------------------------------ Plot results ------------------------------
%
plot (Power,'k','LineWidth',6)  % Plot direct VI power
hold
grid on
xlabel('Sample Number')
ylabel('Total Apparent Power')
title('Total Power')
plot (Piii,'y','LineWidth',4)   % Plot real power determined by LaGrange
plot (P,'r','LineWidth',2)      % Plot real power determined by dq

%
%------------------------ End of Program ---------------------------------
%
```

Appendix E – *MatLab* source code – Comparison of phase currents


```
%
%*************************************************************************
%
%                     Kobe_phaseA_comparison.m
%
%   This program extracts data from the waveforms captured at Keob-Weiland
%   on March 9, 2009, and performs power calculations to compare three
%   different power representations.
%
%   The calculations are the following:
%
%   1. Total ower as computed by the product of V & I over all phases (FDB)
%   2. Total power as computed using dq-Theory.
%   3. Total ower as computed using LaGrange minimization.
%
%   This is a sub-program to look at the differences between the active
%   current as determined by LaGrange and the actual input current.
%
%*************************************************************************
%
% Clean slate
%
clear all     %   clear workspaces
clc           %   clear screen
close all     %   close any open files
double all;   %   use double precision variables
%
%
%*************************************************************************
%
%   Read Kobe data files and populate variable matrix
%
D = csvread('Clean_dataset8.csv');
%
%-------------------------------------------------------------------------
%
%   extract vectors from dataset
%
for i=1:300
    t(i)=D(i,1);        % Time index
    Ia(i)=D(i,2);       % Phase A current
    Ib(i)=D(i,3);       % Phase B current
    Ic(i)=D(i,4);       % Phase C current
    Va(i)=D(i,5);       % Phase A voltage
    Vb(i)=D(i,6);       % Phase B voltage
    Vc(i)=D(i,7);       % Phase C voltage
end
%
%---------------- Incorporate CT and PT turns ratios ----------------------
%
%   CT ratio is 400:5 (80:1)
%   PT ratio is 60:1
```

Appendix E Continued – *MatLab* source code – Comparison of phase currents


```
%
VA=Va*60;
VB=Vb*60;
VC=Vc*60;
%
IA=Ia*80;
IB=Ib*80;
IC=Ic*80;
%
%-------------------------- Define Constants ------------------------------
%
CT=sqrt(2/3)*[1 -0.5 -0.5; 0 sqrt(3)/2 -sqrt(3)/2];    % Clarke transform
CTI=sqrt(2/3)*[1 0; -0.5 sqrt(3)/2; -0.5 -sqrt(3)/2];  % Inverse Clarke
%                                                      %   transform
% ==================== Compute total power - method I ====================
%
PA=VA.*IA;  % Phase A VI
PB=VB.*IB;  % Phase B VI
PC=VC.*IC;  % Phase C VI
Power=(VA.*IA + VB.*IB + VC.*IC);
%
% ==================== Compute total power - method II ====================
%
%------------------------ Generate ABC matrices --------------------------
%
Vabc=[VA; VB; VC];
Iabc=[IA; IB; IC];
%
%--------------------- Determine power using dq method --------------------
%
Vdq=CT*Vabc;        % Determine d & q voltage
Idq=CT*Iabc;        % Determine d & q current
Valpha=Vdq(1,:);    % Separate parts of V and I (for easy identification)
Vbeta=Vdq(2,:);
Ialpha=Idq(1,:);
Ibeta=Idq(2,:);
%
P=Valpha.*Ialpha + Vbeta.*Ibeta;    % Determine Real Power
Q=Vbeta.*Ialpha - Valpha.*Ibeta;    % Determine Reactive Power
%
% ==================== Compute total power - method III ====================
%
%-------------------------- Define Lambda -------------------------------
%
%   Lm=Lambda/2 with Lambda being defined by (X-8)
%
%   Determine active and passive currents
%
for i=1:300
    Lm(i)=(VA(i)*IA(i)+VB(i)*IB(i)+VC(i)*IC(i))/(VA(i)^2+VB(i)^2+VC(i)^2);
    IPa(i)=IA(i)-Lm(i)*VA(i);
    IPb(i)=IB(i)-Lm(i)*VB(i);
```

Appendix E Continued – *MatLab* source code – Comparison of phase currents


```
    IPc(i)=IC(i)-Lm(i)*VC(i);
    IAa(i)=Lm(i)*VA(i);
    IAb(i)=Lm(i)*VB(i);
    IAc(i)=Lm(i)*VC(i);
end
%
% ------------------ Determine total active power -------------------------
%
Piii=(VA.*IAa + VB.*IAb + VC.*IAc);
%
% ============================ End Computations ============================
%
%   This section plots out the actual mmeasured input current on the
%   same set of axes as the computed active current.  This is done for
%   all three phases.
%
    subplot (3,1,1); plot (IA,'k','LineWidth',2) % Phase A voltage
    hold
    subplot (3,1,1); plot (IAa,'r','LineWidth',2) % Phase A voltage
    title('Individual Phase Currents')
    ylabel('\phi A (I)')
    grid on
    subplot (3,1,2); plot (IB,'k','LineWidth',2) % Phase B voltage
    hold
    subplot (3,1,2); plot (IAb,'r','LineWidth',2) % Phase B voltage
    ylabel('\phi A (I)')
    grid on
    subplot (3,1,3); plot (IC,'k','LineWidth',2) % Phase C voltage
    hold
    subplot (3,1,3); plot (IAc,'r','LineWidth',2) % Phase C voltage
    grid on
    xlabel('Sample Number')
    ylabel('\phi C (I)')
%
%------------------------ End of Program --------------------------------
%
```

Appendix F – *MatLab* source code – Uncompensated EAF harmonic content


```
%
%*************************************************************************
%
%                     Kobe_uncompensated.m
%
%   This program downloads the Kobe data for phase voltage and current
%   waveforms and plot harmonic content for the both the 1st cycle and
%   the 2nd cycle of uncompensated waveforms.
%
%   This program will work for any of the captured data sets by changing
%   the number at the end of the data set file name.
%
%*************************************************************************
%
% Clean slate
%
clear all     %   clear workspaces
clc           %   clear screen
close all     %   close any open files
double all;   %   use double precision variables
%
%
%*************************************************************************
%
%   Read Kobe data files and populate variable matrix
%
D = csvread('Clean_dataset8.csv');
%
%-------------------------------------------------------------------------
%
%   extract vectors from dataset
%
for i=1:300
    t(i)=D(i,1);        % Time index
    Ia(i)=D(i,2);       % Phase A current
    Ib(i)=D(i,3);       % Phase B current
    Ic(i)=D(i,4);       % Phase C current
    Va(i)=D(i,5);       % Phase A voltage
    Vb(i)=D(i,6);       % Phase B voltage
    Vc(i)=D(i,7);       % Phase C voltage
end
%
%---------------- Incorporate CT and PT turns ratios ----------------------
%
%   CT ratio is 400:5 (80:1)
%   PT ratio is 60:1
%
VA=Va*60;
VB=Vb*60;
VC=Vc*60;
%
IA=Ia*80;
```

Appendix F Continued – *MatLab* source code – Uncompensated EAF harmonic content


```
IB=Ib*80;
IC=Ic*80;
%
%++++++++++++++++++++++++++++ Plot results ++++++++++++++++++++++++++++++
%
%************************ Begin Sccreen Prompts *************************
%
reply='';      % Create empty matirx, then present screen propmt
while isempty(reply)
reply = input('Select desired output:\n   For uncompensated 1st cycle plots enter "1" \n↙
For uncompensated 2nd cycle plots enter "2" \n   Any other value to end program.\n',↙
's');
end
%
%********************** Begin creen selection 1 *************************
%
if reply=='1'% If screen response is 1 execute this section, else skip.
%
Fs=150*60;          %  Sample frequency
%
   for i=1:150             % Put abc currents into vector.
         x(i)=IA(i);       % i=1-150 is 1st cycle
         y(i)=IB(i);
         z(i)=IC(i);
   end
%
% Plot harmonic bar graph
%
[XfreDomain, frequencyRange]=positiveFFT(x,Fs);
[YfreDomain, frequencyRange]=positiveFFT(y,Fs);
[ZfreDomain, frequencyRange]=positiveFFT(z,Fs);
%
X=sqrt(2)*abs(XfreDomain);
Y=sqrt(2)*abs(YfreDomain);
Z=sqrt(2)*abs(ZfreDomain);
%
% ----------------- Plot bar graphs as subplots --------------------------
%
subplot (3,1,1); bar(frequencyRange,X,.15);
title('Magnitude of 1st Cycle Input Current Harmonics')
ylabel('RMS (A)')
axis([0,1200,0,250])
grid on
%
%
subplot (3,1,2); bar(frequencyRange,Y,.15);
ylabel('RMS (A)')
axis([0,1200,0,250])
grid on
%
%
subplot (3,1,3); bar(frequencyRange,Z,.15);
```

Appendix F Continued – *MatLab* source code – Uncompensated EAF harmonic content


```
ylabel('RMS (A)')
axis([0,1200,0,250])
grid on
xlabel('Frequency (Hz)')
%
end
%
%********************** Begin creen selection 2 *************************
%
if reply=='2'% If screen response is 2 execute this section, else skip.
%
Fs=150*60;          %  Sample frequency
%
   for i=151:300   % i=151-300 is 2nd cycle
       tempx(i)=IA(i);
       tempy(i)=IB(i);
       tempz(i)=IC(i);
   end
% create y for 2nd cycle
   for i=1:150
       x(i)=tempx(i+150);
       y(i)=tempy(i+150);
       z(i)=tempz(i+150);
    end
%
% Plot harmonic bar graph
%
[XfreDomain, frequencyRange]=positiveFFT(x,Fs);
[YfreDomain, frequencyRange]=positiveFFT(y,Fs);
[ZfreDomain, frequencyRange]=positiveFFT(z,Fs);
%
X=sqrt(2)*abs(XfreDomain);
Y=sqrt(2)*abs(YfreDomain);
Z=sqrt(2)*abs(ZfreDomain);
%
% ----------------- Plot bar graphs as subplots --------------------------
%
subplot (3,1,1); bar(frequencyRange,X,.15);
title('Magnitude of 2nd Cycle Input Current Harmonics')
ylabel('RMS (A)')
axis([0,1200,0,250])
grid on
%
%
subplot (3,1,2); bar(frequencyRange,Y,.15);
ylabel('RMS (A)')
axis([0,1200,0,250])
grid on
%
%
subplot (3,1,3); bar(frequencyRange,Z,.15);
ylabel('RMS (A)')
```

Appendix F Continued – *MatLab* source code – Uncompensated EAF harmonic content


```
axis([0,1200,0,250])
grid on
xlabel('Frequency (Hz)')
%
end
%
%  Compute total harmonic distortion
%
sum=X(3)^2;
for j=3:75
    sum=sum+X(j)^2;
end
THDX=(sqrt(sum)/X(2))*100
%
sum=Y(3)^2;
for j=3:75
    sum=sum+Y(j)^2;
end
THDY=(sqrt(sum)/Y(2))*100
%
sum=Z(3)^2;
for j=3:75
    sum=sum+Z(j)^2;
end
THDZ=(sqrt(sum)/Z(2))*100
%
%*************************** End of Program ****************************
%
```

Appendix G – *MatLab* source code – *dq*-compensated EAF harmonic content


```
%
%*************************************************************************
%
%                   Kobe_dq_compensation_revised.m
%
%   This program downloads the Kobe data for phase voltage and current
%   waveforms and performs a standard dq compensation to remove reactive
%   power.  Both the 1st cycle and the 2nd cycle of the corrected input
%   waveform are plotted for review.
%
%   The program will fork for any of the captured data sets by changing
%   the number at the end of the data set file name.
%
%*************************************************************************
%
% Clean slate
%
clear all     %   clear workspaces
clc           %   clear screen
close all     %   close any open files
double all;   %   use double precision variables
%
%*************************************************************************
%
%   Read Kobe data files and populate variable matrix
%
D = csvread('Clean_dataset8.csv');
%
%-------------------------------------------------------------------------
%
%   extract vectors from dataset
%
for i=1:300
    t(i)=D(i,1);        % Time index
    Ia(i)=D(i,2);       % Phase A current
    Ib(i)=D(i,3);       % Phase B current
    Ic(i)=D(i,4);       % Phase C current
    Va(i)=D(i,5);       % Phase A voltage
    Vb(i)=D(i,6);       % Phase B voltage
    Vc(i)=D(i,7);       % Phase C voltage
end
%
%---------------- Incorporate CT and PT turns ratios ----------------------
%
%   CT ratio is 400:5 (80:1)
%   PT ratio is 60:1
%
VA=Va*60;
VB=Vb*60;
VC=Vc*60;

IA=Ia*80;
```

Appendix G Continued – *MatLab* source code – *dq*-compensated EAF harmonic content


```
IB=Ib*80;
IC=Ic*80;
%
%------------------------- Generate ABC matrices -------------------------
%
Vabc=[VA; VB; VC];
Iabc=[IA; IB; IC];
%
%-------------------------- Define Constants -----------------------------
%
CT=sqrt(2/3)*[1 -0.5 -0.5; 0 sqrt(3)/2 -sqrt(3)/2];     % Clarke transform
CTI=sqrt(2/3)*[1 0; -0.5 sqrt(3)/2; -0.5 -sqrt(3)/2];   % Inverse Clarke
%                                                       %   transform
%-------------------------------------------------------------------------
%
Vdq=CT*Vabc;         % Determine d & q voltage
Idq=CT*Iabc;         % Determine d & q current
Valpha=Vdq(1,:);     % Separate parts of V and I (for easy identification)
Vbeta=Vdq(2,:);
Ialpha=Idq(1,:);
Ibeta=Idq(2,:);
%
P=Valpha.*Ialpha + Vbeta.*Ibeta;     % Determine Real Power
Q=Vbeta.*Ialpha - Valpha.*Ibeta;     % Determine Reactive Power
%
for i=1:300          % Generate a reactive power vector that is all zeros
    Qzero(i)=0;
end
%
%------------------ Determine Compensating Currents ----------------------
%
for j=1:300
    M(j)=1/(Valpha(j)^2+Vbeta(j)^2);     % Determine coefficient
    IalphaC(j)=M(j)*( -Valpha(j)*P(j)-Vbeta(j)*Qzero(j));   % Direct I
    IbetaC(j)=M(j)*( -Vbeta(j)*P(j)+Valpha(j)*Qzero(j));    % Quadrature I
end
%
Icor=[IalphaC; IbetaC];   % Assemble compensating current vector
IabcCOR=CTI*Icor;         % Determine abc compensating currents
Ires=Iabc+IabcCOR;        % Determine abc current after compensation
%
% ------------ Extract corrected abc current values ----------------------
%
Iacor=Ires(1,:);     %  Phase A corrected current
Ibcor=Ires(2,:);     %  Phase B corrected current
Iccor=Ires(3,:);     %  Phase C corrected current
%
%+++++++++++++++++++++++++++++ Plot results ++++++++++++++++++++++++++++++
%
%************************ Begin Sccreen Prompts ************************
%
reply='';      % Create empty matirx, then present screen propmt
```

Appendix G Continued – *MatLab* source code – *dq*-compensated EAF harmonic content


```
while isempty(reply)
reply = input('Select desired output:\n   For dq-compensated 1st cycle plots enter "1"↙
\n   For dq-compensated 2nd cycle plots enter "2" \n   Any other value to end program.↙
\n', 's');
end
%
%********************** Begin creen selection 1 ************************
%
if reply=='1'% If screen response is 1 execute this section, else skip.
%
Fs=150*60;          %  Sample frequency
%
   for i=1:150     % i=1-150 is 1st cycle
      x(i)=Iacor(i);
      y(i)=Ibcor(i);
      z(i)=Iccor(i);
   end
%
% Plot harmonic bar graph
%
[XfreDomain, frequencyRange]=positiveFFT(x,Fs);
[YfreDomain, frequencyRange]=positiveFFT(y,Fs);
[ZfreDomain, frequencyRange]=positiveFFT(z,Fs);
%
X=sqrt(2)*abs(XfreDomain);
Y=sqrt(2)*abs(YfreDomain);
Z=sqrt(2)*abs(ZfreDomain);
%
% ----------------- Plot bar graphs as subplots --------------------------
%
subplot (3,1,1); bar(frequencyRange,X,.15);
title('Magnitude of 1st Cycle Input Current Harmonics')
ylabel('RMS (A)')
axis([0,1200,0,150])
grid on
%
%
subplot (3,1,2); bar(frequencyRange,Y,.15);
ylabel('RMS (A)')
axis([0,1200,0,150])
grid on
%
%
subplot (3,1,3); bar(frequencyRange,Z,.15);
ylabel('RMS (A)')
axis([0,1200,0,150])
grid on
xlabel('Frequency (Hz)')
%
end
%
%********************** Begin Screen selection 2 ************************
```

Appendix G Continued – *MatLab* source code – *dq*-compensated EAF harmonic content


```
%
if reply=='2'% If screen response is 2 execute this section, else skip.
%
Fs=150*60;          %  Sample frequency
%
   for i=151:300   % i=151-300 is 2nd cycle
       tempx(i)=Iacor(i);
       tempy(i)=Ibcor(i);
       tempz(i)=Iccor(i);
   end
% create xyz for 2nd cycle
   for i=1:150
       x(i)=tempx(i+150);
       y(i)=tempy(i+150);
       z(i)=tempz(i+150);
    end
%
% Plot harmonic bar graph
%
[XfreDomain, frequencyRange]=positiveFFT(x,Fs);
[YfreDomain, frequencyRange]=positiveFFT(y,Fs);
[ZfreDomain, frequencyRange]=positiveFFT(z,Fs);
%
X=sqrt(2)*abs(XfreDomain);
Y=sqrt(2)*abs(YfreDomain);
Z=sqrt(2)*abs(ZfreDomain);
%
% ----------------- Plot bar graphs as subplots ----------------------------
%
subplot (3,1,1); bar(frequencyRange,X,.15);
title('Magnitude of 2nd Cycle Input Current Harmonics')
ylabel('RMS (A)')
axis([0,1200,0,150])
grid on
%
%
subplot (3,1,2); bar(frequencyRange,Y,.15);
ylabel('RMS (A)')
axis([0,1200,0,150])
grid on
%
%
subplot (3,1,3); bar(frequencyRange,Z,.15);
ylabel('RMS (A)')
axis([0,1200,0,150])
grid on
xlabel('Frequency (Hz)')
%
end
%
%  Compute total harmonic distortion
%
```

Appendix G Continued – *MatLab* source code – *dq*-compensated EAF harmonic content


```
sum=X(3);
for j=3:75
    sum=sum+X(j);
end
THDX=(sqrt(sum)/X(2))*100

sum=Y(3);
for j=3:75
    sum=sum+Y(j);
end
THDX=(sqrt(sum)/Y(2))*100

sum=Z(3);
for j=3:75
    sum=sum+Z(j);
end
THDX=(sqrt(sum)/Z(2))*100

%
%*************************** End of Program ****************************
%
```

Appendix H – *MatLab* source code – LaGrange-compensated content


```
%*************************************************************************
%
%                       Kobe_LaGrange_comensation.m
%
%   This program extracts data from waveforms captured at Kobe-Weiland
%   on March 9, 2009 and performs calculations to determine Active
%   Current and Passive Current.  Both the 1st cycle and the 2nd cycle
%   of the corrected input waveform are plotted for review.
%
%   The program will wrk for any of the captured data sets by changing
%   the number at the end of the data set file name.
%
%*************************************************************************
%
% Clean slate
%
clear all      % clear workspaces
clc            % clear screen
close all      % close any open files
double all;    % use double precision for all data
%
%*************************************************************************
%
%   Read data files and populate allocate variable matrix
%
D = csvread('Clean_dataset8.csv');
%
%-------------------------------------------------------------------------
%
%   extract vectors from dataset
%
for i=1:300
    t(i)=D(i,1);
    Ia(i)=D(i,2);   % Phase A instanteneous measured current
    Ib(i)=D(i,3);   % Phase B instanteneous measured current
    Ic(i)=D(i,4);   % Phase C instanteneous measured current
    Va(i)=D(i,5);   % Phase A instanteneous measured voltage
    Vb(i)=D(i,6);   % Phase B instanteneous measured voltage
    Vc(i)=D(i,7);   % Phase C instanteneous measured voltage
%
end
%
%---------------- Incorporate CT and PT turns ratios ----------------------
%
%   CT ratio is 400:5 (80:1)
%   PT ratio is 60:1
%
%   The results of these calcuations are that the voltages are in Volts
%   and the currents are in Amperes.
%
Va=Va*60;
Vb=Vb*60;
```

Appendix H Continued – *MatLab* source code – LaGrange-compensated content


```
Vc=Vc*60;

Ia=Ia*80;
Ib=Ib*80;
Ic=Ic*80;
%
%--------------------------- Define Lambda --------------------------------
%
%   Lm=Lambda/2 with Lambda being defined by (X-8)
%
%   Determine active and passive currents
%
for i=1:300
    Lm(i)=(Va(i)*Ia(i)+Vb(i)*Ib(i)+Vc(i)*Ic(i))/(Va(i)^2+Vb(i)^2+Vc(i)^2);
    IPa(i)=Ia(i)-Lm(i)*Va(i);
    IPb(i)=Ib(i)-Lm(i)*Vb(i);
    IPc(i)=Ic(i)-Lm(i)*Vc(i);
    IAa(i)=Lm(i)*Va(i);
    IAb(i)=Lm(i)*Vb(i);
    IAc(i)=Lm(i)*Vc(i);
end
%
%+++++++++++++++++++++++++++ Plot results ++++++++++++++++++++++++++++++
%
%************************ Begin Sccreen Prompts *************************
%
reply='';      % Create empty matirx, then present screen propmt
while isempty(reply)
reply = input('Select desired output:\n   For LaGrange compensated 1st cycle plots enter↙
"1" \n   For LaGrange compensated 2nd cycle plots enter "2" \n   Any other value to end↙
program.\n', 's');
end
%
%********************** Begin creen selection 1 *************************
%
if reply=='1'% If screen response is 1 execute this section, else skip.
%
Fs=150*60;          %  Sample frequency
%
   for i=1:150     % i=1-150 is 1st cycle
      x(i)=IAa(i);
      y(i)=IAb(i);
      z(i)=IAc(i);
   end
%
% Plot harmonic bar graph
%
[XfreDomain, frequencyRange]=positiveFFT(x,Fs);
[YfreDomain, frequencyRange]=positiveFFT(y,Fs);
[ZfreDomain, frequencyRange]=positiveFFT(z,Fs);
%
X=sqrt(2)*abs(XfreDomain);
```

Appendix H Continued – *MatLab* source code – LaGrange-compensated content


```
Y=sqrt(2)*abs(YfreDomain);
Z=sqrt(2)*abs(ZfreDomain);
%
% ----------------- Plot bar graphs as subplots --------------------------
%
subplot (3,1,1); bar(frequencyRange,X,.15);
title('Magnitude of 1st Cycle Input Current Harmonics')
ylabel('RMS (A)')
axis([0,1200,0,200])
grid on
%
%
subplot (3,1,2); bar(frequencyRange,Y,.15);
ylabel('RMS (A)')
axis([0,1200,0,200])
grid on
%
%
subplot (3,1,3); bar(frequencyRange,Z,.15);
ylabel('RMS (A)')
axis([0,1200,0,200])
grid on
xlabel('Frequency (Hz)')
%
end
%
%********************** Begin Screen selection 2 *************************
%
if reply=='2'% If screen response is 2 execute this section, else skip.
%
Fs=150*60;          %  Sample frequency
%
   for i=151:300   % i=151-300 is 2nd cycle
       tempx(i)=IAa(i);
       tempy(i)=IAb(i);
       tempz(i)=IAc(i);
   end
% create xyz for 2nd cycle
   for i=1:150
       x(i)=tempx(i+150);
       y(i)=tempy(i+150);
       z(i)=tempz(i+150);
    end
%
% Plot harmonic bar graph
%
[XfreDomain, frequencyRange]=positiveFFT(x,Fs);
[YfreDomain, frequencyRange]=positiveFFT(y,Fs);
[ZfreDomain, frequencyRange]=positiveFFT(z,Fs);
%
X=sqrt(2)*abs(XfreDomain);
Y=sqrt(2)*abs(YfreDomain);
```

Appendix H Continued – *MatLab* source code – LaGrange-compensated content


```
Z=sqrt(2)*abs(ZfreDomain);
%
% ----------------- Plot bar graphs as subplots --------------------------
%
subplot (3,1,1); bar(frequencyRange,X,.15);
title('Magnitude of 2nd Cycle Input Current Harmonics')
ylabel('RMS (A)')
axis([0,1200,0,200])
grid on
%
%
subplot (3,1,2); bar(frequencyRange,Y,.15);
ylabel('RMS (A)')
axis([0,1200,0,200])
grid on
%
%
subplot (3,1,3); bar(frequencyRange,Z,.15);
ylabel('RMS (A)')
axis([0,1200,0,200])
grid on
xlabel('Frequency (Hz)')
%
end
%
%
%  Compute total harmonic distortion
%
sum=X(3)^2;
for j=3:75
    sum=sum+X(j)^2;
end
THDX=(sqrt(sum)/X(2))*100

sum=Y(3)^2;
for j=3:75
    sum=sum+Y(j)^2;
end
THDY=(sqrt(sum)/Y(2))*100

sum=Z(3)^2;
for j=3:75
    sum=sum+Z(j)^2;
end
THDZ=(sqrt(sum)/Z(2))*100
%
%
%************************** End of Program ****************************
%
```

Appendix I – *MatLab* source code – Total powers with LaGrange


```
%*************************************************************************
%
%                       Kobe_LaGrange_power_needed.m
%
%   This program extracts data from waveforms captured at Kobe-Weiland
%   on March 9, 2009 and performs calculations to determine Active
%   Current and Passive Current.
%
%   The program then calculates total three-phase power in the
%   compensated (active) waveform and the correcting (passive) waveform.
%   of the corrected input waveform are plotted for review.
%
%   The program will work for any of the captured data sets by changing
%   the number at the end of the data set file name.
%
%*************************************************************************
%
% Clean slate
%
clear all      % clear workspaces
clc            % clear screen
close all      % close any open files
double all;    % use double precision for all data
%
%*************************************************************************
%
%   Read data files and populate allocate variable matrix
%
D = csvread('Clean_dataset8.csv');
%
%-------------------------------------------------------------------------
%
%   extract vectors from dataset
%
for i=1:300
    t(i)=D(i,1);
    Ia(i)=D(i,2);    % Phase A instanteneous measured current
    Ib(i)=D(i,3);    % Phase B instanteneous measured current
    Ic(i)=D(i,4);    % Phase C instanteneous measured current
    Va(i)=D(i,5);    % Phase A instanteneous measured voltage
    Vb(i)=D(i,6);    % Phase B instanteneous measured voltage
    Vc(i)=D(i,7);    % Phase C instanteneous measured voltage
%
end
%
%---------------- Incorporate CT and PT turns ratios ----------------------
%
%   CT ratio is 400:5 (80:1)
%   PT ratio is 60:1
%
%   The results of these calcuations are that the voltages are in Volts
%   and the currents are in Amperes.
```

Appendix I Continued – *MatLab* source code – Total powers with LaGrange


```
%
Va=Va*60;
Vb=Vb*60;
Vc=Vc*60;

Ia=Ia*80;
Ib=Ib*80;
Ic=Ic*80;
%
%--------------------------- Define Lambda -------------------------------
%
%   Lm=Lambda/2 with Lambda being defined by (X-8)
%
%   Determine active and passive currents
%
for i=1:300
    Lm(i)=(Va(i)*Ia(i)+Vb(i)*Ib(i)+Vc(i)*Ic(i))/(Va(i)^2+Vb(i)^2+Vc(i)^2);
    IPa(i)=Ia(i)-Lm(i)*Va(i);
    IPb(i)=Ib(i)-Lm(i)*Vb(i);
    IPc(i)=Ic(i)-Lm(i)*Vc(i);
    IAa(i)=Lm(i)*Va(i);
    IAb(i)=Lm(i)*Vb(i);
    IAc(i)=Lm(i)*Vc(i);
end
%
%  Determine total active power
%
Pactive=(Va.*IAa+Vb.*IAb+Vc.*IAc);
PAaverage=mean(Pactive);
%
Ppassive=(Va.*IPa+Vb.*IPb+Vc.*IPc);
PPaverage=mean(Ppassive);
%
%   Generate a vector of average power for plotting purposes
%
for i=1:300
    PAave(i)=PAaverage;
end
%
%++++++++++++++++++++++++++++ Plot results ++++++++++++++++++++++++++++++
%
%************************ Begin Sccreen Prompts *************************
%
reply='';      % Create empty matirx, then present screen propmt
while isempty(reply)
reply = input('Select desired output:\n   For Total Active Power plot enter "1" \n   For↙
Total Passibe Power plot enter "2" \n   Any other value to end program.\n', 's');
end
%
%********************** Begin creen selection 1 *************************
%
if reply=='1'% If screen response is 1 execute this section, else skip.
```

Appendix I Continued – *MatLab* source code – Total powers with LaGrange


```
%
plot (Pactive,'k','LineWidth',2)       % Total Power
hold
grid on
xlabel('Sample Number')
ylabel('Apparent Power (VA)')
title('Total Three-phase Power')
axis ( [0 300 0 8E6])
plot (PAave,'r','LineWidth',2)       % Total Power
end
%
%********************** Begin Screen selection 2 ************************
%
if reply=='2'% If screen response is 2 execute this section, else skip.
%
plot (Ppassive,'k','LineWidth',2)       % Total Power
hold
grid on
xlabel('Sample Number')
ylabel('Apparent Power (VA)')
title('Total Three-phase Power')
axis ( [0 300 -10 10])
%plot (Pave,'r','LineWidth',2)       % Total Power
end
%
%*************************** End of Program *****************************
%
```

Appendix J *Mathematica* equivalence proof

In[1]:=
```
Clear[Evaluate[Context[] <> "*"]]

va = Vrms * Sqrt[2] * Cos[ω * t]
vb = Vrms * Sqrt[2] * Cos[(ω * t - 2 π / 3)]
vc = Vrms * Sqrt[2] * Cos[(ω * t + 2 π / 3)]
ia = Irms * Sqrt[2] * Cos[(ω * t + ϕ)]
ib = Irms * Sqrt[2] * Cos[(ω * t - (2 π / 3) + ϕ)]
ic = Irms * Sqrt[2] * Cos[(ω * t + (2 π / 3) + ϕ)]

m = ((va * ia) + (vb * ib) + (vc * ic)) / (va^2 + vb^2 + vc^2)

TrigExpand[m]

pwr = va * ia + vb * ib + vc * ic

TrigExpand [pwr]

iaa = (m * va)

iab = (m * vb)

iac = (m * vc)

patot = (va * iaa) + (vb * iab) + (vc * iac)

TrigExpand[paot]

ipa = ia - (m * va)

ipb = ib - (m * vb)

ipc = ic - (m * vc)

pptot = (va * ipa) + (vb * ipb) + (vc * ipc)

TrigExpand[pptot]
```

Out[2]= $\sqrt{2}\ \text{Vrms}\ \text{Cos}[t\,\omega]$

Out[3]= $-\sqrt{2}\ \text{Vrms}\ \text{Sin}\left[\frac{\pi}{6} - t\,\omega\right]$

Out[4]= $-\sqrt{2}\ \text{Vrms}\ \text{Sin}\left[\frac{\pi}{6} + t\,\omega\right]$

Out[5]= $\sqrt{2}\ \text{Irms}\ \text{Cos}[\phi + t\,\omega]$

Out[6]= $-\sqrt{2}\ \text{Irms}\ \text{Sin}\left[\frac{\pi}{6} - \phi - t\,\omega\right]$

Out[7]= $-\sqrt{2}\ \text{Irms}\ \text{Sin}\left[\frac{\pi}{6} + \phi + t\,\omega\right]$

Appendix J Continued *Mathematica* equivalence proof

Out[8]=
$$\left(2\,\text{Irms}\,\text{Vrms}\,\text{Cos}[t\,\omega]\,\text{Cos}[\phi+t\,\omega]+2\,\text{Irms}\,\text{Vrms}\,\text{Sin}\left[\frac{\pi}{6}-t\,\omega\right]\text{Sin}\left[\frac{\pi}{6}-\phi-t\,\omega\right]+2\,\text{Irms}\,\text{Vrms}\,\text{Sin}\left[\frac{\pi}{6}+t\,\omega\right]\text{Sin}\left[\frac{\pi}{6}+\phi+t\,\omega\right]\right)\Big/\left(2\,\text{Vrms}^2\,\text{Cos}[t\,\omega]^2+2\,\text{Vrms}^2\,\text{Sin}\left[\frac{\pi}{6}-t\,\omega\right]^2+2\,\text{Vrms}^2\,\text{Sin}\left[\frac{\pi}{6}+t\,\omega\right]^2\right)$$

Out[9]=
$$\frac{\text{Irms}\,\text{Cos}[\phi]}{\text{Vrms}}$$

Out[10]=
$$2\,\text{Irms}\,\text{Vrms}\,\text{Cos}[t\,\omega]\,\text{Cos}[\phi+t\,\omega]+2\,\text{Irms}\,\text{Vrms}\,\text{Sin}\left[\frac{\pi}{6}-t\,\omega\right]\text{Sin}\left[\frac{\pi}{6}-\phi-t\,\omega\right]+2\,\text{Irms}\,\text{Vrms}\,\text{Sin}\left[\frac{\pi}{6}+t\,\omega\right]\text{Sin}\left[\frac{\pi}{6}+\phi+t\,\omega\right]$$

Out[11]=
$$3\,\text{Irms}\,\text{Vrms}\,\text{Cos}[\phi]$$

Out[12]=
$$\left(\sqrt{2}\,\text{Vrms}\,\text{Cos}[t\,\omega]\left(2\,\text{Irms}\,\text{Vrms}\,\text{Cos}[t\,\omega]\,\text{Cos}[\phi+t\,\omega]+2\,\text{Irms}\,\text{Vrms}\,\text{Sin}\left[\frac{\pi}{6}-t\,\omega\right]\text{Sin}\left[\frac{\pi}{6}-\phi-t\,\omega\right]+2\,\text{Irms}\,\text{Vrms}\,\text{Sin}\left[\frac{\pi}{6}+t\,\omega\right]\text{Sin}\left[\frac{\pi}{6}+\phi+t\,\omega\right]\right)\right)\Big/\left(2\,\text{Vrms}^2\,\text{Cos}[t\,\omega]^2+2\,\text{Vrms}^2\,\text{Sin}\left[\frac{\pi}{6}-t\,\omega\right]^2+2\,\text{Vrms}^2\,\text{Sin}\left[\frac{\pi}{6}+t\,\omega\right]^2\right)$$

Out[13]=
$$-\left(\sqrt{2}\,\text{Vrms}\,\text{Sin}\left[\frac{\pi}{6}-t\,\omega\right]\left(2\,\text{Irms}\,\text{Vrms}\,\text{Cos}[t\,\omega]\,\text{Cos}[\phi+t\,\omega]+2\,\text{Irms}\,\text{Vrms}\,\text{Sin}\left[\frac{\pi}{6}-t\,\omega\right]\text{Sin}\left[\frac{\pi}{6}-\phi-t\,\omega\right]+2\,\text{Irms}\,\text{Vrms}\,\text{Sin}\left[\frac{\pi}{6}+t\,\omega\right]\text{Sin}\left[\frac{\pi}{6}+\phi+t\,\omega\right]\right)\right)\Big/\left(2\,\text{Vrms}^2\,\text{Cos}[t\,\omega]^2+2\,\text{Vrms}^2\,\text{Sin}\left[\frac{\pi}{6}-t\,\omega\right]^2+2\,\text{Vrms}^2\,\text{Sin}\left[\frac{\pi}{6}+t\,\omega\right]^2\right)$$

Out[14]=
$$-\left(\sqrt{2}\,\text{Vrms}\,\text{Sin}\left[\frac{\pi}{6}+t\,\omega\right]\left(2\,\text{Irms}\,\text{Vrms}\,\text{Cos}[t\,\omega]\,\text{Cos}[\phi+t\,\omega]+2\,\text{Irms}\,\text{Vrms}\,\text{Sin}\left[\frac{\pi}{6}-t\,\omega\right]\text{Sin}\left[\frac{\pi}{6}-\phi-t\,\omega\right]+2\,\text{Irms}\,\text{Vrms}\,\text{Sin}\left[\frac{\pi}{6}+t\,\omega\right]\text{Sin}\left[\frac{\pi}{6}+\phi+t\,\omega\right]\right)\right)\Big/\left(2\,\text{Vrms}^2\,\text{Cos}[t\,\omega]^2+2\,\text{Vrms}^2\,\text{Sin}\left[\frac{\pi}{6}-t\,\omega\right]^2+2\,\text{Vrms}^2\,\text{Sin}\left[\frac{\pi}{6}+t\,\omega\right]^2\right)$$

Appendix J Continued *Mathematica* equivalence proof

Out[15]=
$$\left(2\,\text{Vrms}^2\,\text{Cos}[t\,\omega]^2\left(2\,\text{Irms}\,\text{Vrms}\,\text{Cos}[t\,\omega]\,\text{Cos}[\phi+t\,\omega]+2\,\text{Irms}\,\text{Vrms}\,\text{Sin}\left[\frac{\pi}{6}-t\,\omega\right]\text{Sin}\left[\frac{\pi}{6}-\phi-t\,\omega\right]+2\,\text{Irms}\,\text{Vrms}\,\text{Sin}\left[\frac{\pi}{6}+t\,\omega\right]\text{Sin}\left[\frac{\pi}{6}+\phi+t\,\omega\right]\right)\right)\Big/$$
$$\left(2\,\text{Vrms}^2\,\text{Cos}[t\,\omega]^2+2\,\text{Vrms}^2\,\text{Sin}\left[\frac{\pi}{6}-t\,\omega\right]^2+2\,\text{Vrms}^2\,\text{Sin}\left[\frac{\pi}{6}+t\,\omega\right]^2\right)+$$
$$\left(2\,\text{Vrms}^2\,\text{Sin}\left[\frac{\pi}{6}-t\,\omega\right]^2\left(2\,\text{Irms}\,\text{Vrms}\,\text{Cos}[t\,\omega]\,\text{Cos}[\phi+t\,\omega]+2\,\text{Irms}\,\text{Vrms}\,\text{Sin}\left[\frac{\pi}{6}-t\,\omega\right]\text{Sin}\left[\frac{\pi}{6}-\phi-t\,\omega\right]+2\,\text{Irms}\,\text{Vrms}\,\text{Sin}\left[\frac{\pi}{6}+t\,\omega\right]\text{Sin}\left[\frac{\pi}{6}+\phi+t\,\omega\right]\right)\right)\Big/$$
$$\left(2\,\text{Vrms}^2\,\text{Cos}[t\,\omega]^2+2\,\text{Vrms}^2\,\text{Sin}\left[\frac{\pi}{6}-t\,\omega\right]^2+2\,\text{Vrms}^2\,\text{Sin}\left[\frac{\pi}{6}+t\,\omega\right]^2\right)+$$
$$\left(2\,\text{Vrms}^2\,\text{Sin}\left[\frac{\pi}{6}+t\,\omega\right]^2\left(2\,\text{Irms}\,\text{Vrms}\,\text{Cos}[t\,\omega]\,\text{Cos}[\phi+t\,\omega]+2\,\text{Irms}\,\text{Vrms}\,\text{Sin}\left[\frac{\pi}{6}-t\,\omega\right]\text{Sin}\left[\frac{\pi}{6}-\phi-t\,\omega\right]+2\,\text{Irms}\,\text{Vrms}\,\text{Sin}\left[\frac{\pi}{6}+t\,\omega\right]\text{Sin}\left[\frac{\pi}{6}+\phi+t\,\omega\right]\right)\right)\Big/$$
$$\left(2\,\text{Vrms}^2\,\text{Cos}[t\,\omega]^2+2\,\text{Vrms}^2\,\text{Sin}\left[\frac{\pi}{6}-t\,\omega\right]^2+2\,\text{Vrms}^2\,\text{Sin}\left[\frac{\pi}{6}+t\,\omega\right]^2\right)$$

Out[16]= paot

Out[17]=
$$\sqrt{2}\,\text{Irms}\,\text{Cos}[\phi+t\,\omega]-\left(\sqrt{2}\,\text{Vrms}\,\text{Cos}[t\,\omega]\left(2\,\text{Irms}\,\text{Vrms}\,\text{Cos}[t\,\omega]\,\text{Cos}[\phi+t\,\omega]+2\,\text{Irms}\,\text{Vrms}\,\text{Sin}\left[\frac{\pi}{6}-t\,\omega\right]\text{Sin}\left[\frac{\pi}{6}-\phi-t\,\omega\right]+2\,\text{Irms}\,\text{Vrms}\,\text{Sin}\left[\frac{\pi}{6}+t\,\omega\right]\text{Sin}\left[\frac{\pi}{6}+\phi+t\,\omega\right]\right)\right)\Big/$$
$$\left(2\,\text{Vrms}^2\,\text{Cos}[t\,\omega]^2+2\,\text{Vrms}^2\,\text{Sin}\left[\frac{\pi}{6}-t\,\omega\right]^2+2\,\text{Vrms}^2\,\text{Sin}\left[\frac{\pi}{6}+t\,\omega\right]^2\right)$$

Out[18]=
$$-\sqrt{2}\,\text{Irms}\,\text{Sin}\left[\frac{\pi}{6}-\phi-t\,\omega\right]+\left(\sqrt{2}\,\text{Vrms}\,\text{Sin}\left[\frac{\pi}{6}-t\,\omega\right]\left(2\,\text{Irms}\,\text{Vrms}\,\text{Cos}[t\,\omega]\,\text{Cos}[\phi+t\,\omega]+2\,\text{Irms}\,\text{Vrms}\,\text{Sin}\left[\frac{\pi}{6}-t\,\omega\right]\text{Sin}\left[\frac{\pi}{6}-\phi-t\,\omega\right]+2\,\text{Irms}\,\text{Vrms}\,\text{Sin}\left[\frac{\pi}{6}+t\,\omega\right]\text{Sin}\left[\frac{\pi}{6}+\phi+t\,\omega\right]\right)\right)\Big/$$
$$\left(2\,\text{Vrms}^2\,\text{Cos}[t\,\omega]^2+2\,\text{Vrms}^2\,\text{Sin}\left[\frac{\pi}{6}-t\,\omega\right]^2+2\,\text{Vrms}^2\,\text{Sin}\left[\frac{\pi}{6}+t\,\omega\right]^2\right)$$

Out[19]=
$$-\sqrt{2}\,\text{Irms}\,\text{Sin}\left[\frac{\pi}{6}+\phi+t\,\omega\right]+\left(\sqrt{2}\,\text{Vrms}\,\text{Sin}\left[\frac{\pi}{6}+t\,\omega\right]\left(2\,\text{Irms}\,\text{Vrms}\,\text{Cos}[t\,\omega]\,\text{Cos}[\phi+t\,\omega]+2\,\text{Irms}\,\text{Vrms}\,\text{Sin}\left[\frac{\pi}{6}-t\,\omega\right]\text{Sin}\left[\frac{\pi}{6}-\phi-t\,\omega\right]+2\,\text{Irms}\,\text{Vrms}\,\text{Sin}\left[\frac{\pi}{6}+t\,\omega\right]\text{Sin}\left[\frac{\pi}{6}+\phi+t\,\omega\right]\right)\right)\Big/$$
$$\left(2\,\text{Vrms}^2\,\text{Cos}[t\,\omega]^2+2\,\text{Vrms}^2\,\text{Sin}\left[\frac{\pi}{6}-t\,\omega\right]^2+2\,\text{Vrms}^2\,\text{Sin}\left[\frac{\pi}{6}+t\,\omega\right]^2\right)$$

Appendix J Continued *Mathematica* equivalence proof

Out[20]=

$$\sqrt{2}\ \text{Vrms}\,\text{Cos}[t\,\omega]\left(\sqrt{2}\ \text{Irms}\,\text{Cos}[\phi+t\,\omega]-\left(\sqrt{2}\ \text{Vrms}\,\text{Cos}[t\,\omega]\left(2\,\text{Irms}\,\text{Vrms}\,\text{Cos}[t\,\omega]\,\text{Cos}[\phi+t\,\omega]+2\,\text{Irms}\,\text{Vrms}\,\text{Sin}\left[\frac{\pi}{6}-t\,\omega\right]\text{Sin}\left[\frac{\pi}{6}-\phi-t\,\omega\right]+2\,\text{Irms}\,\text{Vrms}\,\text{Sin}\left[\frac{\pi}{6}+t\,\omega\right]\text{Sin}\left[\frac{\pi}{6}+\phi+t\,\omega\right]\right)\right)\Big/\left(2\,\text{Vrms}^2\,\text{Cos}[t\,\omega]^2+2\,\text{Vrms}^2\,\text{Sin}\left[\frac{\pi}{6}-t\,\omega\right]^2+2\,\text{Vrms}^2\,\text{Sin}\left[\frac{\pi}{6}+t\,\omega\right]^2\right)\right)-\sqrt{2}\ \text{Vrms}\,\text{Sin}\left[\frac{\pi}{6}-t\,\omega\right]\left(-\sqrt{2}\ \text{Irms}\,\text{Sin}\left[\frac{\pi}{6}-\phi-t\,\omega\right]+\left(\sqrt{2}\ \text{Vrms}\,\text{Sin}\left[\frac{\pi}{6}-t\,\omega\right]\left(2\,\text{Irms}\,\text{Vrms}\,\text{Cos}[t\,\omega]\,\text{Cos}[\phi+t\,\omega]+2\,\text{Irms}\,\text{Vrms}\,\text{Sin}\left[\frac{\pi}{6}-t\,\omega\right]\text{Sin}\left[\frac{\pi}{6}-\phi-t\,\omega\right]+2\,\text{Irms}\,\text{Vrms}\,\text{Sin}\left[\frac{\pi}{6}+t\,\omega\right]\text{Sin}\left[\frac{\pi}{6}+\phi+t\,\omega\right]\right)\right)\Big/\left(2\,\text{Vrms}^2\,\text{Cos}[t\,\omega]^2+2\,\text{Vrms}^2\,\text{Sin}\left[\frac{\pi}{6}-t\,\omega\right]^2+2\,\text{Vrms}^2\,\text{Sin}\left[\frac{\pi}{6}+t\,\omega\right]^2\right)\right)-\sqrt{2}\ \text{Vrms}\,\text{Sin}\left[\frac{\pi}{6}+t\,\omega\right]\left(-\sqrt{2}\ \text{Irms}\,\text{Sin}\left[\frac{\pi}{6}+\phi+t\,\omega\right]+\left(\sqrt{2}\ \text{Vrms}\,\text{Sin}\left[\frac{\pi}{6}+t\,\omega\right]\left(2\,\text{Irms}\,\text{Vrms}\,\text{Cos}[t\,\omega]\,\text{Cos}[\phi+t\,\omega]+2\,\text{Irms}\,\text{Vrms}\,\text{Sin}\left[\frac{\pi}{6}-t\,\omega\right]\text{Sin}\left[\frac{\pi}{6}-\phi-t\,\omega\right]+2\,\text{Irms}\,\text{Vrms}\,\text{Sin}\left[\frac{\pi}{6}+t\,\omega\right]\text{Sin}\left[\frac{\pi}{6}+\phi+t\,\omega\right]\right)\right)\Big/\left(2\,\text{Vrms}^2\,\text{Cos}[t\,\omega]^2+2\,\text{Vrms}^2\,\text{Sin}\left[\frac{\pi}{6}-t\,\omega\right]^2+2\,\text{Vrms}^2\,\text{Sin}\left[\frac{\pi}{6}+t\,\omega\right]^2\right)\right)$$

Out[21]= 0

Appendix K – *MatLab* source code – Typical EAF phase and neutral currents


```
%*************************************************************************
%
%                       Kobe_Waveform_Analysis.m
%
%   This program extracts data from waveforms captured at Kobe-Weiland
%   on March 9, 2009 and performs plots the phase currents plus
%   the neutral current.
%
%*************************************************************************
%
% Clean slate
%
clear all      % clear workspaces
clc            % clear screen
close all      % close any open files
double all;    % use double precision for all data
%
%*************************************************************************
%
%   Read data files and populate allocate variable matrix.  The filename
%     is of the form "Clean_dataset#.csv" where # is the number of the
%     data set of interest.
%
D = csvread('Clean_dataset1.csv');
%
%-------------------------------------------------------------------------
%
%   Extract vectors from dataset
%
for i=1:300
    t(i)=D(i,1);
    Ia(i)=D(i,2);
    Ib(i)=D(i,3);
    Ic(i)=D(i,4);
    Va(i)=D(i,5);
    Vb(i)=D(i,6);
    Vc(i)=D(i,7);
end
%
%---------------- Incorporate CT and PT turns ratios ---------------------
%
%   CT ratio is 400:5 (80:1)
%   PT ratio is 60:1
%
Va=Va*60;  % Not used in this program
Vb=Vb*60;  % Not used in this program
Vc=Vc*60;  % Not used in this program

Ia=Ia*80;
Ib=Ib*80;
Ic=Ic*80;
%
```

Appendix K Continued – *MatLab* source code – Typical EAF phase and neutral currents


```
%----------------------------- Current Curves ----------------------------
%
It=Ia+Ib+Ic;
plot(t, Ia,'k','LineWidth',1)
hold,grid on
plot(t, Ib,'r','LineWidth',1)
plot(t, Ic,'b','LineWidth',1)
plot(t, It,'g','LineWidth',1)
xlabel('Time [Seconds]')
ylabel('Current [Amperes]')
title('EAF phase and neutral currents')
%
%------------------------ End of Program --------------------------------
%
```

Appendix L – Harmonic analyzer instrument readings

Single Phase Readings - 10/14/10 16:51:19

			Voltage
Frequency	59.96	RMS	288.4
Power		Peak	414.8
Watts	-44.00	DC Offset	-0.1
VA	185.00	Crest 1.44	1.65
Vars	160.00	THD Rms	2.09
Peak W	-276.00	THD Fund	2.09
Phase	105° lag	HRMS	6.0
Total PF	-0.24	KFactor	22.13
DPF	-0.25		

Single Phase Readings - 03/16/11 16:51:19

Harmonics	Freq.	1 Phase V Mag	%V RMS	1 Phase V Ø°
DC	0.00	0.06	0.02	0
1	59.96	288.38	99.99	0
2	119.92	0.03	0.01	112
3	179.88	0.66	0.23	169
4	239.85	0.02	0.01	50
5	299.81	4.80	1.66	50
6	359.77	0.02	0.01	89
7	419.73	1.23	0.43	-177
8	479.69	0.05	0.02	-149
9	539.65	0.30	0.10	129
10	599.62	0.03	0.01	54
11	659.58	2.56	0.89	158
12	719.54	0.02	0.01	122
13	779.50	1.91	0.66	168
14	839.46	0.05	0.02	112
15	899.42	0.33	0.11	104
16	959.38	0.05	0.02	-178
17	1019.35	0.83	0.29	-146
18	1079.31	0.02	0.01	120
19	1139.27	0.33	0.11	-121
20	1199.23	0.03	0.01	121
21	1259.19	0.05	0.02	-90
22	1319.15	0.02	0.01	-8
23	1379.12	0.27	0.09	-9
24	1439.08	0.02	0.01	41
25	1499.04	0.16	0.05	8
26	1559.00	0.02	0.01	117
27	1618.96	0.03	0.01	79
28	1678.92	0.03	0.01	-167
29	1738.88	0.28	0.10	129
30	1798.85	0.02	0.01	136
31	1858.81	0.20	0.07	130

PSCAD
APPLICATION NOTES

Electric Arc Furnace Modeling and Validation

Modern power systems have a variety of connected nonlinear loads, the ability to study and understand power quality issues is becoming more important. It is necessary to understand the sources of power disturbances and equally imperative to determine practical means to mitigate these power quality problems.

A major contributer to power quality issues, specifically voltage flicker, is the Electric Arc Furnace. The electric arc furnace is a highly variable non-linear load, which according to some studies, possesses what is described as a chaotic pattern.

In response to high client interest, the Manitoba HVDC Research Centre has begun development of an Electric Arc Furnace model. The arc furnace model employs non-linear differential equations1 as opposed to the traditional piece-wise linear method resulting in more accurate and realistic simulation.

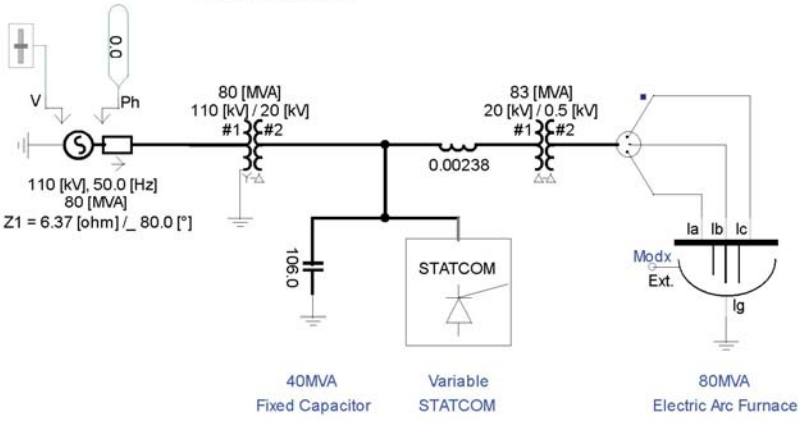

Figure 1 PSCAD Electric Arc Furnace System

The new PSCAD electric arc furnace model was studied as a part of the electrical network as depicted in Figure 1. The voltage-current characteristic of an electric arc furnace is depicted in Figure 2. In a simulated attempt to reduce voltage flicker, the size of the STATCOM in the network was varied, while the size of the capacitors and parameters of the arc furnace remained fixed. The power of the new arc furnace model within the PSCAD environment became apparent when a selection of different sized STATCOMs were evaluated in the model. PSCAD was also able to simulate the UIE Flickermeter to "block 4" which means an instantaneous value of flicker is generated. When averaged over the length of the simulation run, Block 4 gives an indication of the level of voltage flicker occuring on the bus. Normally this "instantaneous flicker" is collected and scaled over 10 minutes to provide a Pst value[2]. By first running the simulation without compensation, we get a benchmark upon

MANITOBA·HVDC RESEARCH CENTRE

Manitoba HVDC Research Centre Inc.
244 Cree Crescent
Winnipeg, Manitoba, Canada R3J 3W1
T +1 204 989 1240 F +1 204 989 1277
info@pscad.com

www.pscad.com

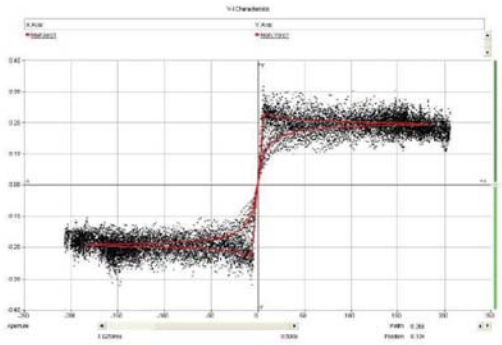

Figure 2 V-I Characteristic of an Electric Arc (including reference plot and scatter, using the advanced plotting capabilities of the LieWire 2)

This graph shows a plot of the differential equation in red. The scatter plot on top shows the same equation plotted, but with sinusoidal and Gaussian noise added in an attempt to model the random nature of the Electric Arc Furnace.

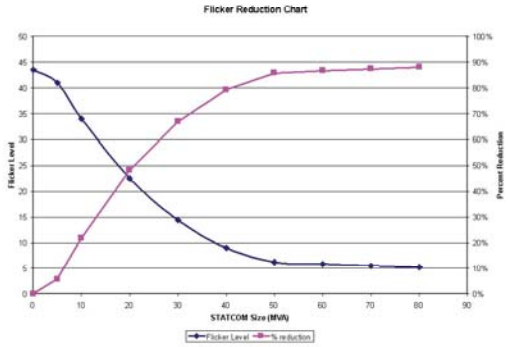

Figure 3 Flicker Reduction

From this graph, one can quickly see the most effective size of STATCOM needed to reduce the flicker, starting from a 22% reduction for a 10 MVA STATCOM to an 88% reduction for an 80MVA STATCOM.

which to compare the compensated results. And, we are able to quite easily calculate the percent flicker reduction achieved by the various runs. Referring to Figure 3, we can determine the most economical size of STATCOM that would be needed to reduce the voltage flicker to an acceptable level.

In a continued effort to provide realistic and accurate validated models to end-users, the Centre welcomes interested parties to participate in the development of the arc furnace model by providing us with actual recorded data from industrial arc furnace installations, or any other information that may be of interest. If you wish to participate, please contact us at support@pscad.com.

by Dan Kell

References

[1] *E.Acha, A. Semlyen, and N. Rajakovic, "A Harmonic Domain Computational Package for Nonlinear Problems and its Application to Electric Arcs," IEEE Transactions on Power Delivery, vol. 5, no. 3, pp 1390-1395, July 1990*

[2] *J. Wikston, "The UIE/IEC Flickermeter Description," IEEE PES, Tutorial on Voltage Fluctuations and Lamp Flicker in Electric Power Systems, pp. 11, Feb. 2001*

Appendix N – *MatLab* source code – Development of modified Euler method


```
%**************************************************************************
%
%                    Test_Modified_Euler_Development_1.m
%
%   This program implements a series of solutions to solve the
%   Ordinary Differential Equation (ODE) that is the relationship between
%   voltage and current for a single phase Electric Arc Furnace (EAF).
%
%   The following solutions are modeled:  (1) 4th order Runge-Kutta, (2)
%   Euler method, & (3) Modified Euler method.
%
%   This program drives the arc with a sinusoidal current and determines
%   arc radius based on the ODE.  The arc voltage is then calculated as
%   on the radius and voltage.
%
%   The program plots curves for arc radius vs time, arc voltage vs time,
%   and arc current vs arc voltage.
%
%**************************************************************************
%
% Clean slate
%
clear all      % clear workspaces
clc            % clear screen
close all      % close any open files
double all;    % use double precision for all data
%
%**************************************************************************
%
f=60
w=2*pi*f
%
%**************************************************************************
%
% Generate one cycle of a current waveform.  Pick 70 KA (RMS) arc current,
% the value used in the PSCad demonstration program.
%
Imax=70000*sqrt(2);
%
%**************************************************************************
%**************************************************************************
%
% EAF Parameters
%
k1=3000
k2=1.0
k3=12.5
%
% Equation variables
%
n=2
```

Appendix N Continued – *MatLab* source code – Development of modified Euler method


```
m=0
%
% Defined Values:
%   R is the arc radius in cm.
%   V is the arc voltage in Volts.
%   A is the arc current in Amperes.
%
%--------------------------------------------------------------------------
%
%  Initial values - used for all methods
%
h=0.000001                          % Pick step size
x = 0:h:1/60;                       % Pick evaluation interval
y = zeros(1,length(x));             % Clear output vector
y(1) = 15;                          % Define initial value
lengthx= length(x)
%
% Create handle to derivative of function and define same
%
F_xy = @(t,R) ( ((k3*(Imax*sin(w*t))^2)/(k2*R^(m+3))) - (k1/k2)*R^(n-1) );
%
% ***************** START 4 th order Runge-Kutta *************************
%
% for i=1:(length(x)-1)                               % calculation loop
%     k_1 = F_xy(x(i),y(i));
%     k_2 = F_xy(x(i)+0.5*h,y(i)+0.5*h*k_1);
%     k_3 = F_xy((x(i)+0.5*h),(y(i)+0.5*h*k_2));
%     k_4 = F_xy((x(i)+h),(y(i)+k_3*h));
%
%     y(i+1) = y(i) + (1/6)*(k_1+2*k_2+2*k_3+k_4)*h;  % main equation
% end
%
% ****************** END 4 th order Runge-Kutta *************************
%
% ******************** START Simple Euler method *************************
%
% for i=1:(length(x)-1)                                 % calculation loop
%     k_1 = F_xy(x(i),y(i));                            % slope at i
%
%     y(i+1) = y(i) + (k_1)*h;                          % main equation
% end
%
%
% ********************** END Simple Euler method *************************
%
% ******************** START Modified Euler method *************************
%
for i=1:(length(x)-1)                           % calculation loop
    k_1 = F_xy(x(i),y(i));                      % slope at i
%
    Ypred = y(i) + (k_1)*h;                     % prediction for y
```

Appendix N Continued – *MatLab* source code – Development of modified Euler method


```
    k_2 = F_xy(x(i+1),Ypred);                % slope at predicted point
%
     Fave = (k_1 + k_2)/2;                   % average value of slope
%
         y(i+1) = y(i) + h*Fave;             % main equation
%
end
%
% ********************** END Modified Euler method ***********************
%
%------------------------------------------------------------------------
%
%     Determine Voltage
%
for i=1:(length(x)-1)   %calculation loop
    Varc(i+1)=(k3/y(i)^(m+2))* Imax*sin(w*x(i));
    Iarc(i+1)=Imax*sin(w*x(i));
end
%
%
%************************** Plot Curves *********************************
%
%----------------------- Arc Radius Curve -------------------------------
%
plot(x, y,'b','LineWidth',1)
grid on
xlabel('Time [Seconds]')
ylabel('Arc Radius [cm]')
title('Variation of the arc radius with time for one period')
axis([0 0.018 0 90])
%
%----------------------- Voltage for one period curve --------------------
%
% plot(x,Varc,'b','LineWidth',1)
% grid on
% xlabel('Time [Seconds]')
% ylabel('Voltage [V]')
% title('Arc Voltage for one period')
% axis([0 0.018 -300 300])
%
%----------------------- Voltage vs Current ------------------------------
%
% plot(Iarc,Varc,'b','LineWidth',1)
% grid on
% xlabel('Arc Current [Amperes]')
% ylabel('Voltage [Volts]')
% title('Voltage-current realtionship for one period')
% axis([-100e3 100e3 -400 400])
%
% ************** End Test_Modified_Euler_Development_1.m ******************
```

Appendix O – *PSCad* EAF model screen shots

The following images are taken from the *PSCad* EAF model:

EAF model graphic:

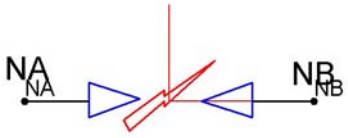

EAF BRANCH code:

```
#IF gnd == 1
   BRN = $NA  $G  BREAKER  1.0
#ELSE
   BRN = $NA  $NB  BREAKER  1.0
#ENDIF
```

EAF *FORTRAN* code:

```
#SUBROUTINE EAF Subroutine
#STORAGE LOGICAL:10  REAL:18  INTEGER:16
#LOCAL REAL K1, K2, K3
#LOCAL INTEGER m, n, noise
#LOCAL REAL V, Rini, R
#LOCAL REAL Stdv
!
     CALL EAF($BRN, $SS, $K1, $K2, $K3, $m, $n, $noise,
     + $Rini, V, R, $Stdv)
#OUTPUT REAL Iarc (#CBR:BRN)
#OUTPUT REAL Varc (V)
#OUTPUT REAL Rarc (R)
```

EAF SCRIPT code: (Not Used)

EAF PARAMETERS screen shot (default values):

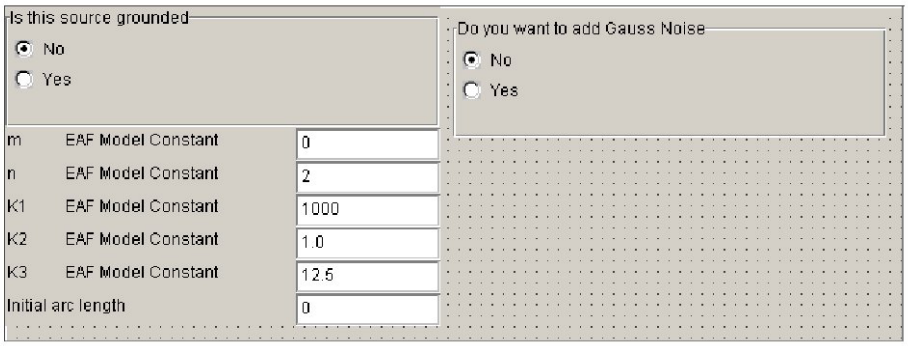

Appendix O Continued – *PSCad* EAF model screen shots

EAF PARAMETERS screen shot (default values):

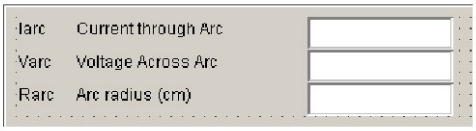

EAF PARAMETERS screen shot (add Gauss noise):

Appendix P – *FORTRAN* source code – EAF model

```
!
! This Fortran code goes with PSCad Version 11
!
!*********************************************************************
!
!                              EAF.f
!
! Leonard W. White                                NSF FREEDM Center
! lwwhite@ncsu.edu                                NC State University
!
! This is the source for a Single Phase Electric Arc Furnace model
! intended for use with PSCad.  The model uses the current through
! the branch to solve the non-linear differential equation used to
! define the arc radius.  The arc radius is then used to compute the
! voltage across the arc.
!
! The following are the called variables:
!
! BRN            PSCad branch number
! SS
! K1, K2, & K3   Real EAF constants
! m, n           Integer EAF constants
! noise          Integer test variable to determine the type of noise,
!                added to the arc radius computation
! Rinitial       Initial arc radius
! C              A test variable for future use
! Vft            Voltage between the 'from' node to the 'to' node
!
!*********************************************************************
!
!23456 This is FORTRAN: Remember to procede code by at lease six spaces.
!                       Maximum line length is 72 characters.
!                       A character in Col 6 is used for line extension.
!
      SUBROUTINE EAF (BRN, SS, K1, K2, K3, m, n, noise, Rinitial,
     1Vft, R, Std)
!
! ***************************** Inclued Block *************************
!
      INCLUDE 'nd.h'         !  Dimensioning information (always first)
      INCLUDE 's0.h'         !  Various variables
      INCLUDE 's1.h'         !  Internal variables, e.g. DELT, TIME, etc.
      INCLUDE 's2.h'         !  This is obsolete based on latest info
      INCLUDE 'branches.h'   !  Branch information and calls
      INCLUDE 'fnames.h'     !  Character data for file names
      INCLUDE 'emtstor.h'    !  Storage arrays and variables
      INCLUDE 'emtconst.h'   !  Various math constants, e.g., pi, etc.
!
! ************************ Data Type Declarations **********************
!
      REAL K1, K2, K3, Rinitial, Vft, Varc              ! Called values
      REAL Vf, Vt, Rlast, Rnew, Ilast, Inew, KA, KB     ! Program values
      REAL S1, S2, Rpred, Savg, Varc, R, Std            ! Program values
      Integer BRN, SS, m, n, noise  ! Called values
      Integer NF, NT    ! Program values
      REAL VAR, Gcoef    ! Gauss test values
!
! ******************* Startup test and initializations ****************
!
!      None are needed for present version
!
!*****************
      ISTORF = NSTORF        ! Set up storage vectors for next time thru
      NSTORF = NSTORF + 2    ! subroutine.
 !
      IF (TIMEZERO) THEN
!
```

```
          Rlast = Rinitial          ! Set initial arc length as desired
          Ilast = 0.0               ! Set initial current to zero
          STORF(ISTORF) = Rlast     ! Store arc length for next loop
          STORF(ISTORF+1) = Ilast   ! Store current for next loop
!
      END IF
!
      SOURCE(BRN,SS) = .TRUE.
!
      Inew = CBR(BRN,SS)*1000       ! CBR gets current through node
      Rlast = STORF(ISTORF)         ! Get value from previous loop
      Ilast = STORF(ISTORF+1)       ! Get value from previous loop
!
!
! ******************** Compute updated arc length, Rnew ***************
!
!  Method of compoutation is Euler's Modified Method, which has overall
!  second order accuracy.
!
!---------------------------------------------------------------------
!
! Simplify equation quotents for improved speed of computation
!
      KA = K3/K2
      KB = K1/K2
!
! Compute slope at last value of R and I
!
      S1 = (((KA*Ilast*Ilast)/(Rlast**(m+3))) - (KB*(Rlast**(n-1))))
!
      Rpred = (Rlast + (S1*DELT))  ! Compute predicted value of R, Rpred
!
! Compute slope at predicted values of R and I
!
      S2 = (((KA*Inew*Inew)/(Rpred**(m+3))) - (KB*(Rpred**(n-1))))
!
      Savg = ((S1+S2)/2)           ! Comput average slope
!
      Rnew = (Rlast + (Savg*DELT)) ! Compute new value of R, Rnew
!
! ****************** Insert correction for Gauss noise here ***********
      IF (noise .EQ. 0) THEN
         CONTINUE      ! Don't modify arc radius value
      ELSE
         CALL GAUSS(VAR)  ! Determine Gauss modification variable
         Gcoef = Std*VAR + 1.0  ! Multiply by desired standard
                                !   devition and add one to determine
                                !   Gauss multiplication coefficient
         Rnew = Rnew*Gcoef      ! Modify arc radius value

      END IF
! =====================================================================
!
! Compute voltage across Arc
!
      Varc = K3*Inew/(Rnew**(m+2))  ! From voltage equation
      Inew = Inew/1000
!
      R = Rnew
! Set branch conductance
      GEQ(BRN,SS) = (Rnew**(m+2))/K3
!
      NF = IEF(BRN,SS)  ! Get the 'from' node number
      NT = IET(BRN,SS)  ! Get the 'to' node number
!
      CALL SETMXINV(SS,NF,NT)
```

```
! Restore new values
      STORF(ISTORF) = Rnew
      STORF(ISTORF+1) = Inew

      Vf = VDC(NF,SS)    ! Get voltage between 'from' node and ground

      Vt = VDC(NT,SS)    ! Get voltage between 'to' node and ground

!
      Vft = VDC(NF,SS) - VDC(NT,SS)  ! Determine voltage between nodes
!
      RETURN
      END

!  ***********************************************************************
!  ***********************************************************************
!
! +++++++++++++++++++++++++++++++++++++++++++++++++++++++++++++++++++++++++
!
! The method used in this Subroutine is based on a paper by Fox, et al:
! "Fast, accurate algorithm for numerical simulation of exponentially
! correlated colored noise."  Published in Physical Review A, Vol. 38,
! No. 11, December 1, 1988.
!
! +++++++++++++++++++++++++++++++++++++++++++++++++++++++++++++++++++++++++
!
      SUBROUTINE GAUSS (Gnoise)
!
      INTEGER Iset
      REAL Gnoise, Gnoise_ST, R1, R2, Rroot, Fact
      DATA Iset /0/    ! Iset is a test variable
!
! Two Gauss noise factors are generated on each pass through the
! routine. One is imediately used, then the second one is used on the
! next pass through. After both are used the routine resets Iset to
! zero to generate two more values the next time the routine is called.
!
      IF (Iset .EQ. 0) THEN     ! Evaluate test variable
100      R1 = 2.0*RAN1 (TIME) - 1.0  ! Generate random numbers
         R2 = 2.0*RAN1 (TIME) - 1.0  ! between -1 & +1
         Rroot = R1*R1 + R2*R2 ! Rroot is beteen 0 & +2
!
      IF (( Rroot .GE. 1.0) .OR. (Rroot .EQ. 0.0)) GOTO 100
! Redoo until final value of Rroot is greater than 0 and less than or
! equal to 1
         Fact = SQRT (-2.0*LOG(Rroot)/Rroot) ! Generate factor
         Gnoise_ST = R1*Fact  ! Save a stored value of noise
         Gnoise = R2*Fact     ! Use this noise value then return
         Iset = 1             ! Flip the test variable
      ELSE  ! This code is executed if to use the
          Gnoise = Gnoise_ST  ! Set noise value to be used to the
                              !   stored value
          Iset = 0            ! Reset test variable
      ENDIF

      RETURN
      END
```